Assembly and Physico-Chemical Characterization of Supramolecular Polyelectrolyte Nanostructures

Dissertation presented to the Department of Mining and Metallurgical Engineering and Materials Science

(E.T.S.I. Bilbao / UPV-EHU)

for the degree of Doctor Europeus in Chemistry

by

JAGOBA JON ITURRI RAMOS

Thesis advisor: Dr. Sergio E. Moya

University Tutor: Dr. José Ramón Sarasua Oiz

Donostia-San Sebastian

2011

Universidad del País Vasco
Euskal Herriko Unibertsitatea

This PhD thesis has been performed at:

CICbiomaGUNE

Biosurfaces Unit

Donostia-San Sebastian (SPAIN)

Universität Leipzig

Institut für Medizinische Physik und Biophysik

Leipzig (GERMANY)

Zhejiang University

Department of Polymer Science and Engineering

Hangzhou (CHINA)

Acknowledgements

From these lines I would like to acknowledge my supervisor Dr. Sergio E. Moya, Dr. José Ramón Sarasua (UPV-EHU) as my tutor at university, and the financial support from the Spanish Ministry of Science and Innovation (MAT2007-0458).

A last mention, although very special, goes to those who, in one way or another, have inspired both my life and my work during these last four (+27) years. My most sincere gratitude to all of you.

Outline

Abstract

This PhD thesis describes, from a physico-chemical point of view, the assembly and the responsiveness of supramolecular structures based on stimuli-responsive polyelectrolyte chains.

Firstly, the layer-by-layer electrostatic adsorption of oppositely charged poly (allyl amine hydrochloride) (PAH)/poly (sodium styrene sulfonate) (PSS) and of poly (diallyl dimethylammonium chloride)/PSS polyelectrolyte pairs has been used for the formation of polyelectrolyte multilayers (PEMs). Secondly, the Atom Transfer Radical Polymerization (ATRP) technique of (meth)acrylate-based monomers, such as the sulfo propyl methacrylate (SPM) or N-isopropyl acrylamide (NIPAAm), has been employed to synthesize brush-like structures from chemically modified surfaces.

By means of different techniques such as the Quartz Crystal Microbalance with Dissipation (QCM-D), Ellipsometry and both Raman and Infra-red (IR) spectroscopies, some important issues regarding the mechanism of assembly and the water content of these systems have been studied. Furthermore, the subsequent exposure of multilayers and brushes to external stimuli (high ionic strengths, temperature increases, surfactants…) has been also analyzed to determine the effect on the structure and the water content of the films.

Resumen

Este trabajo de tesis describe, desde un punto de vista físico-químico, el ensamblado y la capacidad responsiva de estructuras supramoleculares basadas en polielectrolitos.

En primer lugar, se utilizó la adsorción electrostática capa-a-capa de polielectrolitos de carga opuesta como en el caso de los pares de polielectrolitos poly (allyl amine hydrochloride) (PAH)/poly (sodium styrene sulfonate) (PSS) y poly (diallyl dimethylammonium chloride)/PSS para la formación de sistemas multicapas (PEMs). En segundo lugar, se empleó la técnica de Polimerización Radicalaria de Transferencia Atómica (ATRP) para monómeros basados en (met)acrilatos, tales como el sulfo propyl methacrylate (SPM) o la N-isopropyl acrylamide (NIPAAm), para obtener la síntesis de estructuras de tipo cepillo a partir de superficies químicamente modificadas.

El uso de técnicas tales como la Quartz Crystal Microbalance with Dissipation (QCM-D), la Elipsometría y las espectroscopías Raman e Infrarroja (IR), permitió el estudio de algunos aspectos importantes relacionados con el mecanismo de ensamblado y del contenido acuoso de estos sistemas. Adicionalmente, se analizó el efecto generado en la estructura y el contenido acuoso de multicapas y cepillos por una posterior exposición frente a diversos estímulos externos (elevadas fuerzas iónicas, incrementos en la temperatura, surfactantes…).

Overview

Around 400 BC, the Greek philosopher Democritus already imagined that all matter in the universe evolved from the organization of atomistic components to form the Earth and solar system, stars and galaxies. A similar approach to that of Democritus was done two millennia later by the French philosopher Descartes, who also envisioned an ordered universe arising through the organization of small objects into larger assemblages.[1] Although the language of Democritus and Descartes stemmed from mere lucubration, their explanation about structural organization of life seems to be surprisingly synonymous with the current approach offered by supramolecular chemistry.[2]

Supramolecular Chemistry

Supramolecular chemistry is, according to the IUPAC definition, "the field of chemistry related to species of greater complexity than molecules that are held together and organized by means of intermolecular interactions. The objects of supramolecular chemistry are super-molecules and other poly-molecular entities that result from the spontaneous association of a large number of components into a specific phase (membranes, vesicles, micelles, solid state structures, *etc*)".[3-8]

Supramolecular chemistry has been often inspired by nature. Indeed, a wide variety of complex naturally occurring nanostructures like tobacco mosaic virus, collagen or ferritin can be considered as supramolecular assemblies. Moreover, DNA has a supramolecular nature since exists in a double helical form where the two single strands are held together by a number of hydrogen bonds. Interaction occurs between the acidic atoms (hydrogen bonding donors) from

the purine bases (guanine and adenine) and the oxygen and nitrogen atoms (hydrogen bonding acceptor) of the pyrimidine bases (cytosine and thymine). It is the challenge of supramolecular chemistry to synthetically create nanostructures with such precision and specificity as seen in biological systems.[9-15]

Supramolecular chemistry is strongly related to the *self-assembly* concept. Self-assembly can be defined as the process in which components, either separate or linked, spontaneously form ordered aggregates. Then, a self-assembled system consists of a group of molecules or segments of a macromolecule that interact through weak and non-covalent interactions (van der Waals forces, Coulomb interactions, hydrophobic interactions, and hydrogen bonds) and lead the system from some less ordered state (a solution, disordered aggregate, or random coil) to a final state that is more ordered (a crystal or folded macromolecule). Such association is either reversible or allows the components to adjust their positions within an aggregate once it has formed. We find examples of self assembly in the formation of molecular crystals, the organization of lipids into lipid bilayers or vesicles, the formation of monolayers of thiols, as well as the folding of polypeptide chains into proteins .[16-21]

Self-assembly is not only scientifically interesting and technologically important[22-23] but it is also centrally important in life. The cell, for instance, is composed of an astonishing range of complex structures such as lipid membranes, folded proteins, structured nucleic acids, protein aggregates, molecular machines, and many others that form by self-assembly. Besides, self-assembly provides one of the most general strategies now available for generating nanostructures and routes to a range of materials with regular structure such as molecular crystals, liquid crystals,

and semi-crystalline and phase-separated polymers. Most of these constructs can be designed for a specific purpose. For instance, one could find self-assembled monolayers (SAMs) in micro-fabrication and nano-electronics, lipid bilayers as biomembranes and liquid crystals in displays .[24-38] All this turns self-assembly into a powerful way of making materials and organizing them into functional assemblies.

Polymers appear among the most relevant examples of materials that can organize into supramolecular structures.[39-43] There are plenty of examples of polymers forming fibers monolayers, complexes and thin films held together by weak interactions.[44-46]

In this thesis two examples of polymeric supramolecular structures will be studied: the layer-by-layer (LbL) buildup of multilayers and the synthesis of polymer brushes, which will be explained in detail further below. Both systems are based on the use of polyelectrolytes as building blocks.

Polyelectrolytes

Polyelectrolytes are polymeric chains bearing an electrolyte group as repeating unit, which dissociates in water and provides either a positive or negative charge, or both charges at the same time (zwiterionic polyelectrolytes).[47-49] Polyelectrolytes can be classified into ‘weak’ and ‘strong’: strong polyelectrolytes keep their charged/dissociated state at the whole pH range, while for weak polyelectrolytes the degree of charge will depend on the pH value. While an uncharged linear polymer chain is usually found in a random conformation in solution, linear polyelectrolyte chains in an aqueous environment adopt an extended conformation. Such chain

extension is explained by the repulsion originated between the charged monomers that repel each other within a chain or among different chains. However, when the ionic strength in the bulk solution is increased, the charges of polyelectrolyte will be screened and the polyelectrolyte chain will consequently adopt a randomly coiled conformation.[50] Polyelectrolytes are used in different fields such as cosmetics or food industry since, for instance, they can act as thickeners, emulsifiers or moisturizers and similar processes mostly related to modifying flow and stability properties.[51] Polyelectrolytes are easy to assemble, pattern or synthesize from surfaces, and have been therefore extensively used in the fabrication of thin films. In addition, polyelectrolytes have capability to respond to external stimuli through structural changes in the nanometric scale that render them particularly appealing for the fabrication of responsive surfaces.[52-55]

Layer by layer technique

The layer-by-layer (LbL) deposition technique is based on the alternatively assembly of oppositely charged polyelectrolytes on charged surfaces.

R. K. Iler, in 1966, reported for the first time the alternate deposition layers of positively and negatively charged colloidal particles.[56] But, it was Decher, around 30 years later from Iler's experiment, who followed the same technique to coat positively charged solid substrates with a planar surface.[57] The protocol consisted in the immersion of the surface in a solution containing an anionic polyelectrolyte, poly (sodium styrene sulfonate) (PSS), in order to form a monolayer of the polyanion. Thus, a large number of charged monomers in the interface were exposed to the solution and thus the surface charge was effectively reversed. After thorough rinse in pure water

the substrate was subsequently immersed in the solution containing a cationic polyelectrolyte, Poly (allylamine hydrochloride) (PAH) which adsorbs on top of the polyanion. By repeating both steps in a cyclic fashion, a thin polymer film with a layered structure was obtained, giving thus raise to the term *layer-by-layer*. A schematic view of the process is depicted in Fig. 1.

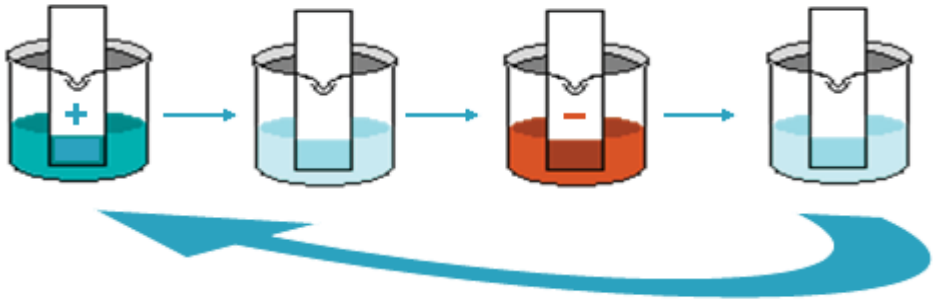

Figure 1 Scheme of the layer-by-layer technique.

During each layer deposition step, the polyelectrolytes from the solution are electrostatically attracted by the oppositely charged polyelectrolytes constituting the last layer of the film on the solid substrate. This polyelectrolyte deposition then leads to charge overcompensation at the solid/liquid interface which, in turn, causes electrostatic repulsion with excess material in solution and limits the adsorbing layer to monolayer coverage. The structure of the film formed was reported to exhibit a somewhat "fuzzy" but layered structure, instead of a purely stratified architecture, where each polyelectrolyte layer interpenetrates with its neighboring layers.[58] The chain interpenetration leads to a film roughening where a progressively larger number of adsorption sites are generated. Therefore, an increase in the adsorbed polymer, and thus in layer thicknesses, can be expected to take place as the number of deposited layers is increased.

However, the equilibrium is reached quickly and the thickness per layer lies typically between 1 and 10 nm depending on the system under analysis. [59-60]

The LbL technique has been successfully employed to construct films based on either natural (polysaccharides, polypeptides) or synthetic polyelectrolytes [PSS, PAH…).[61] In general, the LbL assembly of polyelectrolytes has been reported to follow two different mechanisms. The first class of multilayers embraces those multilayers whose mass and thickness grow linearly with the number of deposition steps, which are the most common and most widely studied, and are known as "linear" polyelectrolyte multilayers (PEMs).[62]

The second class comprehends those films whose mass and thickness grow with the number of deposited layer pairs more rapidly than in the case of linear PEMs. These films are denoted as supralinear or "exponential" PEMs.[63] The buildup, unlike that of linear systems, is based on the diffusion "in" and "out" of at least one of the polyelectrolytes through the whole film, during each layer pair deposition step. The choice of the polyelectrolyte pair forming the multilayer will undoubtedly determine the assembly regime. For instance, multilayers formed by PAH and PSS have been reported as linearly growing systems while exponentially growing films were mainly observed with polypeptides and polysaccharides such as poly(glutamic acid) (PGA)/(PAH) or Poly (L-lysine) (PLL)/alginate systems.[64-66.] Many additional parameters such as the ionic strength and pH of the deposition solutions, the adsorption time or the rinsing procedure used during formation of films can influence both the properties of PEMs and the type of growing regime followed along the buildup. Indeed, increasing the salt concentration during the assembly can lead to a transition from a linear growth regime to an exponential growth regime for some

systems. Such scenario was reported by Guzman et al. for a system composed of Poly (diallyl dimethylammonium chloride) (PDADMAC) polycation in combination with polyanionic Poly (sodium styrene sulfonate) (PSS). The film was shown to shift from a linear to a exponential growth over certain ionic strength values of the bulk solution.[67] Such change was reflected in the corresponding average thickness per layer being assembled, which passed from around 7 nm at low salt concentrations, to around 25 nm when the ionic strength went over 0.3 M.

LbL technique is not only restricted to polyelectrolytes, since it could be also employed for the construction of multicomposite films of other charged materials through layer-by-layer adsorption from aqueous solution.[68] Indeed, much of the work on these polyelectrolyte multilayers has focused on generalizing and expanding the technique to various combinations of charged components, including synthetic polyelectrolytes, biopolymers such as proteins,[69] clay minerals,[70] dendrimers,[71] metal colloids,[72.] silica,[73.] and other inorganic particles.[74] Applications have surfaced almost simultaneously and include conducting layers,[75] permeation-selective membranes,[76] enzyme-active thin films,[77] sensors,[78] light-emitting thin films,[79] selective area patterning,[80] electrochromic films,[81] and electrocatalysis,[82] among others.

Furthermore, LbL assembly is not only limited to planar surfaces and can be effective in other geometries as well.[83] The use of nano- and micro- sized spherical particles (polystyrene latex, silicon dioxide) allows for the fabrication of three dimensional structures in addition to the well-advanced fabrication of two dimensional films (Fig. 2a). This offers a wide range of

opportunities for non-covalent tuning of the chemical and physical properties of the surface of colloidal particles.

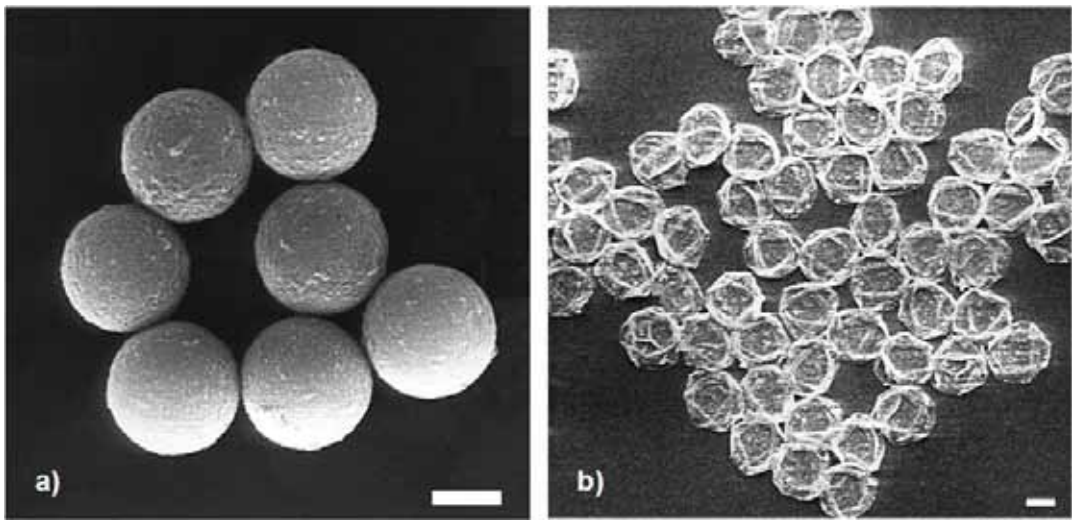

Figure 2 SEM micrographs of Melamine-Formaldehyde particles coated with nine layers (PSS and PAH) prior to the dissolution of the core (a) and of the remaining polyelectrolyte shell after removal of the core at pH 1.3 (b). The scale bar corresponds to 1 nm. (Picture taken from ref. 83)

The assembly on colloidal particles demands for especial care in order to avoid bridging flocculation between colloids induced by the added polyelectrolytes instead of layer growth. First, the initial colloidal substrate as well as each of the employed polyelectrolyte species has to be sufficiently charged. Otherwise adsorbed layers may be partially removed upon adsorption of the next polyelectrolyte layer. Furthermore, weakly charged substrates or polyelectrolyte species facilitate bridging flocculation. Second, the saturation conditions have to be provided. If the latter requirement is not met an uncontrolled layer growth or bridging flocculation may occur.

Working with such kind of spherical PEMs brings the possibility to use characterization methods which differ from those employed for planar substrates. Thereby, one could measure

electrophoresis, dynamic light scattering particle sizing, single particle light scattering, and even fluorescence intensity measurements, when using fluorophore-labeled polyelectrolytes to assemble the multilayer, to determine structural properties.

In addition, research on spherical PEMs can be taken a step further by coating of soluble, or otherwise degradable, colloidal templates for the film formation. In such case, subsequent removal of the core could lead to three-dimensional polyelectrolyte complexes in the form of hollow polyelectrolyte shells (Figure 2b), which find major applications on the encapsulation of active materials for the controlled release and targeting.[84] Examples of colloidal templates employed for the formation of hollow capsules are both Melamine-Formaldehyde and SiO_2 nano-sized particles which can be dissolved in acidic solutions of hydrochloric (HCl) and fluorhydric (HF) acids, respectively.

Polyelectrolyte brushes

Also in this thesis, polyelectrolyte brushes prepared by the grafting from approach will be studied. The configuration of polymers attached by one end to the solid/solvent interface started attracting a great deal of interest both experimentally and theoretical1y along the 1980s.[85-89] Such interest was in-line with the increased use of these polymers as dispersion stabilizers, adhesives, etc. The term “polymer brush” refers to the case where long chain polymer molecules attached by one end to a surface or interface have a density of attachment points high enough, so the sterical repulsions between neighboring chains force them to stretch away from the interface, sometimes much farther than the typical un-stretched size of a chain (Fig. 3a).[90] Such situation,

in which polymer chains stretch along the direction normal to the grafting surface (like the bristles in a brush, hence the name), differs quite considerably from the typical behavior of flexible polymer chains in a solution, where the long molecules adopt random-walk configurations.

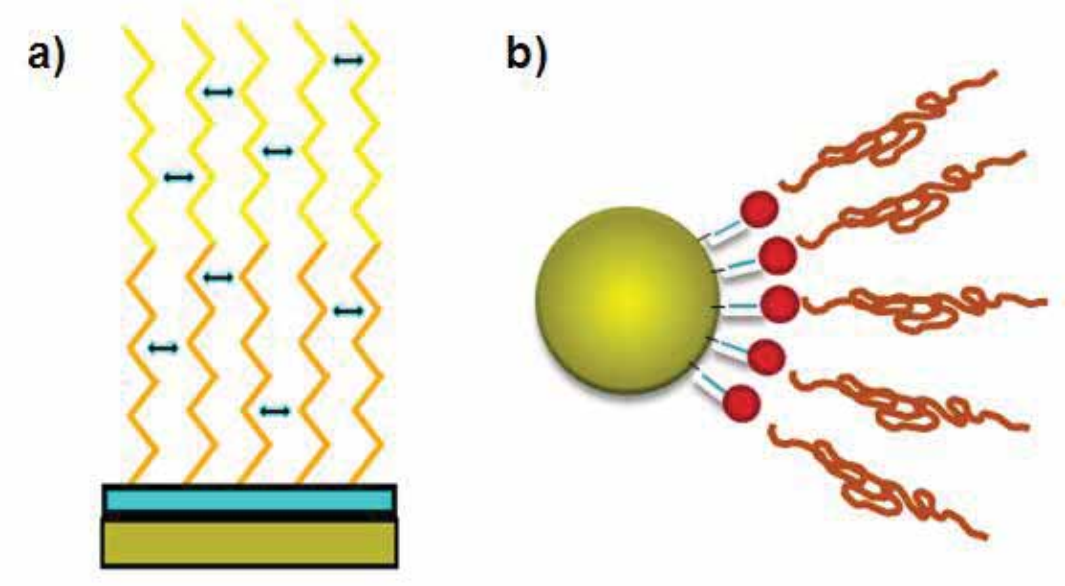

Figure 3. Scheme of a polyelectrolyte brush (a) on a planar surface and (b) grafted from a colloidal particle.

The anchorage of the chains in a brush is generally based on two methods called "*grafting to*" (to the surface) and "*grafting from*" (from surface). In the first case, when the coating is produced "to", the pre-formed polyelectrolyte chains are endowed with a terminal functional group in its structure and then react with the surface to obtain the desired layer. Normally the density of coating thus obtained by this method is low and the film thickness, small. In general polymer chains are voluminous and therefore when grafting one polymer molecule by a single covalent binding the access of other chains to the area where the chain has been attached is limited. The

second method, the "grafting from" technique, allows for the in situ formation of the polyelectrolyte film on the surface from a previously bound self-assembled monolayer (SAM) incorporating an appropriate polymerization initiator.[91-93] Initiators employed, either silanes or thiols, are on the rule of small molecules with surface areas of 20 $Å^2$, much smaller than the average cross sectional area of a polymer chains (~180-200 $Å^2$) and can therefore result in denser layer.[94] Hence, monomers migrate to these active sites of initiation and polymerize, forming a polyelectrolyte layer of higher density and thickness as the film obtained by the procedure explained above.

The features of the surface to modify often define what approach to follow for the brush synthesis. For solid substrates, the “grafting from” protocol has generally become the most attractive way to prepare thick, covalently tethered polymer brushes with a high grafting density. The immobilization of initiators onto the substrate, forming a 2-D Self-Assembled Monolayer (SAM), is followed by in situ surface-initiated polymerization (SIP) to generate the tethered polymer brush. In this regard, different polymerization strategies, such as free-radical, cationic, anionic, or ring opening metathesis polymerization (ROMP), have been applied to form the brush-like structures on surfaces.[95] Among these types of polymerization methods, atom transfer radical polymerization (ATRP) has attracted significant interest for its living/controlled character, thus providing a control over molecular weight and polydispersity, its tolerance of functional groups, and the mild experimental conditions required.[96-97] However, all the methods above mentioned would be suitable for polymerizing different types of monomers on a variety of flat surfaces and particles (Fig. 3b). As the chains are growing from the surface, the only limits to

propagation are the diffusion of monomer to the polymerization-active chain ends, or the blockage of the active radical. This results in thick tethered polymer brushes with high grafting density. The first highly successful demonstration of the grafting from technique for the synthesis of brush layers was reported by Rühe and co-workers who succeeded in preparing various polyelectrolyte brushes from planar surfaces with high grafting densities and high molecular weights by this approach.[98-99] Since then, polymer brushes have become a central model in many important problems in polymer science, and are relevant even in biophysics and surfactant science (where the chains in question are only marginally long enough to be called polymers).

In the specific case where the polymer chain grafted bears an electrolyte group as repeating unit, a polyelectrolyte brush results. Unlike the previously described end-grafted uncharged macromolecules, structure and properties of polyelectrolyte brushes are dominated by electrostatic interactions both between the charged polymer segments in a single chain and between neighboring polyelectrolyte chains. Then, while at low ionic strengths of the bulk solution, the properties of the polyelectrolyte brush are mainly governed by those intrinsic electrostatic interactions, an increase in ionic strength leads to the reduction of the electrostatic repulsion, the so-called salted regime.[100] In this regime, the difference in osmotic pressures between the film and the bulk becomes smaller and the brushes may undergo a transition toward a more coiled state. Consequently, both the volume and the thickness of the brush are reduced while, on the contrary, rigidity of the film increases.

In addition to collapse induced by the screening of electrostatic charges, brushes can also collapse, when the counterions are replaced by ions with high affinity to the charges on the brushes, leading to overall neutral brushes. For instance, poly ([2-(methacryloyloxy)ethyl] trimethyl ammonium chloride)(PMETAC) brushes have been reported to collapse via specific interactions in the presence of certain ions like ClO_4^-, SCN^-, and I^- but, unlike the electrostatic case, initial structure cannot be immediately recovered in the presence of pure water.[101] Besides the collapse, the exchange of counterions affects wettability and mechanical properties of the brush. For example, PMETAC brushes have been also shown to change their wettability from very hydrophilic to relatively hydrophobic upon exchanging Cl counterions by perchlorate.[102] Another interesting effect can be found when the counterions employed have some additional properties such as reversible redox chemistry, application of alternating negative and positive potentials permits switching between the reduced state and oxidized state, resulting in reversible changes in water contact angles.[103]

Polyelectrolyte brushes have become the subject of intense research, mainly due to the great number of possible application that they can have in nanotechnology and nanofabrication.[104] For example their capability to respond to both ionic strength and to the specific nature of the electrolytes in solution could be used in nano-actuators or controllable barriers in microfluidic devices.[100] Polyelectrolyte brushes can also be used to immobilize metallic nano-particles that can be used by catalysis, or to control protein adsorption on surfaces, in the so called "polyelectrolyte-mediated protein adsorption" (PMPA) phenomena. PMPA effect was found to take place in both planar and spherical polyelectrolyte brushes and resulted from increasing the ionic strength in the system. This promoted a shift between a protein-adsorbing to an anti-fouling

state in which sterical repulsion between the protein and the brush layer prevails and the proteins do not adsorb anymore.[105]

Besides their possible applications brushes pose a number of fundamental questions of high interest. For example, although the synthesis and the collapse upon changes in the environmental conditions have been rather extensively studied for polyelectrolyte brushes, less work has been done in studying the role of water on these systems. Water in a brush can come both from the water associated to the electrolyte groups in the repeating unit and from those water molecules entrapped within the brush-like structure. Several factors, i.e. the grafting density or the chain length, will thus have a direct impact on the final water content values obtained. This becomes a main issue that is worth to be studied. More specifically, knowledge of the water content of the brush will allow for the subsequent calculation of the water percentage released through shrinkage of the film, which is reported here for the first time.

Objectives

Despite extensive studies done so far, several issues regarding polyelectrolyte multilayers and brushes still remain unknown. The focus of this thesis is to bring a deeper insight in the process of self assembly of polyelectrolytes into organized supramolecular structures and to understand their behavior under specific conditions: i.e. changes in the ionic strength, presence of surfactant, temperature. Understanding the basic properties of these systems is very important for their application in the design of devices with tailored properties.

More specifically, the objectives of this thesis are the following:

-To have a more detailed understanding of the mechanisms of self assembly of polyelectrolyte multilayers

-To study the evolution of the water content in polyelectrolyte multilayers during polyelectrolyte assembly, as well as the effect of the ionic strength in the assembly.

-To determine how specific counter ion polyelectrolyte interactions affect the physical properties of both multilayers and brushes.

-To study the stability of polyelectrolyte layers and find out the ways to selectively remove polyelectrolyte multilayers

-To characterize the growth of polyelectrolyte brushes and their water content.

-To determine the effect that the chain grafting density has in the structure and aqueous content of polyelectrolyte brushes.

-To quantify, in terms of percentage of water lost, the collapse induced in the brush through different external stimuli.

-To combine polyelectrolyte multilayers and polyelectrolyte brushes for the fabrication of complex 3D architectures.

The thesis has been divided in two sections: a first section (Chapters 1-3) dealing with polyelectrolyte multilayers and a second section (Chapter 4-6) centered on the analysis of polyelectrolyte brushes.

Chapter I will address the buildup and the water content of several polyelectrolyte combinations assembled by the Layer-by-Layer technique. For the first time, the combination of acoustic Quartz Crystal Microbalance with Dissipation (QCM-D) and of optical Spectroscopic Ellipsometry in a single device will be used for the in situ determination of the evolution of the water content during polyelectrolyte assembly. The in situ studies will be applied to linear (PAH/PSS) and exponentially growing (PDADMAC/PSS) PEMs under different conditions of assembly. A model is proposed to explain the differences observed between linear and exponential PEMs.

Chapter 2 will analyze the response of PEMs upon increases in the ionic strength and in presence of specific counterions such as ClO_4^- or $H_2PO_4^-$. Complementary measurements by QCM-D on planar substrates and by ζ-potential of spherical PEMs will allow for the determination of specific interactions between the counterions and the polyelectrolyte pair.

In **Chapter 3**, the interaction between multilayered systems and ionic surfactants will be studied. Although one of the main features of PEMs is their stability under harsh conditions, there are situations where removal would turn desirable: for instance, deprotection of a coated surface or, on the contrary, to promote degradation of capsules in order to release its content. It will be shown that PEMs can be selectively removed with the TTAB cationic surfactant. PEMs with PSS as polyanion will be removed depending on the nature of the counter polycation,

PDADMAC or PAH, although in all case the positive charged surfactant interacts with PSS. Confocal Raman Microscopy and Infrared Microscopy will be employed to study the mechanism of interaction of the surfactant with the polyelectrolytes, the stoichiometry of the surfactant polyelectrolyte complexes and also to gain insight in the interaction between polyelectrolytes.

Chapter 4 will analyze in situ the synthesis of PE brushes of different compositions: PSPM, PMETAC and PNIPAAm, and their water content, in a similar manner as done in Chapter 1 for PEMs, by means of QCM-D combined with ellipsometry. Additionally, it will be analyzed how the density of thiol initiator, from 1 % to 100 % in the thiol solution used to fabricate the initiating monolayer, affects the mass of the brush and its water content.

In **Chapter 5**, exposure of brushes to changes in the ionic strength and the temperature, or to an exchange of the counterions promoting specific interactions with the counterions of the brush will be presented. Both variations in the film thickness and in the water content resulting from the structural collapse will be studied by means of QCM-D technique. Comparison of these results with those obtained in the previous chapter will then allow for the calculation of the water percentage lost.

Finally, in the last chapter of this thesis (**Chapter 6**) brushes and PEMs will be combined for the fabrication of three dimensional porous structures. Brushes will be used as templates for the LbL assembly of PEMs assembly. The use of a soft material as template for the PEM results in a higher adsorption of polyelectrolytes than on hard surfaces. In addition, PDADMAC/PSS PEMs will form a porous structure on top of the brush.

References

(1) Ozin, G. A.; Hou, K.; Lostch, B. V.; Cademartiri, L.; Puzzo, D. P.; Scotognella, F.; Ghadimi, A.; Thomson, J. Materials Today 2009, 12, 12.

(2) Lehn, J. M. Angew. Chem. Int. Ed. 1990, 29, 1304.

(3) Nguyen, S. T.; Gin, D. L.; Hupp, J. T.; Zhang, X. PNAS 2001, 98, 11849

(4) Rebek, J., Jr. Angew. Chem. Int. Ed. Engl. 1990, 29, 245.

(5) Amabilino, D. B.; Stoddart, J. F. Chem. Rev. 1995, 95, 2715.

(6) Fyfe, M. C. T.; Stoddart, J. F. Acc. Chem. Res. 1997, 30, 393.

(7) Harada, A.; Li, J.; Kamachi, M. Nature 1992, 356, 325.

(8) Harada, A.; Li, J.; Kamachi, M. Nature 1994, 370, 126-128.

(9) Lehn, J. M Polym. Int. 2002, 51, 825.

(10) Philp, D.; Stoddart, J. F. Angew. Chem. Int. Ed. Engl. 1996, 35, 1154.

(11) Batten, S. R.; Robson, R. Angew. Chem. Int. Ed. 1998, 37, 1460.

(12) Reinhoudt, D. N.; Stoddart, J. F.; Ungaro, R. Chem. Eur. J. 1998, 4, 1349.

(13) de Mendoza, J. Chem. Eur. J. 1998, 4, 1373.

(14) Whitesides, G. M.; Mathias, J. P.; Seto, C. T. Science 1991, 254, 1312.

(15) Davis, A. V.; Yeh, R. M; Raymon, K. N. PNAS 2002, 99, 4793

(16) Kim, K.; Lee, I. S.; Centrone, A.; Hatton, T. A.; Myerson, A. S. J. Am. Chem. Soc. 2009, 131, 18212

(17) Cha, T.; Guo, A.; Zhu, X. Y. Biophys J. 2006, 90, 1270.

(18) Ghadiri, M. R.; Soares, C.; Chong, C. J. Am. Chem. Soc. 1992, 114, 825.

(19) Thomas, E. L. Science 1999, 286, 1307.

(20) Kumar, A.; Abbott, N. A.; Kim, E.; Biebuyck, H. A.; Whitesides, G. M. Acc. Chem. Res. 1995, 28, 219.

(21) Grantcharova, V., Alm, E. J., Baker, D. & Horwich, A. L. Curr. Opin. Struct. Biol. 2001, 11, 70.

(22) Whitesides, G. M.; Boncheva M. PNAS 2002, 99, 4769

(23) Whitesides, G. M.; Grzybowski, B. Science 2002, 295, 2418.

(24) Love, J. C., et al., Chem. Rev. 2005, 105, 1103.

(25) Xia, Y. N., and Whitesides, G. M., Ann. Rev. Mater. Sci. 1998, 28, 153.

(26) Keller, S. W, et al., J. Am. Chem. Soc. 1994, 116, 8817.

(27) Lvov, Y., et al., J. Am. Chem. Soc. 1995, 117, 6117.

(28) Lvov, Y., et al., Langmuir 1993, 9, 481.

(29) Chan, W. C. W., and Nie, S., Science 1998, 281, 2016.

(30) Bruchez, Jr. M., et al. , Science 1998, 281, 2013.

(31) Friedman, R. S., et al., Nature 2005, 434, 1085.

(32) Khang, D. Y, et al., Science 2006, 311, 208.

(33) Lopez, C., et al., Adv. Mater. 2003, 15, 1679.

(34) Zakhidov, A. A., et al., Science 1998, 282, 897.

(35) Tang, C. B., et al., Science 2008, 322, 429.

(36) Loudet, J. C.; Barois, P.; Poulin, P. Nature 2000, 407, 611.

(37) Aizenberg, J.; Black, A. J.; Whitesides, G. M. Nature 1999, 398, 495.

(38) Srinivasan, U.; Liepmann, D.; Howe, R. T.; J. Microelectromech. Syst. 2001, 10, 17.

(39) Li, H.; Huck, W. T. S. Curr. Opin. Solid State Mater. Sci. 2002, 6, 3.

(40) Ishizu, K.; Tsubaki, K.; Mori, A.; Uchida, S. Prog. Polym. Sci. 2003, 28, 27.

(41) Moore, J. S. Curr. Opin. Colloid Interface Sci. 1999, 4,108.

(42) Tsukruk, V. V. Prog. Polym. Sci. 1997, 22, 247.

(43) Brunsveld, L.; Folmer, B. J. B.; Meijer, E. W.; Sijbesma, R. P. Chem. Rev. 2001, 101, 4071.

(44) Kidoaki, S.; Ohya, S.; Nakayama, Y.; Matsuda, T. Langmuir 2001, 17, 2402.

(45) Gillies, E. R.; Jonsson, T. B.; Fréchet, J. M. J. J. Am. Chem. Soc., 2004, 126 (38), 11936.

(46) Hu, J.; Liu, S. Y. Macromolecules 2010, 43, 8315.

(47) Eisenberg, H. Biophys. Chem. 1977, 7, 3.

(48) Mortimer, D. A. Polym, Int, 1991, 25, 2941

(49) Schanze, K. S.; Shelton, A. H. Langmuir 2009, 25, 13698

(50) Brilliantov, N. V.; Kuznetsov, D. V.; Klein, R. Phys. Rev. Lett. 1998, 81, 1433

(51) Hara, M. Polyelectrolytes, Science and Technology, Ed. Marcel Dekker, New York. 1993

(52) Uhlmann, P.; Ionov, L.; Houbenov, N.; Nitschke, M.; Grundke, K.; Motornov, M.; Minko, S.; Stamma, M. Prog. Org. Coat. 2006, 55, 168.

(53) Nath, N.; Chilkoti, A. Adv. Mater. 2002, 14, 1243.

(54) Cohen Stuart, M.; Huck, W. T. S.; Genzer, J.; Müller, M.; Ober, O.; Stamm, M.; Sukhorukov, G. B.; Szleifer, I.; Tsukruk, V. V.; Urban, M.; Winnik, F.; Zauscher, S.; Luzinov, I.; Minko, S. Nat. Mater. 2010, 9, 101.

(55) Grigoriev, D. O.; Köhler, K.; Skorb, E.; Shchukin, D. G.; Möhwald, H. Soft Matter 2009, 5, 1426

(56) Iler, R. K. J. Colloid Interface Sci. 1966, 21, 569.

(57) Decher, G.; Hong, J. D.; Schmitt, J. Thin Solid Films 1992, 210/211, 831.

(58) Decher, G. Science 1997, 277, 1232

(59) Lösche, M.; Schmitt, J.; Decher, G.; Bouwman, W. G.; Kjaer, K. Macromolecules 1998, 31, 8893

(60) Hübsch, E,; Ball, V.; Senger, B.; Decher, G.; Voegel, J.C.; Schaaf, P. Langmuir 2004, 20, 1980.

(61) Zhang, J.; Senger, B.; Vautier, D.; Picart, C.; Schaaf, P.; Voegel, J. C.; Lavalle, P. Biomaterials 2005, 26, 335

(62) Ramsden, J. J.; Lvov, Y. M.; Decher, G. Thin Solid Films 1995, 254, 246-251

(63) Picart, C.; Mutterer, J.; Richert, L.; Luo, Y.; Prestwich, G. D.;Schaaf, P.; Voegel, J. C.; Lavalle, P. Proc. Natl. Acad. Sci. U.S.A. 2002, 99, 1253

(64) El Haitami, A. E.; Martel, D.; Ball, V.; Nguyen, H. C.; Gonthier, E.; Labbé, P.; Voegel, J. C.; Schaaf, P.; Senger, B.; Boulmedais, F. Langmuir 2009, 25, 2282

(65) Elbert, D. L.; Herbert, C. B.; Hubbell, J. A. Langmuir 1999, 15, 5355.

(66) Boulmedais, F.; Ball, V.; Schwinte, P.; Frisch, B.; Schaaf, P.; Voegel, J. C. Langmuir 2003, 19, 440

(67) Guzmán, E.; Ritacco, H.; Rubio, J. E. F.; Rubio, R. G.; Ortega, F. Soft Matter, 2009, 5, 2130–2142

(68) Dubas, S. T.; Schlenoff, J. B. Macromolecules 1999, 32, 8153.

(69) Lvov, Y.; Decher, G.; Sukhorukov, G. Macromolecules 1993, 26, 5396.

(70) Kleinfeld, E. R.; Ferguson, G. S. Science 1994, 265, 370.

(71) Watanabe, S.; Regan, S. L. J. Am. Chem. Soc. 1994, 116, 8855.

(72) Feldheim, D. L.; Grabar, K. C.; Natan, M. J.; Mallouk, T. C. J. Am. Chem. Soc. 1996, 118, 7640.

(73) Lvov, Y.; Ariga, K.; Onda, M.; Ichinose, I.; Kunitake, T. Langmuir 1997, 13, 6195.

(74) Kotov, N. A.; Dekany, I.; Fendler, J. H. J. Phys. Chem. 1995, 99, 13065.

(75) Cheung, J. H.; Fou, A. F.; Rubner, M. F. Thin Solid Films 1994, 244, 985.

(76) Stroeve, P.; Vasquez, V.; Coelho, M. A. N.; Rabolt, J. F. Thin Solid Films 1996, 284, 708.

(77) Onda, M.; Lvov, Y.; Ariga, K.; Kunitake, T. Biotechnol. Bioeng 1996, 51, 163.

(78) Sun, Y.; Zhang, X.; Sun, C.; Wang, B.; Shen, J. Macromol.Chem. Phys. 1996, 197, 147.

(79) Fou, A. C.; Onitsuka, O.; Ferreira, M.; Rubner, M. F.; Hsieh, B. R. J. Appl. Phys. 1996, 79, 7501.

(80) Hammond, P. T.; Whitesides, G. M. Macromolecules 1995, 28, 7569.

(81) Laurent, D.; Schlenoff, J. B. Langmuir 1997, 13, 1552.

(82) Stepp, J.; Schlenoff, J. B. J. Electrochem. Soc. 1997, 144, L155.

(83) G. B. Sukhorukov, E. Donath, H. Lichtenfeld, E. Knippel, M. Knippel, A. Budde, H. Möhwald. Colloids Surf. A: Phys. Eng. Aspects 1998, 137, 253.

(84) C. Gao, S. Leporatti, S. Moya, E. Donath, H. Möhwald. Chem. Eur. J. 2003, 9, 915.

(85) Cosgrove, T.; Heath, T.; van Lent, B.; Leermakers, F.; Scheutjens, J. Macromolecules 1987, 20, 1692.

(86) Milner, S. T.; Witten, T. A.; Cates, M. E. Macromolecules 1988, 21, 2610.

(87) Milner, S. T.; Witten, T. A.; Cates, M. E. Macromolecules 1989, 22, 853.

(88) Misra, S.; Varanasi, S.; Varanasi, P.P. Macromolecules 1989, 22, 4173.

(89) Murat, M.; Grest, G. S. Macromolecules 1989, 22,4054.

(90) Milner, S. T. Science, 1991, 251, 905.

(91) Advincula, R.; Zhou, Q.; Park, M.; Wang, S.; Mays, J.; Sakellariou, G.; Pispas, S.; Hadjichristidis, N. Langmuir 2002, 18, 8672.

(92) Jordan, R.; Ulman, A. J. Am. Chem. Soc. 1998, 120, 243.

(93) Ingall, M. D. K.; Honeyman, C. H.; Mercure, J. V.; Bianconi, P. A.; Kunz, R. R. J. Am. Chem. Soc. 1999, 121, 3607.

(94) Jones, D. M.; Brown, A. A.; Huck W. T. S.. Langmuir 2002, 18, 1265.

(95) Steenackers, M.; Küller, A.; Ballav, N.; Zharnikov, M.; Grunze, M.; Jordan, R. Small 2007, 10, 1764.

(96) Matyjaszewski, K.; Xia, J. Chem. Rev. 2001, 101, 2921

(97) Pyun, J.; Kowalewski, T.; Matyjaszewski, K. Macromol. Rapid Commun. 2003, 24, 1043

(98) Prucker, O.; Rühe, J. Macromolecules 1998, 31,592

(99) Prucker, O.; Rühe, J. Macromolecules 1998; 31, 602

(100) Moya, S. E.; Azzaroni, O.; Kelby, T.; Donath, E.; Huck, W. T. S. J. Phys. Chem. B 2007, 111, 7034

(101) Azzaroni, O.; Moya, S. E.; Brown, A. A.; Zheng, Z.; Donath, E.; Huck, W. T. S. Adv. Funct. Mater. 2006, 16, 1037

(102) Azzaroni, O.; Brown, A. A.; Huck, W. T. S. Adv. Mater. 2007, 19, 151.

(103) Spruijt, E.; Choi, E. Y.; Huck, W. T. S. Langmuir 2008, 24, 11253

(104) Ballauff, M.; Borisov, O. Curr. Opin. Colloid Interface Sci. 2006, 11, 316

(105) Wittemann, A.; Haupt, B.; Ballauff, M. Phys Chem Chem Phys 2003, 5, 1671.

Materials and methods

Materials

Chemicals

Poly(diallyl dimethylammonium chloride) [PDADMAC 20% in water, Mw~2-3.5×10^5 kDa], poly(sodium 4-styrene sulfonate) [PSS, Mw~70 kDa] and poly(allylamine hydrochloride) [PAH, Mw~15 kDa], methacryloyloxy ethyl trimethylammonium chloride (METAC, Mw=207.5, d_{25}=1.105), sulfo propyl methacrylate potassium salt (SPM, Mw=246), N-isopropyl acrylamide (NIPAAm, Mw=113), N, N-dimethylformamide 99.85% (DMF), copper (I) chloride, copper (II) chloride, and 2,2-bipyridyl were purchased from Aldrich. $LiClO_4$, NaCl and *N*-tetradecyl (myristyl) trimethyl ammonium bromide (TTAB), ≥98%, quaternary salt, were purchased from Fluka. KH_2PO_4 was purchased from Aldrich. ω-mercaptoundecyl bromo isobutyrate initiator thiol was synthesized as described in the literature.[1] All reagents were used without further purification. Ethanol, 96% was purchased from Scharlau S.A. Water was purified using a Nanopure purification system (Thermo Scientific Barnstead). Silica particles,with a dimeter of Ø = 400 nm, were purchased from Kisker, Germany.

Methods

Layer-by-layer assembly

PEMs were assembled on QCM-D sensors (QSX335, Q-Sense AB) with a fundamental resonance frequency of about 4.95 MHz. The sensor coating was purpose designed for ellipsometric measurements and consisted of an opaque bottom layer of titanium, a thin (~1 nm) titania interlayer, and a top layer of about 80 nm silica. The sensors were pre-treated with UV/ozone (BioForce Nanosciences, Ames, IA, USA) for 30 min.

The LBL assembly was performed by alternately passing 1 mg/ml in 0.5 M NaCl polyelectrolyte solutions and washing in milli-Q water or 0.5 M NaCl solutions with a peristaltic pump (ISM935C, Ismatec, Zürich, Switzerland) through the flow cell. Two different assembly protocols were followed. In the first protocol, a 0.5 M NaCl solution was used for washing steps between the deposition of each individual polyelectrolyte and the sample was washed with pure water only at the end of the assembly. In the second protocol, the sample was rinsed with pure water after the deposition of each layer.

For the LbL coating of the silica particles, these were suspended in 1 mg/mL polyelectrolyte and 0.5 mol/L NaCl solution. After each layer deposition, the samples were centrifuged, the supernatant was removed, and the particles were dispersed in water. The centrifugation and washing with water were repeated three times before addition of the next polyelectrolyte layer.

Synthesis of Polymer brushes

Brushes were synthesized from a monolayer of thiols of ω-mercaptoundecyl bromo isobutyrate bound to gold coated quartz sensors (QSX 301, 4.95 MHz, Q-Sense AB). The sensors were pre-treated with UV/ozone for 30 min and then exposed overnight to a 10^{-2} M thiol solution in EtOH. Finally, the quartz sensor was rinsed with EtOH and water, and immediately taken to the next step. Both the thiol solutions and the washing EtOH and milli-Q water were passed through the flow cell with a peristaltic pump. For brush polymerization the gold surface coated with the thiol initiator was incubated for 5 h in a N,N-dimethylformamide (DMF)/water (3:2) solution of monomer/2,2-bipyridine/CuCl (molar ratio 10:2:1). Then, the gold surfaces were consecutively rinsed in DMF/water (3:2) and water.[2]

In case of SPM monomer, the polymerization solution was prepared either as described above or including $CuCl_2$ in a ratio Cu(I)/Cu(II) 4:1 into the reaction mixture. In absence of Cu(II) the polymer chains grow freely. The presence of $CuCl_2$ helps to control the final chain length polydispersity. Polymerization was also kept for 5 hours in this case. The PSPM synthesized in these conditions will be named (4:1) PSPM throughout this thesis.

Preparation of PE Complexes and PE-surfactant Complexes

Complexes of PAH/PSS and PDADMAC/PSS were prepared at different molar ratios in 0.5 M NaCl, centrifuged three times, followed by removal of the supernatant. Varying amounts of TTAB were added to the PE complexes. Afterward, these PSC were centrifuged and washed

three times. The initial TTAB concentration was 100 mM, which is considerably above the critical micelle concentration (CMC). The TTAB micelles at this concentration in aqueous solutions have a shape of prolate ellipsoids with half axes of 18 and 35 Å, respectively.[3]

Surface Patterning

Commercially available flat gold Arrandee© surfaces were patterned with a thiol monolayer using the micro-contact printing technique. The surfaces were cleaned by UV–Ozone treatment for 30 min, prior to stamping. A poly-(dimethyl siloxane) (PDMS) stamp, consisting of 5 μm side squares separated by 3 μm between them, was first cleaned by ultrasonication in ethanol for 5 min and was then incubated for one minute in a 10^{-2} M ω-mercaptoundecyl bromoisobutyrate ethanol solution, dried under a nitrogen gas stream and brought in contact with the gold surface. After a contact of 45 s, the gold surface was rinsed and ultrasonicated in ethanol for 3 min. Then, the sample was immersed in 10^{-2} M solution of 1-undecanethiol in EtOH to fill non patterned regions. Finally, the samples were rinsed and sonicated in ethanol, dried under nitrogen gas, and taken immediately to the surface polymerization step.

Salt Treatment of the Supramolecular Assemblies

Exposure to changes in the ionic strength and to counterions of different nature was performed by passing, through the flow cell, salt solutions of increasing concentrations with the peristaltic

pump, until a plateau in the QCM-D signal was observed. Then, milli-Q water is passed to make the brush rehydrate until the initial state is recovered.

Temperature control

For PNIPAAm brushes the temperature was varied between 23º C and 40º C through application of a temperature increase/decrease cycle, controlled by the QSoft 401software (QSense). The temperature shift took place gradually and allowed the brush for exposure to the cycle-limiting temperatures for periods over 10 min, to ensure the total collapse/swelling of the PNIPAAm.

Techniques

Techniques such as X-ray reflectivity, UV/ Vis and IR spectroscopy, ellipsometry, neutron scattering, and quartz crystal microbalance have been widely employed so far to follow the growth of polyelectrolyte-based films as well as their structures and properties.[4-5]

In the development of this project, and in order to achieve the objectives established, some of the techniques already mentioned, as well as some other different although complementary ones have been applied. A brief theoretical description of the most relevant features of the techniques employed becomes necessary for a better understanding of the results discussed in this project.

- ### Quartz Crystal Microbalance with Dissipation

The quartz crystal microbalance (QCM) is a simple, cost effective, high-resolution mass sensing technique. The signal transduction mechanism of the QCM technique relies on the piezoelectric effect in quartz crystals. Due to the piezoelectric effect, a mechanical oscillation of characteristic frequency, f_0, is produced in the quartz crystal by applying an alternating electric field across the crystal through upper and lower metal electrodes covering the quartz surface. The frequency of such oscillation is determined by the thickness of the crystal (d) and the speed of shear waves in quartz (v_Q).[6] When a mass is loaded on top of the quartz crystal the mobility of the sensor becomes more limited and the oscillation frequency decays. A schematic view of the different

frequency responses obtained from a single quartz sensor when sandwiched between a pair of electrodes is shown in Figure 4.

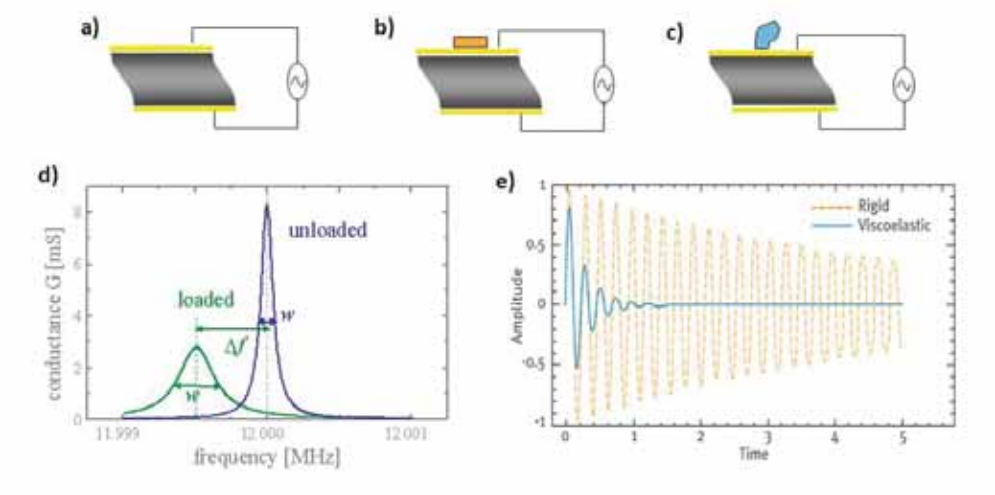

Figure 4 Scheme of an electric circuit applied onto (a) a bare quartz sensor, (b) a quartz sensor with a rigid mass deposited on top and (c) a sensor with a viscoelastic mass. The frequency decrease observed (d) when passing from (a) to any of the other systems will depend on the viscoelastic character of the mass being adsorbed (e, from www.qsense.com).

The derived relationship between the frequency decrease of the oscillating quartz crystal and the bound mass was reported in 1959 by Günter Sauerbrey.[7] Since then, QCM technique has been extensively used in order to detect thin film deposition on the surface of the crystal with a resolution down to ng/cm^2 because it can be operated in vacuum, in gaseous environment or in liquid and its applicability has been shown for a wide range of systems. The ability of QCM to sensitively measure mass changes associated with liquid-solid interfacial phenomena, as well as to characterize energy dissipative or viscoelastic behavior of the mass deposited upon the metal electrode surface of the quartz crystal have turn this technique into a very useful tool in surface science.

Quantitative evaluation of QCM-D data

The Sauerbrey equation[7] links frequency shifts and adsorbed mass per unit area in a very simple way:

$$m_{\mathrm{QCM}} = -C\frac{\Delta f_i}{i} \qquad (1)$$

with the mass sensitivity constant, $C = 18.06 \pm 0.15$ ng·cm^{-2}·Hz^{-1} for sensors with a resonance frequency of 4.95 ± 0.02 MHz, and the overtone number i. The normalized frequency shifts, $\Delta f = \Delta f_i/i$, for the 3rd overtone were employed to determine m_{QCM}. This acoustic mass comprises the mass of the adsorbed polymer and the mass of the solvent that is trapped inside or hydrodynamically coupled to the polymer film. The applicability of Equation (1) is limited to rigid films. For soft and dissipative films, more complex models would be required that account for the viscoelastic properties of the film [8, 9]. For the supramolecular assemblies investigated here, the ratio of dissipation and normalized frequency shifts, $\Delta D/-\Delta f$, was found to be smaller than 0.2×10^{-6}/Hz. Such ratio is the parameter which determines the degree of viscoelasticity of the film. In this case, it indicates that Eq. 1 is a good approximation. The application of the viscoelastic models to selected datasets corroborated that the Sauerbrey equation is indeed a good approximation for the films presented here, with an error below 5%. The experimental noise was typically below 2 ng/cm^2.

The film thickness was further determined by

$$d_{QCM} = {}^{m_{QCM}}\!\!\diagup\!\!_{\rho_{film}}, \qquad (2)$$

with $\rho_{film} = 1.0$ g/cm^3 being the density of the solvated polymer film. In their pure form, the employed polymers exhibit densities between 1.0 and 1.1 g/cm^3, while the density of water or salt solutions is 1.0 g/cm^3. Equation (2) hence overestimates the thickness by at most 10%.

- **Spectroscopic Ellipsometry**

Ellipsometry is one among many optical techniques which are available today for the study of optical properties of thin films. It relies on the fact that the state of polarization of a light wave is altered upon reflection at an interface.[10-12]

In a standard ellipsometry experiment, elliptically polarized light can be produced through reflection of linearly polarized from a flat surface. Reflection associates to a change of phase of the components of E parallel (E_p) and perpendicular (E_s) to the plane of incidence of light. The two components of E, which were in phase (for linearly polarized light), emerge out of phase from the surface (for elliptically polarized light). Figure 5 illustrates how a beam of linearly polarized light incident on a bare surface and a film-covered surface is reflected.

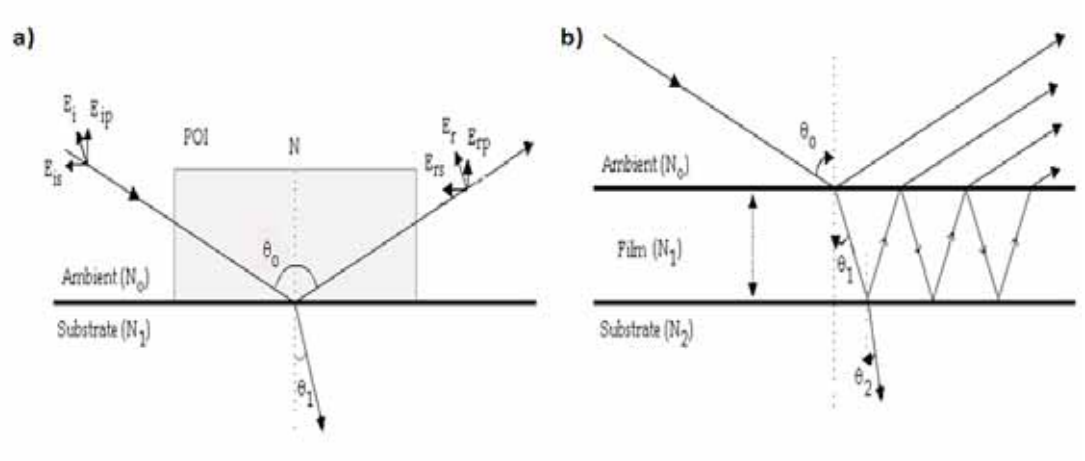

Figure 5. Reflection of polarized light on: (a) bare surface (b) film-covered surface.

The plane of incidence (POI) includes the incident beam and the sample surface normal N, which is in the plane of the paper. The components parallel (E_p) and perpendicular (E_s) to the POI are out of phase after reflection, and both phase and amplitude of the reflected light changes in a distinct way depending on the optical properties of the surface[13]. Thus, an ellipsometric measurement allows one to quantify the phase difference between E_p and E_s, Δ, and the change in the ratio of their amplitudes given by tan Ψ. For a bare reflecting surface, the forms for Δ and Ψ are:

$$\Delta = \delta_{rp} - \delta_{rs} \text{ and } \tan\psi = \frac{|r_p|}{|r_s|} \quad (3)$$

where r_p and r_s are the Fresnel coefficients for the components p and s of light.

Therefore, the resulting change in polarization after reflection from a surface can be measured through a complex reflection coefficient:

$$\rho = (\tan\psi)e^{(i\Delta)} = \frac{r_p}{r_s} \quad (4)$$

which for a model substrate/film/ambient is obtained as a function of N_0, N_1, N_2, λ, L_1, θ_0 where N_0, N_1 and N_2 are the indexes of refraction for the ambient, film and substrate, respectively (Fig. 5). Usually, N_0, λ and θ_0 are known, N_2 can be independently obtained, and N_1 and L_1 (film thickness) can be obtained.

Thus, ellipsometry can be used to study growth or adsorption of very thin films (< 1 nm) on solid surfaces.[14] Although most of the work has so far concerned measurements at the air/solid interface, it is also possible to do measurements in water solution to study, for example, adsorption of surfactants, proteins, and polymers at the liquid/solid interface.[15-19]

Quantitative evaluation of ellipsometric data

Bound masses were determined by numerical fitting of the ellipsometric data to a multilayer model. Data were fitted over the accessible wavelength spectrum, using the software CompleteEASE (Woollam). The model relates the measured ellipsometric responses, Δ and Ψ as a function of λ, to the optical properties of the sensor surface, the adsorbed film and the surrounding solution. The glass windows in the fluid cell were verified not to perturb the polarization of the probing light beam, and the optical properties of the sensor coating were calibrated prior to each measurement.

To extract the properties of the built polymer film from the ellipsometric response, either a five-layer or a three-layer model were used for the assembly of polyelectrolyte multilayers or brushes, respectively. The five layers represented the bulk solution, the polymer film and the three coating layers (silica, titania and titanium) on the sensor that interact with the light beam. Such number of layers decreases to three in case of modeling the growth of the brushes because the gold sensor represents a single layer. The polyelectrolyte film was treated as a single layer, which was assumed to be transparent and homogeneous (Cauchy medium), with a given thickness, d_{opt}, a wavelength-dependent refractive index, $n_{film}(\lambda) = A_{film} + B_{film} / (\lambda/\mu m)^2$, and a negligible extinction coefficient ($k_{film} = 0$). d_{opt}, A_{film} and B_{film} were fitted simultaneously. The semi-infinite bulk solution was also treated as a transparent Cauchy medium, with a refractive index of $n_{sol}(\lambda) = A_{sol} + B_{sol} / (\lambda/\mu m)^2$. For water, $A_{sol} = 1.323$ and $B_{sol} = 0.00322$ were estimated from the literature [20]. For 0.5 M NaCl solutions, $A_{sol} = 1.328$ and $B_{sol} = 0.00322$ were employed [21]. The optical properties and thicknesses of the sensor's coating layers were fixed to the values established during calibration.

The adsorbed mass per unit area was determined from de Fejter's equation [22]:

$$m_{opt} = \frac{d_{opt} \times (n_{film} - n_{sol})}{\left(dn/dc\right)} \qquad (5)$$

To calculate m_{opt}, the refractive indices employed are those at $\lambda = 632.5$ nm, and the refractive index increment used is of $dn/dc = 0.150$ cm^3/g.[23] The errors associated with d_{opt} and n_{film}-$n_{solvent}$ can be rather high for films that exhibit only a few nanometers in thickness. It was also observed that the absolute values for d_{opt} and n_{film}-$n_{solvent}$ are quite sensitive to minor variations in the

optical properties of the solid support. When discussing results in terms of thickness, d_{QCM} was therefore considered rather than d_{opt}. The errors in d_{opt} and $_{Pfilm}$-$n_{solvent}$ are though covariant, i.e., the product $d_{opt}\times(n_{film}-n_{solvent})$ and m_{opt} can be determined with good accuracy[24]. The experimental noise was typically below 1 ng/cm^2.

- **In situ combination of QCM-D and ellipsometry**

Both the formation of polyelectrolyte multilayers and the synthesis of the polyelectrolyte brushes were monitored simultaneously, by QCM-D and ellipsometry, in liquid environment. Measurements were performed using a purpose designed flow cell (Q-Sense AB, Västra Frölunda, Sweden) with a total volume of ~300 µL. The flow cell was attached to a Q-Sense E1 setup, providing access to QCM-D data, and mounted on a spectroscopic rotating compensator ellipsometer (M2000V, Woollam, NE, USA), providing access to ellipsometric data. QCM-D data, Δf and ΔD, were acquired at 6 overtones ($i = 3,\ 5\ \ldots\ 13$, corresponding to resonance frequencies of $f_i \approx 15,\ 25\ \ldots\ 65$ MHz) simultaneously, with sub-second time resolution. Ellipsometric data, Δ and Ψ, were acquired over a wavelength range from $\lambda = 380$ to 1000 nm, simultaneously, at 65º angle of incidence, and with a time resolution of ~5 s. The working temperature was 23°C.

Quantification of the aqueous solvent content.

The masses determined by QCM-D and ellipsometry, respectively, can be employed to calculate the solvent content of the film. To this end, the hydration is defined as the percentage of solvent contributing to the total film mass:

$$\text{Hydration}(\%) = \frac{m_{\text{QCM}} - m_{\text{opt}}}{m_{\text{QCM}}} \times 100 = \frac{m_{\text{sol}}}{m_{\text{QCM}}} \times 100 \qquad (6)$$

- **Zeta Potential**

Electrophoresis is defined as the motion of dispersed particles relative to a fluid under the influence of a spatially uniform electric field.[25-27] Such motion is ultimately caused by the presence of a charged interface between the particle surface and the surrounding fluid. The dispersed particles have an electric surface charge, on which an external electric field exerts an electrostatic Coulomb force. According to the double layer theory, all the charged surfaces in fluids are screened by a diffuse layer of ions, which has the same absolute charge but opposite sign with respect to that of the surface charge. The electric field also exerts a force on the ions in the diffuse layer which has an opposite direction to that acting on the surface charge. This latter force is not actually applied to the particle, but to the ions in the diffuse layer located at some distance from the particle surface, and part of it is transferred all the way to the particle surface through viscous stress. The moving particles, taking into account the hydrodynamic friction due to the viscosity of the dispersant, have a characteristic velocity which is dependent on the

strength of the electric field (measured by the instrument), the dielectric constant and the viscosity of the medium (known from literature) and the zeta potential. These parameters are correlated by the theory developed by Smoluchowski[28] which defines the electrophoretic mobility (μ_e) as:

$$\mu_e = \left(\frac{\varepsilon_r \varepsilon_0 \zeta}{\eta} \right), \quad (7)$$

where ε_r is the dielectric constant of the dispersion medium, ε_0 is the permittivity of free space ($C^2\ N^{-1}\ m^{-2}$), η is the dynamic viscosity of the dispersion medium (Pa s), and ζ is zeta potential (i.e., the electrokinetic potential of the slipping plane in the double layer). This model works for dispersed particles of any shape at any concentration and since its application is limited to the case when particle radius is much greater than the Debye length, the length in which mobile charge carriers screen out the external electric field, validity in our case is totally ensured.

The ζ-potential of LbL coated silica nanoparticles was measured with a NanoSizer (MALVERN Nano-ZS, U.K.) instrument. LbL assembly on the colloids was first traced by measuring the changes in ζ-potential after each layer deposition. All the ζ-potential measurements were performed at 25 °C and with a cell drive voltage of 30 V, using a monomodal analysis model.

- **Raman Spectroscopy**

Measurement of Raman spectra, discovered by Raman and Kirishnanin in 1928, has been developed as a novel qualitative and quantitative optical technique by the scattering of radiation.[29] The technique has long been routinely used to study vibrational, rotational, and other low-frequency modes for obtaining the specific information, such as the molecular composition of matter or the spectral fingerprinting in small amounts of the biological samples, even in the liquid state.[30-31] Raman scattering is an inelastic scattering which is usually generated by a laser with monochromatic light in the visible, near infrared, or near ultraviolet region. A scheme of the process is depicted in Fig. 6,

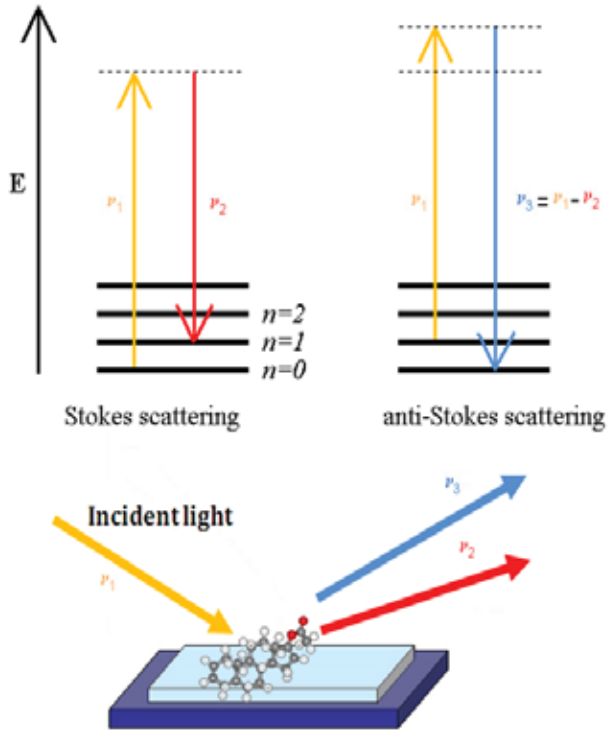

Figure 6 Schematic diagram of the Raman scattering process.

The energy of laser photons may be changed after the excitation laser interacts with the vibrating molecules or the excited electrons in the sample. As the spontaneous effect, photons transfer the excitation energy to change the molecule from the ground state to a virtual state. The excited molecule then returns to a different rotational or vibrational state after emitting a photon. The change in energy between the original state and the new state causes an up-shift or down-shift frequency of the emitted photon different from the excitation wavelength. The Stoke Raman scattering (Stoke shift), which is the one refereed to along this chapter, is that defined when the excited molecule gets higher energy than the ground state, and the emitted photon gets a down-shifted frequency. In contrast, anti-Stoke Raman scattering (anti-Stoke shift) happens when the emitted photon gets an up-shifted frequency. The change or shift in energy indicates molecular information and its photon mode in the target. This vibrational-reach information that supports Raman spectroscopy has become a commonly used tool in chemistry because of its specificity to the chemical bonds or symmetry of molecules.

In this work Micro-Raman analyses were performed using a Renishaw inVia Raman microscope. The laser excitation wavelength was 532 nm with a grating of 1800 mm^{-1}. The microscope was equipped with interchangeable objective lenses with magnifications of 10×, 50×, and 100×. Most measurements were conducted using the 50× objective. The size of the focal spot was approximately 1 μm. Raman spectra were recorded in the region 300-3600 cm^{-1} with a spectral resolution of around 7 cm^{-1}. These measurements cover both the fingerprint and the C-H stretch vibration region. Two to eight accumulation scans at different sample points were used to reduce the spectral noise and to account for possible sample heterogeneities. The system was calibrated to the spectral line of crystalline silicon at 520.7 cm^{-1}. All spectra were baseline corrected. The

PE complexes and PSC, observed by reflectance microscopy, were dispersed on silica slides to minimize the fluorescence background. Raman spectra were measured directly under the microscope in solution and dry state at room temperature. The confocal modus was applied in the case of strong fluorescence.

- **Infra-Red Spectroscopy**

Infra-Red (IR) spectroscopy is an important and popular tool for structural elucidation and compound identification. At temperatures above absolute zero, all the atoms in molecules are in continuous vibration with respect to each other. When the frequency of a specific vibration is equal to the frequency of the IR radiation directed on the molecule, the molecule absorbs the radiation. Infrared spectroscopy is thus based in the detection of the molecular vibrations produced by absorption of different IR frequencies by a sample positioned in the path of an IR beam. The main goal of IR spectroscopic analysis is to determine the chemical functional groups in the sample. Functional groups can be associated with characteristic infrared absorption bands, which correspond to the fundamental vibrations of the functional groups.[32-34] An example of the spectrum monitored is shown in Figure 7.

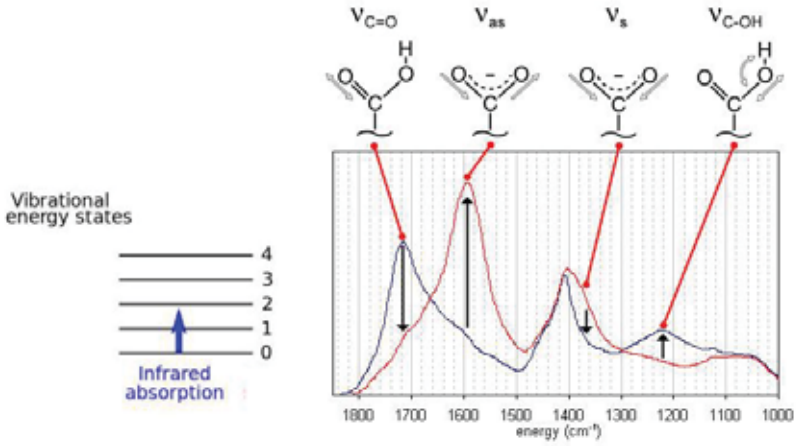

Figure 7 Characteristic Infra-Red (IR) spectra of a carboxylic acid in its acidic form (Blue) and in the deprotonated (carboxylate) state (red).

A molecule can be classed as infrared active (i.e., it absorbs the incident infrared light) whenever there is a change in the dipole moment of the molecule during the course of the vibration. Thus, symmetric vibrations are usually not detected in infrared. In particular, when a molecule has a center of symmetry, all vibrations which are symmetrical with respect to the center are infrared inactive. But, at the same time, the strong IR absorption of water molecules when working in aqueous environments, which overlaps the emitted photons of the target, becomes an important disadvantage that needs to be solved.

In this work, polyelectrolytes were deposited onto the surface of a ZnSe ATR crystal mounted into a commercial horizontal ATR holder. In order to subtract the effect of the water, the degree of hydration of the PE film was adjusted by means a moisture generator (HumiVar, Leipzig, Germany) to relative humidity (RH) values between 3% and 99% with an accuracy of ±0.5%. IR spectra were recorded by means of the Excalibur FTS3100 Fourier transform IR spectrometer (Varian, Darmstadt, Germany) with a resolution of 4 cm^{-1} from 100 scans at room temperature.

- **Atomic Force Microscopy**

A JPK Nanowizard atomic force microscope (JPK Instruments AG, Germany) was used for imaging the PEMs. Measurements were performed under liquid in contact mode using DNP-S cantilevers with a spring constant of approximately 0.12 N/m. Cantilevers were calibrated by measuring the thermal motion of the free cantilever. After being thoroughly rinsed in water, the samples were placed on pre-cleaned microscope slides for scanning.

- **Conductimetry**

The Critical Micellar Concentration (CMC) of TTAB, 4.2 mM, was measured by conductimetry employing a CON 1500 Conductimetry Meter (Eutech Instruments, Thermo Fisher Scientific).

References

(1) Shah, R. R.; Merreceyes, D.; Husemann, M.; Rees, I.; Abbott, N. L.; Hawker, C. J.; Hedrick, J. L. Macromolecules 2000, 33, 597.

(2) Masci, G.; Bontempo, D.; Tiso, N.; Diociaiuti, M.; Mannina, L.; Capitani, D.; Crescenzi, V. Macromolecules 2004, 37, 4464.

(3) Gorski, N.; Kalus, J. Langmuir 2001, 17, 4211.

(4) Caruso, F.; Niikura, K.; Furlong, D. N.; Okahata, Y. Langmuir 1997,13, 3422

(5) Kellogg, G. J.; Mayes, A. M.; Stockton, W. B.; Ferreira, M.; Rubner, M. F.; Satija, K. Langmuir 1996, 12, 5109

(6) Janshoff, A.; Galla, H. J.; Steinem, C. Angew. Chem. Int. Ed. 2000, 39, 4004.

(7) Sauerbrey, G. Z. Phys. 1959, 155, 206.

(8) Domack, A.; Prucker, O.; Rühe, J.; Johannsmann, D. Phys. Rev. 1997, 56, 680.

(9) Voinova, M. V.; Rodahl, M.; Jonson, M.; Kasemo, B. Phys. Scr.1999, 59, 391.

(10) Gonçalves, D.; Irene, E. A. Quim. Nova 2002, 25 (5), 794.

(11) Fowles, G.R. “Introduction to Modern Optics, 2nd ed.” 1975, Dover, New York.

(12) Pedrotti, F.L.; Pedrotti, L.S.; “Introduction to Optics, 2nd ed.” 1993, Prentice Hall, New Jersey.

(13) Irene, E. A.; Woolam, J. A. Mater. Res. Soc. Bulletin 1995, 20, 24.

(14) Landgren, M.; Jönsson, B. J. Phys. Chem. 1993, 97, 1656.

(15) Arnebrant, T.; Bäckström, K.; Jönsson, B.; Nylander, T. J. Colloid Interface Sci. 1989, 128, 303.

(16) Wägnerud, P.; Olofsson, G. J. Colloid Interface Sci. 1992, 153, 392.

(17) Wahlgren, M.; Arnebrant. T. J. Colloid Interface Sci. 1989, 136, 259.

(18) Malmsten, M.; Lindman, B. Langmuir 1990, 6, 357.

(19) Tiberg, F.; Malmsten, M.; Linse, P.; Lindman, B. Langmuir 1991, 7, 2723.

(20) Daimon, M.; Masumura, A. Appl. Opt. 2007, 46, 3811.

(21) Lide, D. R. “Handbook of Chemistry and Physics, 85th ed.” 2004, CRC Press, Boca Raton.

(22) De Feijter, J. A.; Benjamins, J.; Veer, F. A. Biopolymers 1978, 17, 1759.

(23) Halthur, T. J.; Elofsson, U. M. Langmuir 2004, 20, 1739.

(24) Caruso, F.; Niikura, K.; Furlong, D. N.; Okahata, Y. Langmuir 1997, 13, 3422.

(25) Lyklema, J. “Fundamentals of Interface and Colloid Science, Vol. II: Solid–Liquid Interfaces" 1995, Academic Press, London, 1995.

(26) Hunter, R.J. "Foundations of Colloid Science" 1989, Oxford University Press.

(27) Russel, W.B.; Saville, D.A.; Schowalter, W.R. “Colloidal Dispersions” 1989, Cambridge University Press.

(28) v. Smoluchowski, M. Bull. Int. Acad. Sci. Cracovie 1903, 182, 184.

(29) Raman, C. V.; Kirishnan, K. S. Nature 1928, 121, 501.

(30) Gardiner, D. J.; Graves, P. R.; "Practical Raman Spectroscopy" 1989, Springer-Verlag, Berlin/Heidelberg.

(31) Sideroudi, T. I.; Pharmakakis, N. M.; Papatheodorou, G. N.; Voyiatzis, G. A. Lasers Surg. Med. 2006, 38, 695.

(32) Colthup, N.B.; Daly, L.H.; Wiberly, S.E. "Introduction to infrared and Raman spectroscopy" 1975, Academic Press, New York.

(33) Griffith, P.R.; de Haseth, J.A. "Fourier transform infrared spectroscopy" 1986, Wiley, New York.

(34) Settle, F. A. "Handbook of Instrumental Techniques for Analytical Chemistry" 1997, Prentice Hall, New Jersey.

Section I:

Polyelectrolyte Multilayers

Introduction

Since their introduction in the 90s, polyelectrolyte multilayers (PEMs) based on the alternate assembly of oppositely charged polyelectrolytes by means of the so-called layer-by-layer (LbL) technique have gained the attention of the scientific community as an inexpensive, simple and robust route for surface modification and as a tool for device fabrication.[1-12] The stepwise protocol of assembly results in a structure with controllable composition at the nanoscale in the growing direction [13-16], which can include multiple functionalities like proteins, nanoparticles, growth factors, lipids, etc. [17-20], either on top or between the layers. Among many other applications PEMs can be used to increase surface biocompatibility or to endow surfaces or devices with optical, antibacterial or sensing properties [21-26]. Also, PEMs are used for the fabrication of smart surfaces since they can be designed to show a specific response to external stimuli such as pH, ionic strength, temperature, light, magnetic field or specific biological moieties [27].

The alternate assembly of polycations and polyanions on charged surfaces for the fabrication of PEMs is a process mainly driven by electrostatic interactions although some systems have been reported to be additionally stabilized by hydrogen-bonding[28]. During PEM assembly the charges provided by a depositing layer will over-compensate those of the already assembled layers, leaving a remainder of charge in the surface which is the prerequisite for the formation of the next layer. The structural arrangements stemming from the charge compensation inside the multilayer can be described, in a good approximation, by a three-zone model as reported by some authors [29, 30]. According to this model, films can be subdivided into three regions:

I) The region close to the substrate, which is typically composed of only a few layers that are different from those in the next region owing to the influence of the substrate.

II) The "bulk" multilayer film. All anionic layers possess equal thickness, and all cationic layers possess equal thickness. In most cases polyanion/polycation stoichiometry is observed to be 1:1 or at least close to that value in this region of the multilayer.

III) The region close to the surface of the film. This region is typically composed of only a few layers where the charge compensation is achieved mainly by the counterions (extrinsic compensation).

While for a small number of layers forming the PEM, from a couple to approximately 10 layers, only the zones I and III are formed,[31] for systems where the number of layers is increased, the growth in multilayer takes place in the zone II and the gap between zones I and III becomes bigger as more layers are deposited. But generally, since the resulting film contains highly interpenetrated polyelectrolyte chains without a strictly stratified structure, interfaces between the zones are rather diffuse.[29]

In their grow PEMs have been described to follow either a linear or an exponential growing regime depending on the pair of polyelectrolytes chosen for their buildup [32-33]. In the linear regime, for instance, the deposition of a polyelectrolyte with a finite interpenetration range generates a constant mass and thickness increment to the developing film. In most cases, the layer-by-layer buildup is self-limited to constant increments and can be sustained in the same

growing regime for hundreds or even thousands of layers. The explanation for a non-linear buildup regime in the polyelectrolyte multilayer, where the mass that binds per deposition cycle increases as a function of the total film mass, becomes more controversial. Some studies support that the nonlinear buildup could be attributed to the continuous increase of surface roughness, which leads to an increase in the physical surface area available for adsorption. Such growing regime has been proposed to take place when polymers of low charge are used[34-35] or when the charges of a highly charged polymer are compensated with a high salt concentration.[36] Nevertheless, this model does not take into account the possible extension of the active surface toward the interior of the film so that in addition to the increased surface area there might also be an increased penetration depth of the adsorbed polymer. Hence, other models are concerned with the active volume of the polyelectrolyte multilayer. The active volume concept can be realized as that part of a film that is capable of adsorbing the depositing polymer, which corresponds to zone III of the polyelectrolyte zone model. The height of the active volume would be characterized in terms of charge penetration length, as defined by Schlenoff and Dubas.[14] In this theory, the whole film acts as an active volume in which at least one of the polyelectrolytes can freely diffuse, which would reflect more accurately the real situation taking place in the multilayer.

However, besides the pair of polyelectrolytes employed to form the multilayer, some other important factors can affect the buildup regime of the PEM: the ionic strength of the polyelectrolyte solution [37-38], the polyelectrolyte charge density,[39] pH (particularly in weak polyelectrolytes),[40] deposition time,[13] temperature,[30] solvent quality,[41] and/or the polyelectrolyte chain length,[42] have a strong influence in the final structure assembled and, thereby, will determine the properties the system may have.

Here the analysis was, in particular, focused on PAH/PSS and PDADMAC/PSS polyelectrolyte pairs, two standard polyelectrolyte systems which are among the most studied in PEMs. PAH is a weak polyelectrolyte with primary amines as pending groups while PDADMAC is a strong polyelectrolyte whose charge originates from quaternary amines. Their respective multilayer films, in combination with polyanionic PSS, display very different properties[43-44] with regard to stability, pH response, elasticity and conductivity. While for multilayers composed of PAH and PSS the growth scales linearly with the number of assembled layers,[32] for PDADMAC combined with PSS, the growth of the multilayer has been found to follow an exponential trend when assembly takes place in the presence of certain concentrations of NaCl in aqueous medium. Such exponential behavior has been demonstrated in literature to occur as a result of the diffusion of at least one of the polyelectrolytes in and out of the previously assembled layers. [45-48]

Despite ample research on these systems, there are basic questions related to their assembly and to some of their physico-chemical properties that still remain unknown and that will be addressed through the current section.

References

(1) Decher, G.; Hong, J. D.; Schmitt, J. Thin Solid Films 1992, 210–211, 831.

(2) Decher, G. Science 1997, 277, 1232.

(3) Jewell, C.M.; Lynn, D.M. Adv. Drug Delivery Rev. 2008, 60 (9), 979.

(4) Sukhorukov, G. B.; Donath, E.; Lichtenfeld, H.; Knippel, E.; Knippel, M.; Budde, A.; Möhwald, H. Colloids Surf. A 1998, 137, 253.

(5) Donath, E.; Sukhorukov, G. B.; Caruso, F.; Davis, S. A.; Möhwald, H. Angew. Chem. Int. Ed. 1998, 37, 2201.

(6) Yaroslavov, A. A.; Rakhnyanskaya, A. A.; Yaroslavova, E. G.; Efimova, A. A.; Menger, F. M. Adv. Colloids Interface Sci. 2008, 142, 43.

(7) Grigoriev, D. O.; Köhler, K.; Skorb, E.; Shchukin, D. G.; Möhwald, H. Soft Matter 2009, 5, 1426.

(8) Jin, W.; Toutianoush, A.; Tieke, B. Langmuir 2003, 19, 2550.

(9) Rmaile, H. H.; Schlenoff, J. B. J. Am. Chem. Soc. 2003, 125, 6602.

(10) Llarena, I.; Iturri Ramos, J. J.; Donath, E.; Moya, S. E. Macromol. Rapid Commun. 2010, 31, 526.

(11) Dubas, S. T.; Kittitheeranun, P.; Rangkupan, R.; Sanchavanakin, M.; Potiyaraj, P. J. Appl. Polym. Sci. 2009,114, 1574.

(12) Cai, G.; Lee, W.; Min, S. K.; Koo, G.; Cho, B. W.; Lee, S. H.; Han, S. H. J. Nanosci. Nanotechnol. 2009, 9, 7209.

(13) Dubas, S. T.; Schlenoff, J. B. Macromolecules 1999, 32, 8153.

(14) Schlenoff, J. B.; Dubas, S. T. Macromolecules 2001, 34, 592.

(15) Arys, X.; Laschewsky, A.; Jonas, A. M. Macromolecules 2001, 34, 3318.

(16) Schoeler, B.; Kumaraswamy, G.; Caruso, F. Macromolecules 2002, 35, 889.

(17) Moya, S.; Donath, E.; Sukhorukov, G. B.; Auch, M.; Baumler, H.; Lichtenfeld, H.; Mohwald, H. Macromolecules 2000, 33, 4538.

(18) Fischlechner, M.; Zaulig, M.; Meyer, S.; Estrela-Lopis, I.;Cuellar, L.; Irigoyen, J.; Pescador, P.; Brumen, M.; Messner, P.;Moya S.; Donath, E. Soft Matter 2008, 4, 2245.

(19) Delcea, M.; Krastev, R.; Gutberlet, T.; Pum, D.; Sleytr, U. B.; Toca-Herrera, J. L. Soft Matter 2008, 4, 1414.

(20) Benkirane-Jessel, N.; Schwinte, P.; Falvey, P.; Darcy, R.; Haikel, Y.; Schaaf, P.; Voegel, J. C.; Ogier, J. Adv Funct Mater2004, 14, 174.

(21) Zhou, J.; Romero, G.; Rojas, E.; Ma, L.; Moya, S. E.; Gao, C. Biomacromolecules 2010, 345, 241.

(22) Kujawa, P.; Schmauch, G.; Viitala, T.; Badia, A.; Winnik, F. M. Biomacromolecules 2007, 8, 3169.

(23) Lichter, J. A.; Van Vlietpa, K. J.; Rubner, M. F. Macromolecules 2009, 42, 8573.

(24) Lichter, J. A.; Rubner, M. F. Langmuir 2009, 25, 7686.

(25) Fiorentino, D.; Gallone, A.; Fiocco, D.; Palazzo, G.; Mallardi, A. Biosens Bioelectron 2010, 25, 2033.

(26) Jiang, G.; Baba, A.; Ikarashi, H.; Xu, R.; Risheng, X.; Locklin, J.; Kashif, K. R.; Shinbo, K.; Kato, K.; Kaneko, F.; Advincula, R. J Phys Chem C 2007, 111, 18687.

(27) Sukhishvili, S. A. Curr Opin Colloid Interface Sci. 2005, 10, 37.

(28) Zhuk, A.; Pavlukhina, S.; Sukhishvili, S. A. Langmuir 2009, 25, 14025.

(29) Ladam, G.; Schaad, P.; Voegel, J. C.; Schaaf, P.; Decher, G.; Cuisiner, F. Langmuir 2000, 16, 1249.

(30) Salomäki, M.; Kankare, J. Langmuir 2005, 21, 11232.

(31) Lukkari, J.; Salomäki, M.; Ääritalo, T.; Loikas, K.; Laiho, T.; Kankare, J. Langmuir 2002, 18, 8496.

(32) Caruso, F.; Niikura, K.; Furlong, D. N.; Okahata, Y. Langmuir 1997, 13, 3422.

(33) Porcel, C.; Lavalle, P.; Ball, V.; Decher, G.; Senger, B.; Voegel, J-C.; Schaaf, P. Langmuir 2006, 22, 4376.

(34) Schoeler, B.; Poptoshev, E.; Caruso, F. Macromolecules 2003, 36, 5258.

(35) DeLongchamp, D. M.; Kastantin, M.; Hammond, P. T. Chem.Mater. 2003, 15, 1575.

(36) McAloney, R. A.; Sinyor, M.; Dudnik, V.; Goh, M. C. Langmuir 2001, 17, 6655.

(37) Lösche, M.; Scmitt, J.; Decher, G.; Bouwman. W. G.; Kjaer, K. Macromolecules 1998, 31, 8893.

(38) Decher, G.; Schmitt, J. Prog. Colloid Polym. Sci. 1992, 89, 160.

(39) Glinel, K.; Moussa, A.; Jonas, A. M.; Laschewsky, A. Langmuir 2002, 18, 1408.

(40) Shiratori, S. S.; Rubner, M. F. Macromolecules 2000, 33, 4213.

(41) Potoshev, E.; Schoeler, B.; Caruso, F. Langmuir 2004, 20, 829.

(42) Sui, Z.; Salloum, D.; Schlenoff, J. B. Langmuir 2003, 19, 2491.

(43) Mauser, T.; Dejugnat, C.; Sukhorukov, G. B. Macromol. Rapid Commun. 2004, 25, 1781.

(44) Köhler, K.; Shchukin, D. G.; Möhwald, H.; Sukhorukov, G. B. J. Phys. Chem. B 2005, 209, 18250.

(45) Lavalle, P.; Gergely, C.; Cuisinier, F. J. G.; Decher, G.; Schaaf, P.; Voegel, J. C.; Picart, C. Macromolecules 2002, 35, 4458.

(46) Hübsch, E.; Ball, V.; Senger, B.; Decher, G.; Voegel, J. C.; Schaaf, P. Langmuir 2004, 20, 1980.

(47) Picart, C.; Mutterer, J.; Richert, L.; Luo, Y.; Prestwich, G. D.; Schaaf, P.; Voegel, J. C.; Lavalle, P. Proc. Natl. Acad. Sci. U.S.A. 2002, 99, 12531.

(48) Liu, G.; Zou, S.; Fu, L.; Zhang, G. J. Phys. Chem. B 2008, 112, 4167.

Chapter 1:

Assembly and water content of PEMs

1.1. Introduction

Since polyelectrolytes are charged molecules water can appear as solvation molecule around the charged monomers but, besides that, it can also be retained in cavities within a polyelectrolyte multilayer, either between polyelectrolyte molecules forming a given layer or between subsequent layers during assembly.[1-2] The calculation of the water content becomes an issue of main relevance when describing the buildup of such films: the presence of water molecules in the structure may affect the layout of the already deposited polyelectrolyte layers and, therefore, the approach of the subsequent incoming layers could be modified. Besides, it is not known how much the deposition of a new layer on the PEM would affect the content of water of the previously assembled layers.

Quartz crystal microbalance with dissipation monitoring (QCM-D) has proven to be a powerful technique to follow the growth of PEMs and to characterize the mechanism of their assembly. [3-5] The QCM-D responses, i.e., the resonance frequency *f* and the energy dissipation *D* of the shear oscillatory motion of a piezoelectric quartz crystal sensor, change upon adsorption or desorption of material on the surface of that sensor. The measured parameters are highly sensitive to the mass and the mechanical properties of the surface-bound layer. Mass resolution for example is on the order of a few ng/cm^2. Such sensitivity allows then for the in situ monitoring of the LbL assembly of the PEM as a stepwise process where each single layer being deposited is sensed as a change in the resonance frequency of the sensor movement. However, owing to its acousto-mechanical transducer principle, the QCM-D technique is not only sensitive to the adsorbed

molecules, but also to the solvent that is retained within or hydrodynamically coupled to the surface-bound film. It is hence often difficult to extract the adsorbed molecular mass from the QCM frequency response alone, i.e., to discriminate between the contribution of the adsorbate and the contribution of the solvent coupled to it. Thus, to reach a more comprehensive knowledge of the mechanism of polyelectrolyte assembly and, more specifically, for a proper quantification of the mass being adsorbed, additional and complementary experimental techniques are required.

In this regard, spectroscopic ellipsometry is also a frequently used technique for characterizing the assembly of thin films at interfaces.[6-7] Ellipsometry is an optical technique, where the change in the polarization state of an incident light wave upon reflection at an interface is measured. The polarization change is measured in terms of the ellipsometric angles ψ and Δ as a function of the wavelength λ, which can be detected with high accuracy. The simultaneous *in situ* determination of ψ and Δ can provide, by proper data treatment, quantitative information on the refractive index, thickness and mass of thin films at planar interfaces.[8-9] As ellipsometry is sensitive to differences in the optical density between adsorbate and bulk solution it essentially senses the adsorbate mass. Therefore, by comparison of the values for the masses obtained by both QCM-D and ellipsometry, the water content of a PEM can be calculated. Halthur and Elofsson[10] already illustrated how the growth of a multilayer composed of biocompatible polymers could be followed layer by layer by applying both techniques in separate experiments. More recently, Guzman et al.[11], applied the same protocol to analyze the structural changes induced by the employment of increasing NaCl concentrations in the growth of PDADMAC/PSS. In both cases,

the growth of m_{opt} and m_{QCM} of PEMs was studied on different samples because both methods could not be easily applied simultaneously for technical reasons.

In this chapter, the combination of spectroscopic ellipsometry and QCM-D is presented, as novelty, in a single device to study how the content in water, or aqueous solvent, and the amount of deposited polyelectrolyte vary along the layer-by-layer formation of PEMs. The combination of ellipsometry and QCM-D in a single device brings the advantage that the responses of both techniques are measured in parallel and in real time from the same sample under identical experimental conditions. Furthermore, in order to determine the effect of the ionic strength in the buildup of the multilayer, the LBL assembly of PDADMAC/PSS and PAH/PSS systems under study followed two different assembly protocols. The protocols differ exclusively in the ionic strength of the solution used for the washing steps between the depositions of each individual polyelectrolyte. Thus, while in one case the buildup took place in 0.5 M NaCl and the sample was only washed with pure water at the end of the assembly, in the second protocol applied, the sample was rinsed with pure water after the deposition of each layer. Based on these results, basic aspects regarding multilayer buildup will be addressed for both PDADMAC/PSS and PAH/PSS multilayers.

1.2. Results and discussion

1.2.1. Assembly of PAH/PSS multilayers in 0.5 M NaCl

Figure 8 illustrates the combined *in situ* QCM-D/ellipsometry measurements for the assembly of 17 layers of PAH and PSS in 0.5 M NaCl. Fig. 8a shows the variations in frequency and dissipation recorded by the QCM-D device. The dissipation shift remained low throughout the entire assembly process, indicating the formation of a rather rigid film. For such a film, the Sauerbrey equation was determined to be clearly applicable for the calculation of the increase in total film mass (including solvent), or m_{QCM}, after each deposition step, since the ratio of dissipation and normalized frequency shifts, $\Delta D/-\Delta f$, was found to be smaller than 0.2×10^{-6}/Hz, even for the last layer being assembled ($\Delta D/-\Delta f = 0.014\times10^{-6}$). The polymer mass, or m_{opt}, was obtained from the fitting of the real-time variation of Ψ and Δ measured along the multilayer deposition (Fig. 8b).

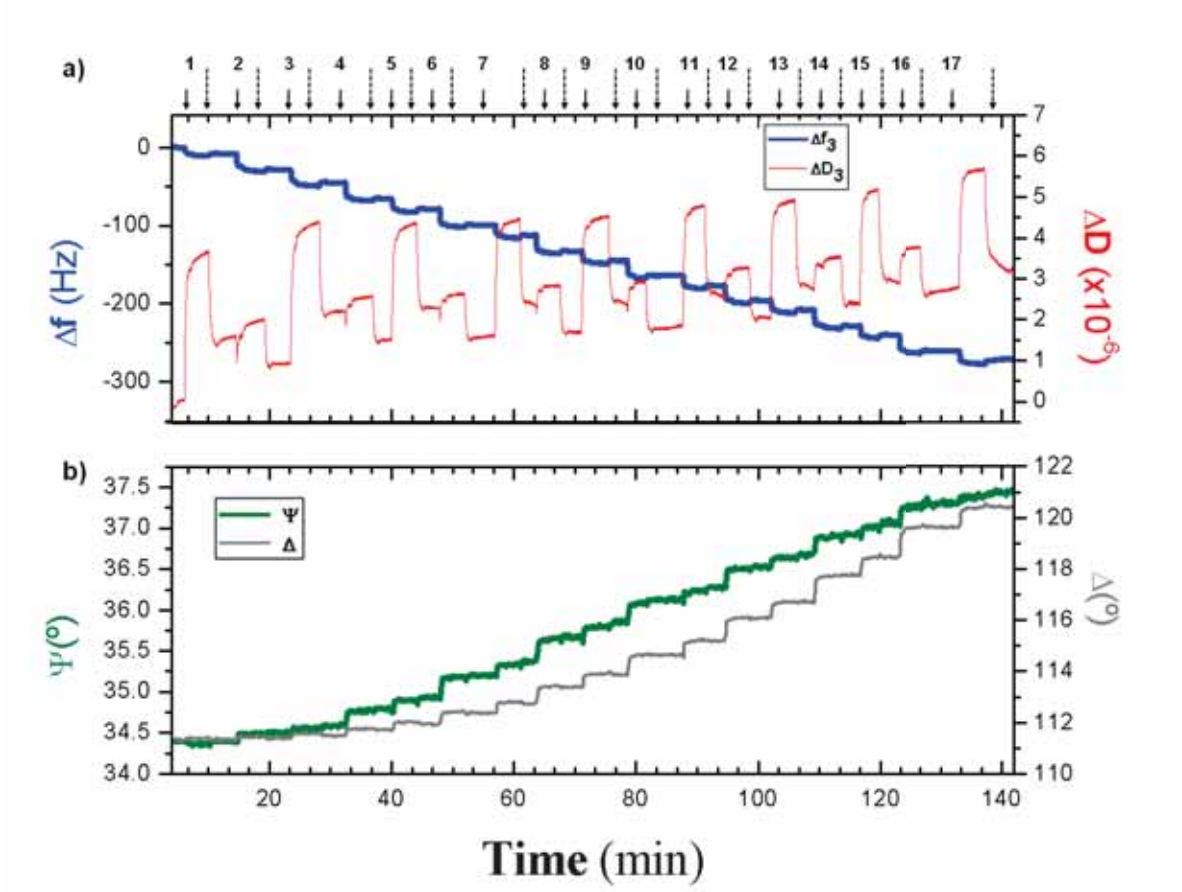

Figure 8 Assembly of 17 layers of PAH and PSS followed *in situ* by the combined QCM-D/ellipsometry device. (a) QCM-D response, i.e., Δ*f* and Δ*D vs.* time for a selected overtone (*i* = 3). (b) Ellipsometric response, i.e., Ψ and Δ *vs.* time for a selected wavelength (λ = 632.5 nm). The starting time of each deposition step and rinses are indicated by solid and dashed *arrows*, respectively, together with the step number. Odd and even numbers correspond to the incubation of PAH and PSS, respectively.

The calculated values for the acoustic thickness (d_{QCM}) and both m_{opt} and m_{QCM} are shown in Fig. 9 as a function of the number of assembled layers. PAH/PSS PEMs have previously been reported to exhibit linear growth [12] and the results obtained confirm this tendency.

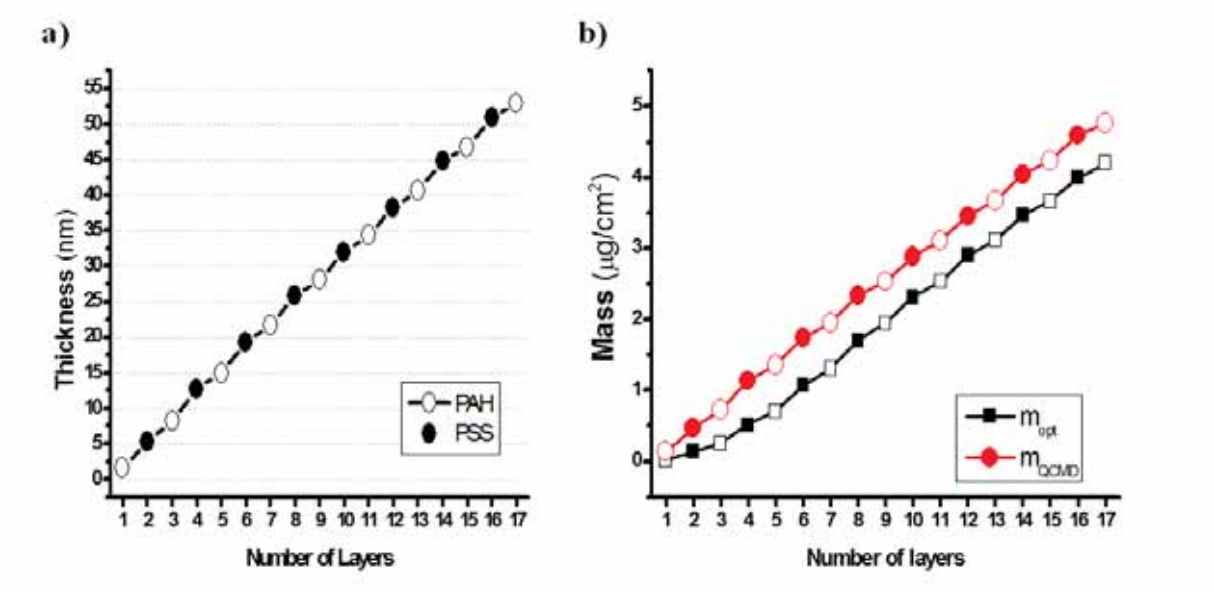

Figure 9 Evolution of the total film thickness (a) and the adsorbed masses (b) as a function of the number of deposited layers of PAH and PSS. Both m_{opt} (*squares*), which reflects the pure polymer mass, and m_{QCM} (*circles*) which includes solvent in the film are displayed. Open and filled symbols indicate adsorption of the polycation or the polyanion, respectively.

The thickness of the PAH/PSS multilayer (Fig.92a) increased linearly, at a rate of 6.4 nm per PAH/PSS incubation cycle. Interesting features arise from the analysis of plots, regarding *in situ* variations of m_{opt} and m_{QCM} as shown in Fig. 9b. Across the first three incubation steps, the polymer mass (m_{opt}) increased more slowly than the total film mass (m_{QCM}), while the increase rate was comparable for all subsequent incubation steps. It is noticeable that the increase in m_{opt} of the first layer is very small, 0.021 μg/cm^2 while the m_{QCM} for this layer is 0.213 μg/cm^2. This means that around the 90% of the total mass corresponds to water or aqueous solution (Fig. 10). The sensed mass of water may either represent water molecules bound to polymer chains or water that is entrapped between chains or layers. It has previously been reported that the first layers of PAH/PSS do not form a homogeneous film and assemble into islands that cover the surface heterogeneously. [13, 14] A part of the solvent that is situated in the interstices between

these islands will also contribute to m_{QCM} [15]. After the third layer, both m_{opt} and m_{QCM} increased by around 0.2 μg/cm^2 for every PAH layer added, and around 0.4 μg/cm^2 for every PSS layer. Concomitantly, the hydration of the multilayer (Fig. 10) continuously decreased along with the number of layers assembled, reaching a value of only 12% after the final 17th layer. An overall densification of the multilayer with increasing number of layers can be inferred.[16]

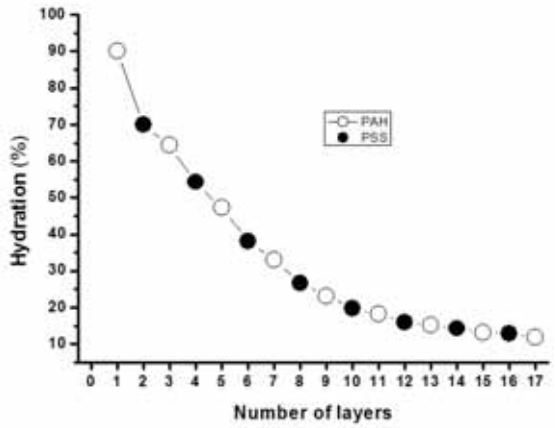

Figure 10 Aqueous solvent content as a function of the number of deposited layers of PAH (*open circles*) and PSS (*filled circles*).

It is quite remarkable that, for more than three layers, the *absolute* amount of water in the PEM did not depend on the number of deposited layer pairs. The global structure of sufficiently thick PEMs has been conceptualized by a three zone model, as explained before: two interfacial zones, which are affected by the presence of the solid support and the bulk solution, respectively, and maintain a constant thickness; and an interior zone, placed between the two interfacial ones, that grows in thickness as additional layers are deposited.[17] The observation that the absolute amount of water in the PEM is constant indicates that the interior zone is essentially water free and that water is primarily entrapped in the interfacial zones. The change in the water content when

passing from even to odd layers suggests that at least some of that water must be situated in the interfacial zone adjacent to the bulk solution. Then, the small differences in water content between PEMs with PAH as last layer and PEMs with PSS as last layer, are due to the particular hydration of the last layer. Clearly, the presence of NaCl retains PAH and PSS in a strongly collapsed state inside the PEM. The presence of water can be associated to the uncompensated charges present in the last layers of the PEM.

1.2.2. Assembly of PAH/PSS multilayers in water

For comparison, PAH/PSS multilayers were also assembled following a protocol that included the washing with water between the layer deposition steps.

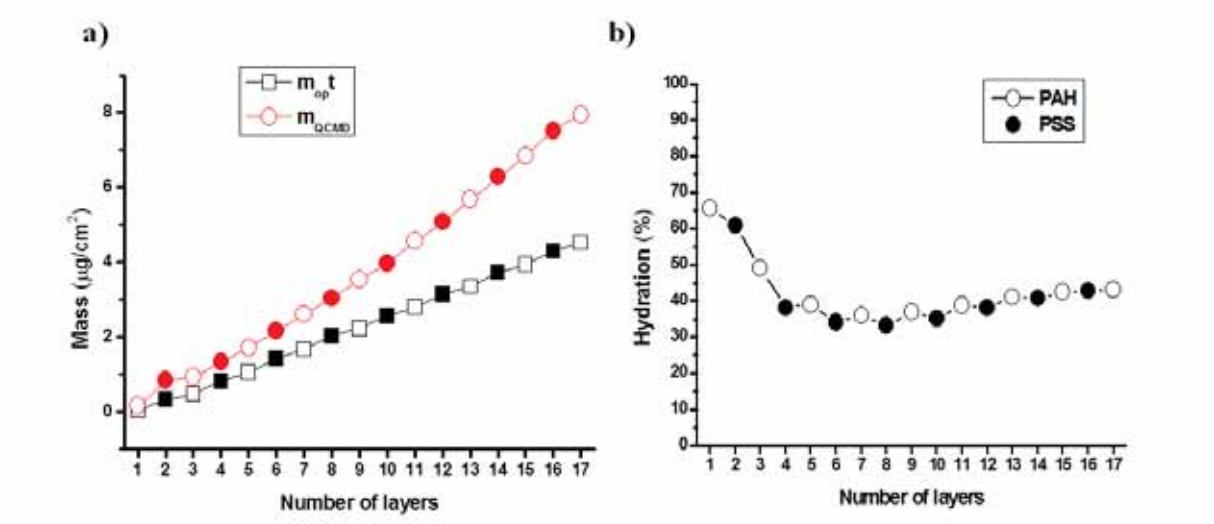

Figure 11 (a) m_{QCMD} (*circles*) and m_{opt} (*squares*) values for PAH/PSS assembly with washes in pure water between deposition steps (b) Hydration plot of the PAH/PSS PEM as a function of the layer number. Open and filled symbols indicate the adsorption of the polycation and the polyanion respectively.

The variations in m_{opt} (Fig. 11a) were identical to the values obtained with NaCl washings (Fig. 9b). The values for m_{QCM}, in contrast, diverged significantly from those previously observed. Starting with the third layer, m_{QCM} increased more strongly than m_{opt}. The divergence between m_{QCM} and m_{opt} provides evidence that the modified deposition procedure leads to the entrapment of water in the PEM. Fig. 11b illustrates that the hydration approaches a final value of 43%, i.e., almost half of the PEM mass is water. Assuming equimolar polyanion and polycation content, this corresponds to a ratio of 7 water molecules per polyelectrolyte monomer. It is interesting that the PAH/PSS PEM soaks more water with increasing layer number when rinsing with water, although the amounts of PAH and PSS that bind per incubation step remain constant. Two scenarios appear plausible to explain this effect. One could assume that while charges are compensated in the interior of the multilayer, the last layer behaves as a polyion and hence soaks water upon reduction of the ionic strength. In this case, the hydration would be coming only from the last layer of the PEM, and the capacity of this last layer to soak water increases with layer number, i.e., the arrangement of the chains as the film growths becomes more favorable for the swelling of the last layer. Alternatively, it may be the interior of the PEM and not only the last layer that swells during the rinsing with pure water. The weak dependence of the water content on the number of exposure cycles for sufficiently large number of layers and the linear growth make the latter scenario more likely.

1.2.3. Assembly of PDADMAC/PSS multilayers in 0.5 M NaCl

The *in situ* combination of QCM-D with ellipsometry was then applied to study the growth of PEMs of a total of 17 layers composed of PDADMAC as polycation and PSS as polyanion, with washes in 0.5 M NaCl between the incubation steps. Fig. 12 shows the responses in the acoustic parameters, Δf and ΔD, and optical parameters, Ψ and Δ, measured for this system.

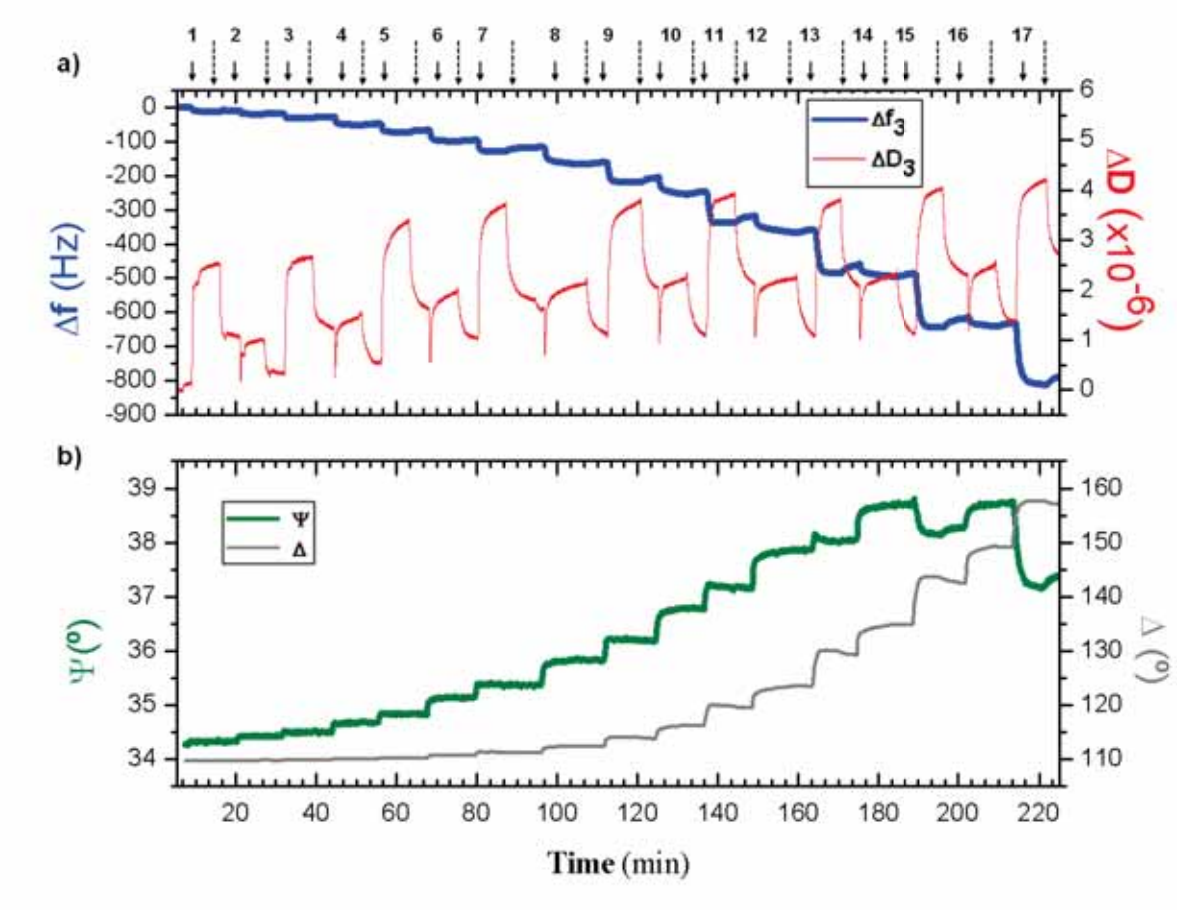

Figure 12 Assembly of 17 layers of PDADMAC and PSS in 0.5 M NaCl followed *in situ* by the combined QCM-D/ellipsometry device. (a) QCM-D response, i.e., Δf and ΔD *vs.* time for a selected overtone ($i = 3$). (b) Ellipsometric response, i.e., Ψ and Δ *vs.* time for a selected wavelength ($\lambda = 632.5$ nm). The starting time of each deposition step and rinses are indicated by solid and dashed *arrows*, respectively, together with the step number. Odd and even numbers correspond to the incubation of PDADMAC and PSS, respectively.

Compared to the frequency shifts, which reached values of -750 Hz, the dissipation shifts remained small ($< 4.5\times10^{-6}$), indicating the formation of an overall rather rigid film. It is notable that the incubation with polyelectrolyte solution induced a rather strong increase in ΔD that was partly reversed after rinsing in salt solution. Furthermore, the dissipation after incubation of the PEM with PDADMAC was always larger, and the film hence softer, than after exposure to PSS. Also in can be observed that the time needed to reach equilibrium in ΔD upon rinsing were rather long, while the optical responses and Δf equilibrated quickly. These observations suggest a rather strong reorganization of the PEM. Thickness, m_{opt} and m_{QCM} were calculated from the raw data for the assembly of the PDADMAC/PSS multilayer (Fig. 13).

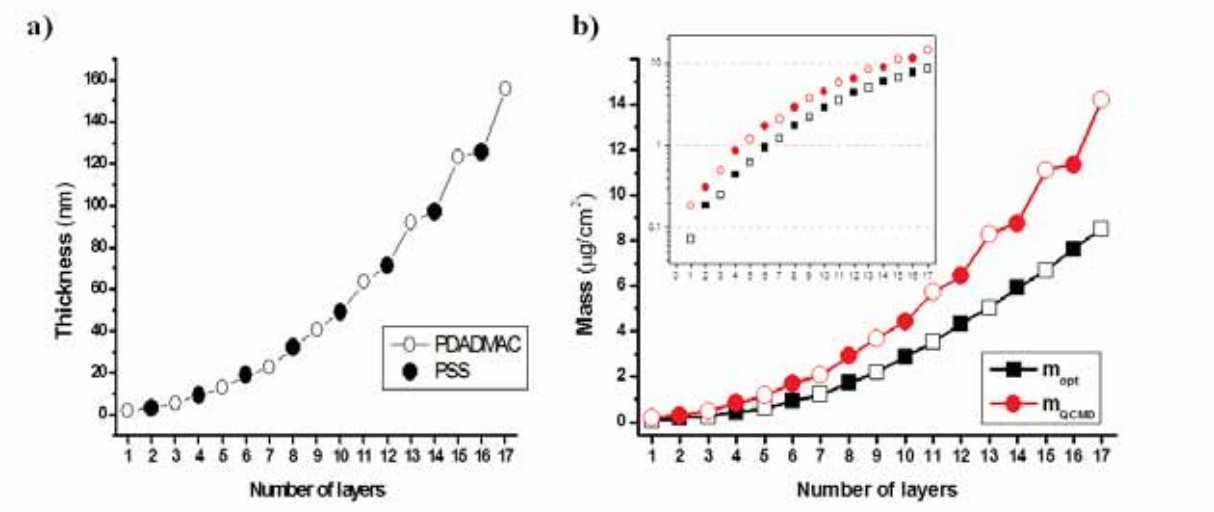

Figure 13 PEM composed of PDADMAC and PSS with a total of 17 layers built in 0.5 M NaCl. (a) Thickness variation per layer assembled. (b) Comparison between m_{opt} (*squares*) and m_{QCM} (*circles*) as a function of layer number. The inset shows the same date in a semi-logarithmic plot. Open and filled symbols indicate adsorption of the polycation or the polyanion, respectively.

After 17 layers, the film reached a thickness of 157 nm (Fig. 13a). From the 11th layer onwards the odd layer numbers, which correspond to PDADMAC, resulted always in more significant increases in the thickness values than the increases observed for even layers, corresponding to PSS. Both m_{QCM} and m_{opt} clearly exhibit supra-linear growth (Fig. 13b). A semi-logarithmic plot of these quantities (Fig. 13, *inset*), however, does not show a clear linear dependence of log(*m*) on layer number. The PEM growth is hence not strictly exponential. A total mass of 14.1 μg/cm^2 and a polymer mass of 8.5 μg/cm^2 (Fig. 13b) were calculated from acoustic and optical data, respectively.

An interesting feature of the mass curves in Fig. 13b is their diverging growth behavior which becomes particularly apparent at large layer numbers. Upon deposition of PDADMAC, the increase in m_{QCM} is large and the increase is m_{opt} is rather small. The opposite situation is observed upon deposition of PSS. This translates into a hydration curve (Fig. 14a) that oscillates, starting at the 9th assembly step, between values of a maximum of 40-45% and a minimum of 30-35%.

The hydration plot also reveals that, when considering odd and even layer numbers separately, the water content decreased throughout the build-up of the PEM. For thick PEMs, the hydration approached plateaus of about 30 and 40% for final incubations with PSS and PDADMAC, respectively. This implies that the amount of assembled polyelectrolyte increased proportionally to the amount of water entrapped. Assuming that the film contains an equimolar amount of cationic and anionic groups, the ratio of water molecules per polyelectrolyte monomer for thick PEMs can be calculated to oscillate between 5:1 and 7:1

for PEMs with PSS and PDADMAC as last layers, respectively. These values might have an over- or underestimation, of at most ±13%, if PDADMAC or PSS, respectively, were the last assembled layer.

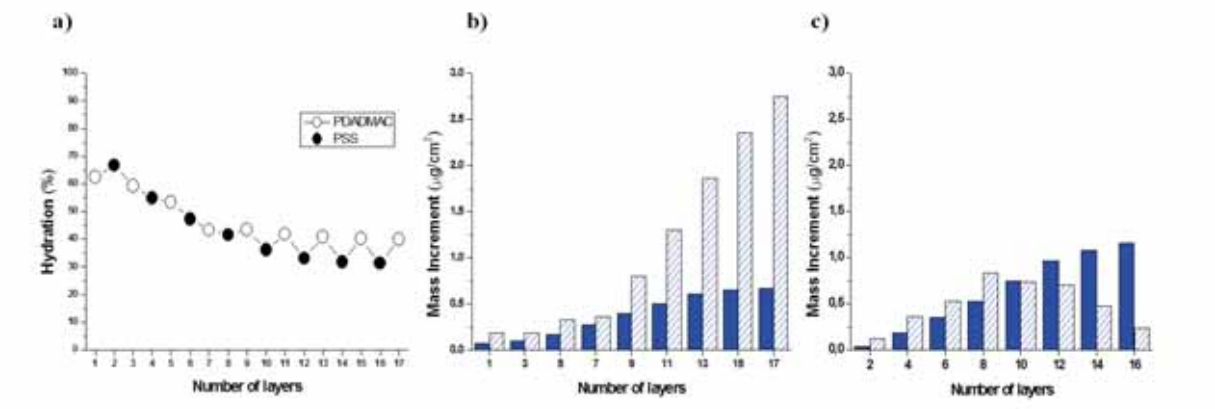

Figure 14 (a) Aqueous solvent content in the film *vs.* number of deposited layers of PDADMAC (*open circles*) and PSS (*filled circles*) plot. Increments in m_{opt} (*solid bars*) and m_{QCM} (*hatched bars*) for a PDADMAC/PSS multilayer grown with 0.5 M NaCl washing steps upon deposition of (b) PDADMAC and (c) PSS.

The increments in both net polymer and total film mass for each incubation step (Fig. 14b-c) were also calculated. Clearly, the increments in total mass upon assembly of PDADMAC increase strongly with layer number, while the increments in net polymer mass seem to have attained a plateau. For PSS, in contrast, the increments in net polymer mass increase monotonously, while the increments in total mass decrease after reaching a maximum at layer number 8.

1.2.4. Assembly of PDADMAC/PSS multilayers in water

PDADMAC and PSS were also assembled by using pure water instead of NaCl solution for the washing between each layer deposition (Fig. 15). From the inspection of the dissipation shifts, drastic changes in the mechanical properties of the multilayer as a function of the salt concentration in solution can be deduced. In NaCl solutions, the dissipation shifts remained small, at levels that are comparable to those in Fig. 12. Exchange of the bulk solution to pure water, however, induced drastic increases in ΔD, indicating a softening of the film. The changes in dissipation were particularly significant for PEMs with PDADMAC as the last layer. Here, the changes in dissipation when changing the solvent increased strongly as the buildup of the multilayer proceeded, reaching values of 100×10^{-6} and more. The strong dissipation shifts were accompanied by strong frequency shifts, indicating that hydration/swelling is responsible for the softening of the film.

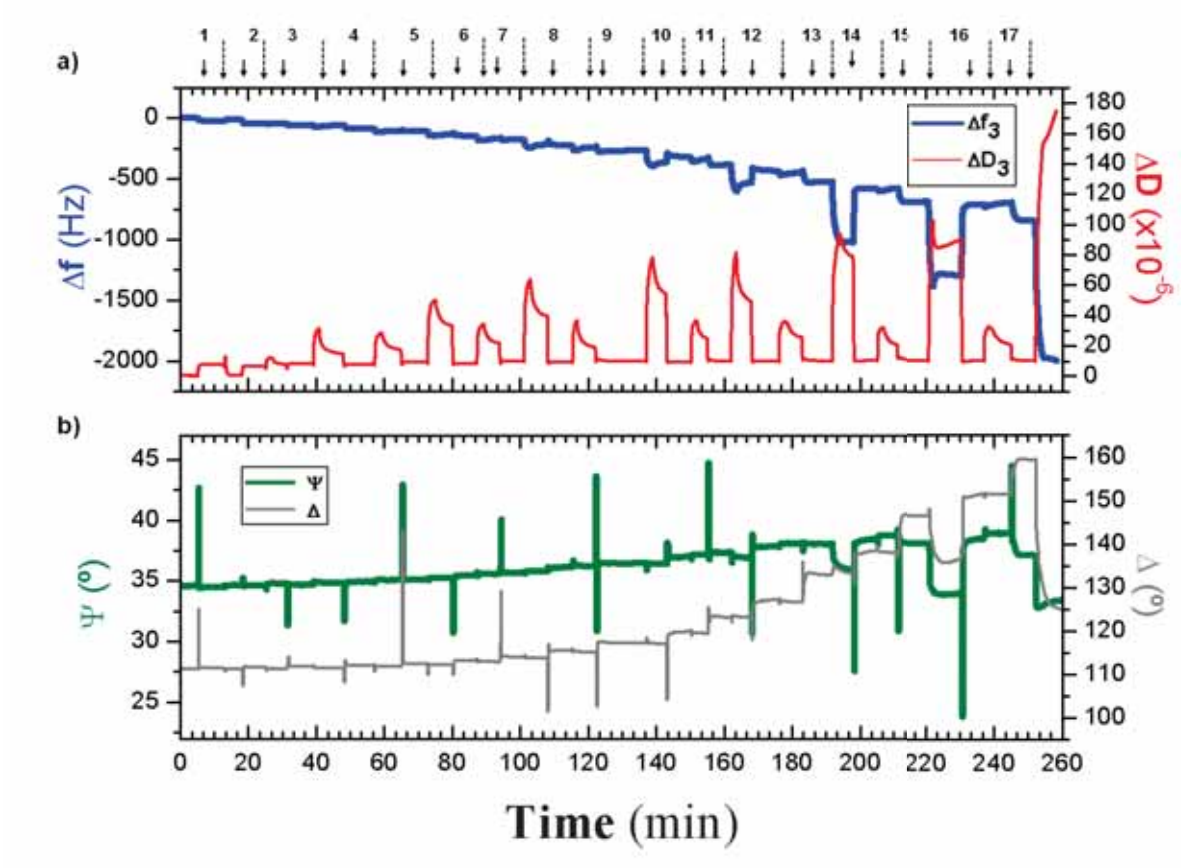

Figure 15 Assembly of 17 PDADMAC/PSS layers with washes in pure water followed *in situ* by the combined QCM-D/ellipsometry device. (a) QCM-D response, i.e., Δf (*blue line*) and ΔD (*red line*) *vs.* time for a selected overtone ($i = 3$). (b) Ellipsometric response, i.e., Ψ (*green line*) and Δ (grey line) *vs.* time for a selected wavelength ($\lambda = 632.5$ nm). The starting time of each deposition step and rinses are indicated by solid and dashed *arrows*, respectively, together with the step number. Odd and even numbers correspond to the assembly of PDADMAC and PSS, respectively. The strong but transient peaks in the ellipsometric response are artifacts that originate from strong scattering of light upon exchange of pure water against polymer-containing NaCl solutions.

Figure 16 shows the variations of d_{QCM}, m_{opt} and m_{QCM} along the multilayer build-up. With the protocol including water rinsing, the PDADMAC/PSS multilayers showed an initial exponential growth of m_{QCM} until the 9th layer, which was followed by strong oscillations in the mass. After 17 incubation steps, a film thickness of 370 nm was reached, which is twice

the value observed in NaCl solution. The total film mass also doubled. In contrast, the polymer mass was only marginally affected by the change in the rinsing method throughout the entire PEM buildup. The oscillatory behavior found for m_{QCM} is also apparent for the thickness of the multilayer (Fig. 16a), illustrating the cycles of swelling and shrinkage that ensue upon deposition of PDADMAC and PSS, respectively. An oscillatory behavior is also evident for the polymer mass, albeit to a lesser degree. Notably, the oscillation of m_{QCM} is out of phase with the oscillation of m_{opt}, i.e., a maximum in m_{QCM} coincides with a minimum in m_{opt}.

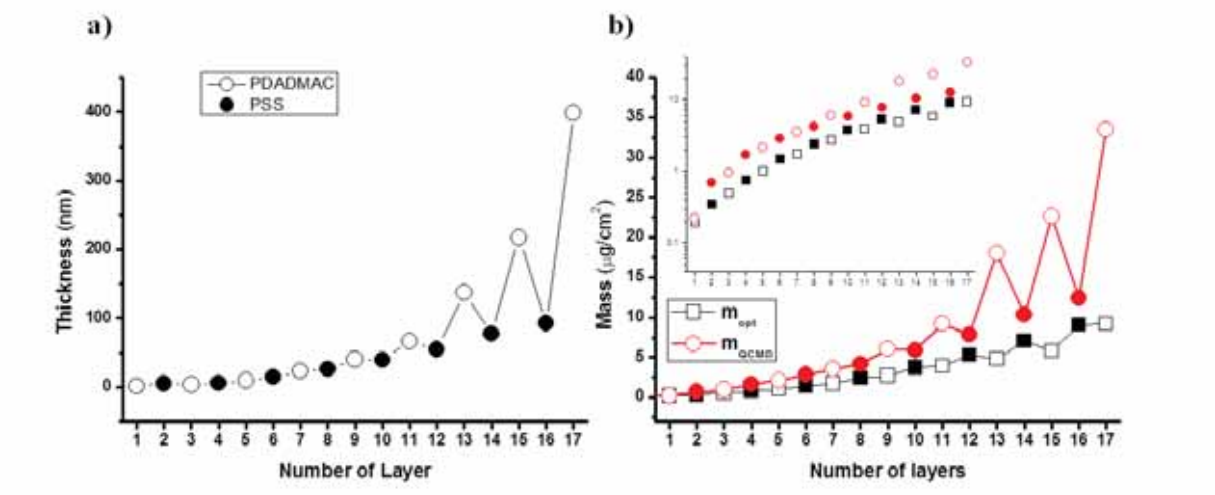

Figure 16 PEM composed of PDADMAC and PSS with a total of 17 layers built with washes in pure water. (a) Evolution of the total film thickness. (b) Comparison between m_{opt} (*black squares*) and m_{QCM} (*red circles*) as a function of layer number. The inset shows the same date in a semi-logarithmic plot. Open and filled symbols indicate adsorption of the polycation or the polyanion, respectively.

The comparison of Fig. 17a with Fig. 14a demonstrates that the hydration was dramatically affected by the change in the protocol of assembly. Except for the first layer, the hydration after rinsing with water remained approximately constant, at about 50%, up to the 7th layer.

Then, the hydration started to oscillate, between about 30% and 70%, upon assembly of PSS and PDADMAC, respectively. Assuming again equimolar presence of cations and anions in the film, the ratio of water molecules per polyelectrolyte monomer reached up to 29:1 for the swollen PEMs after assembly of PDADMAC and diminished to 4:1 for the compact films after PSS assembly.

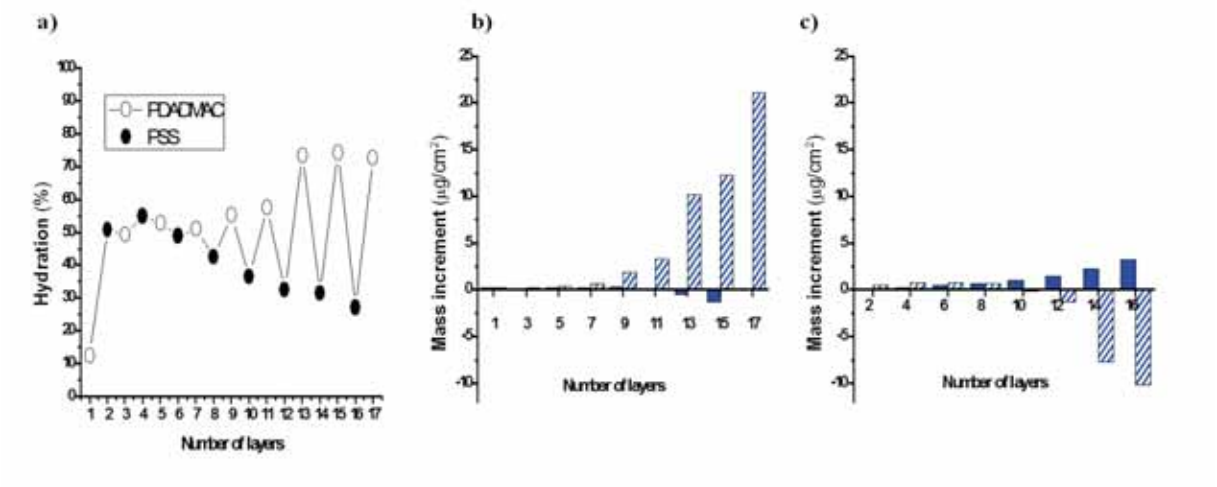

Figure 17 (a) Aqueous solvent content in the film *vs.* number of deposited layers of PDADMAC (*open circles*) and PSS (*filled circles*). Increments in m_{opt} (*solid bars*) and m_{QCM} (*hatched bars*) upon deposition of PDADMAC (b) and PSS (c) for a PDADMAC/PSS multilayer grown with pure water washing steps.

As for the PEM with washing steps of 0.5 M NaCl between layers, the mass increments corresponding to each assembled layer for both m_{opt} and m_{QCM} (Fig. 17b-c) have been also determined. For PDADMAC, constant increments in m_{opt} of 0.2 to 0.3 µg/cm^2 were observed until the 9th layer. For the following layers, very small or even negative increments were found. This net loss of polymer mass most likely indicates removal of PSS from the PEM upon exposure of PDADMAC. At the same time, the increments in m_{QCM} became progressively

bigger, with typically more than 2-fold increases from one assembly step to the next. The mass increments for PSS followed a very different trend. The increments in m_{QCM} were initially constant, at 0.5 to 0.7 μg/cm^2, became zero at layer 10 and then decreased strongly. In contrast, m_{opt} increased progressively.

1.3. Conclusions

In this first chapter, both the growth and the water content of multilayers composed of standard polyelectrolyte pairs PDADMAC/PSS and PAH/PSS have been described. The existing difference in the interaction between the two polycations and the negatively charged PSS, as well as in the structure of the films formed, has been shown to generate drastic differences between the two systems studied. On one hand, linearly growing PAH/PSS PEMs produce a film containing almost no water in its interior when assembled with rinses in salt solution, while assembly with rinses in pure water produces a film that contains more than 40% water. On the other hand, the hydration of the supra-linear PDADMAC/PSS PEMs is tremendously affected by the ionic strength of the washing solution and, additionally, shows a strong dependence on the last layer being deposited. While for multilayers built with NaCl rinses the hydration values oscillate around the 40% in water content, in conditions of low ionic strength the film is capable to soak water up to 70% of the total multilayer mass when the last incubation step is with PDADMAC. Nevertheless, adsorption of a new PSS layer leads the multilayer to a more compact and rigid state, which promotes the release of some of the entrapped water and makes the water content in the film to decrease down to the 30%.

1.4. References

(1) Schonhoff, M.; Ball, V.; Bausch, A. R.; Dejugnat, C.; Delorme, N.; Glinel, K.; von Klitzing, R.; Steitz, R. Colloids Surf. A 2007, 303, 14.

(2) Schlenoff, J. B.; Rmaile, A. H.; Bucur, C. B. J. Am. Chem. Soc. 2008, 130, 13589.

(3) Marx, K. A. Biomacromolecules 2003, 4, 1099.

(4) Notley, S. M., Eriksson, M., Wågberg, L. J. Colloid Interface Sci. 2005, 292 (1), 29.

(5) Liu, G.; Zhao, J.; Sun, Q.; Zhang, G. J. Phys. Chem. B 2008, 112, 3333.

(6) Haberska, K.; Ruzgas, T. Bioelectrochemistry 2009, 76, 153.

(7) Gong, X.; Gao, C. Phys. Chem. Chem. Phys. 2009, 11, 11577.

(8) McCrackin, F. L.; Passaglia, E.; Stromberg, R. R.; Steinberg, H. L. J. Res. Natl. Bur. Stand.,A. 1963, 67A, 363.

(9) Cuypers, P.A.;Corsel, J.W.; Janssen, M. P.; Kop, J. M. M.; Hermens, W. T.; Hemker, H. C. J. Biol. Chem. 1983, 258, 2426.

(10) Halthur, T. J.; Elofsson, U. M. Langmuir 2004, 20, 1739.

(11) Guzman, E.; Ritacco, H.; Rubio, J. E. F.; Rubio, R. G.; Ortega, F. Soft Matter 2009, 5, 2130.

(12) Dejeu, J.; Buisson, L.; Guth, M. C.; Roidor, C.; Membrey, F.; Charraut, D.; Foissy, A. Colloids Surf., A 2006, 288, 26.

(13) Porcel, C.; Lavalle, P.; Ball, V.; Decher, G.; Senger, B.; Voegel, J-C.; Schaaf, P. Langmuir 2006, 22, 4376.

(14) McAloney, R. A.; Sinyor, M.; Dudnik, V.; Goh, M. C. Langmuir 2001, 17, 6655.

(15) Bingen, P.; Wang, G.; Steinmetz, N. F.; Rodahl, M.; Richter, R. P. Anal. Chem. 2008, 80, 8880.

(16) Estrela-Lopis, I.; Leporatti, S.; Clemens, D.; Donath, E. Soft Matter 2009, 5, 214–219.

(17) Ladam, G.; Schaad, P.; Voegel, J. C.; Schaaf, P.; Decher, G.; Cuisiner, F. Langmuir 2000, 16, 1249–1255.

Chapter 2:

Effect of the ionic strength and nature of the counterions in the inner structure and surface potential of PEMs

2.1. Introduction

The presence of salts is one important factor affecting the buildup regime, the response, or the stability of the PEM[1]. For instance, variations in the ionic strength or in the nature of the counter-ions are involved in the intrinsic compensation (screening) of the charges, and lead the multilayers to undergo structural reorganization of the chains which can be reflected as shrinkage of the film or can even originate, in the most dramatic cases, the dissolution of structure-driving bonds which results in the disintegration of the film.

PEMs composed of strong polyelectrolytes present intrinsic charge compensation in the region of the bulk of the film, the so-called zone II, while the film-solution interface (zone III) contains polyions with partial extrinsic charge compensation. The remainder charge in the outermost layers of the PEM, resulting from the previously commented extrinsic over-compensation, can be expected to induce conformational rearrangements in the polyelectrolyte molecules and, eventually, changes in the thickness of the PEM upon variations in the ionic strength. The response of PEMs to ionic strength has indeed been widely investigated in recent years [2-3] and, in particular, PEM films with exponential growth have been proved to be extremely sensitive to the ionic strength of the bulk solution because of their high water and ion content [4].

In contrast to polyelectrolyte gels, which shrink when the ionic strength is increased, PEM films have been usually reported to swell. This swelling would be explained by diffusion of the counter ions of the employed salt solution into the multilayer what leads to an extrinsic compensation of the polymer charges. The weakening of the electrostatic interactions between

the charged polymeric chains results in a looser structure, and a reversible swelling of the film is observed. At a critical salt concentration, the ionic bonds that hold the layers together tend to break [5]. A quantitative approach to salt infiltration-swelling process was even provided by Dubas and Schlenoff [6] who defined the volume swelling coefficient as

$$Q_{swell} = \% \text{ swelling} / [\text{salt}],$$

where Q_{swell} was calculated for multilayers of different compositions. Nevertheless, in this chapter it will be shown that PEMs composed of PDADMAC/PSS display an unexpected trend in response to changes in the ionic strength. In contrast to previously reported responsive multilayers, these highly hydrated films shrink in a reversible fashion upon exposure to relatively high salt concentrations [7-8]. PEMs showing variations in thickness to this extent upon changes in the ionic strength could be used as a nanoactuator or as barrier with tuneable thickness in a nanodevice. In regard to their response these systems would be comparable with either polyelectrolyte gels or polyelectrolyte brushes, which also collapse reversibly with increasing ionic strength [9-10]. The main advantage of PEMs compared with systems such as polyelectrolyte brushes, for instance, is the much simpler route of assembly and the possibility of coating almost any charge surface provided. However, such shrinking behaviour is only observed for multilayers deposited in high ionic strength (0.5 M NaCl) where PDADMAC is placed as the top layer since the response of the PEM is blocked by the addition of one PSS layer on top. Then PEMs composed of PDADMAC and PSS offer a unique tool for fabricating a smart surface based on simple nanoscale design principles.

The use of different counterions may have additional effects in the multilayer structure. This is the case of perchlorate (ClO_4^-), a voluminous anion which creates a more hydrophobic environment in the layer and thus has a pronounced influence on the water content in the multilayer[11]. Besides, another interesting example would be the assembly of LbL multilayers in the presence of counterions which follow the Hofmeister series of ion affinity.[12] The Hofmeister series classifies ions according to their capability to stabilize or precipitate proteins, which is related to the effects of those ions on the structure of the solvent[13]. Ions, such as citrate, sulphate, phosphate, and Al^{3+}, can be classified as "structure maker" or cosmotropes. They stabilize proteins or hydrophobic aggregates and reduce the solubility of hydrophobic species. Conversely, other ions are classified as "disorder maker" or chaotropes when they unfold proteins, destabilize hydrophobic aggregates, and increase the solubility of hydrophobic species, for example, I^-, NO_3^-, NH_4^+, and the above mentioned ClO_4^-.[14] Then, when affinity of the counterions to the monomers is strong the film formation may be significantly reduced or even not occur. [12, 14-15] In this regard, the response of PAH/PSS and PDADMAC/PSS polyelectrolyte multilayers is addressed in this chapter due to the presence in the environment of ions at the extremes of the Hofmeister series, such as ClO_4^- and $H_2PO_4^-$, which can have a specific interaction either with PDADMAC or with PAH, respectively. The interaction of the PEMs with $LiClO_4$ and KH_2PO_4 salts was studied by means of QCM-D and AFM, to determine the stability and the topographical variations of the films.

Furthermore, in order to know if these polyelectrolyte-counterion specific interactions, in addition to electrostatic ionic strength based effects, may lead to specific properties of the LbL film, the electrophoretic behavior of both PAH/PSS and PDADMAC/PSS coated sub-

micrometer silica particles was analyzed by ζ-potential measurements in presence of the above mentioned salts. The response of the PEM coated silica particles in NaCl was studied and employed as reference for comparison with the other systems.

2.2. Results and discussion

2.2.1. Effect of the Ionic Strength on PEM structure

The assembly of multilayers composed of PDADMAC and PSS polyelectrolyte pairs has been shown, in the previous chapter, to be highly dependent on the ionic strength of the solution used for the intermediate rinse between each layer adsorption. These systems exhibited strong and fully reversible swelling, when applying water washings along the buildup, with water contents ranging between values of 70% and more if the incubation step was with PDADMAC, and the 40% for PSS-capped films (Fig. 9). A similar oscillatory behavior could be observed for those PEMs assembled in 0.5 M NaCl but to a much lower degree (Fig. 6).

An extended analysis about the variations in the ionic strength that PDADMAC/PSS systems display was then done, by means of QCM-D, by exchanging the bulk solution from 0.5 M NaCl to water after the assembly of the PEM. Thereby, PEMs with PDADMAC as the top layer showed a negative change in frequency of 600 Hz [Fig. 11(a)]. Such change can only be attributed to an uptake of water since the optical mass has shown not to undergo variations along the exchange. Then, from the measured frequency shifts a variation in the thickness from 190 nm in 0.5 M NaCl to 300 nm (~58%) was calculated, with an increase in water content from a 50% to a 69%. As the dissipation of the PEM also increases a shift of the viscoelastic character to a softer state is deduced.

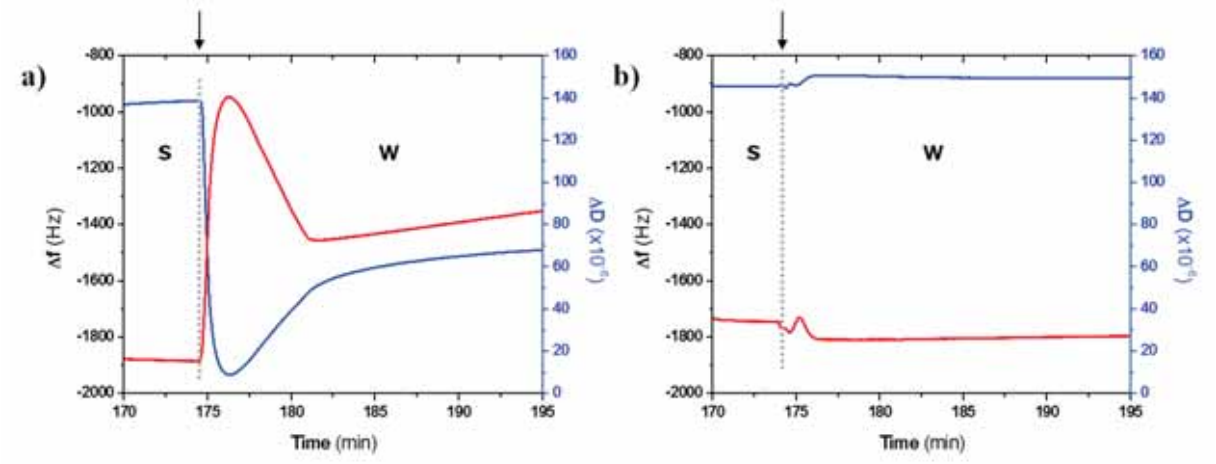

Figure 18 Changes in Frequency and Dissipation for PDADMAC/PSS PEMs after exchange of bulk solution from 0.5 M NaCl to water, immediately after PEM assembly of (a) 17 layers, with PDADMAC on top, and for (b) 16 layers, where PSS is the outermost layer.

In contrast, when PSS is the top layer, the thickness and the water content of the PEM do not increase when going in bulk from a salt solution to water, which indicates no apparent changes in the PEM structure [Fig. 18(b)]. In fact, the changes measured for frequency and dissipation are consistent with those expected exclusively for an exchange of salt with water, that is, the changes in frequency due to change to less dense medium and a smaller friction. The response of the assembled PDADMAC/PSS PEMs to the ionic strength was then studied with QCM-D. Figure 19 displays the in situ frequency and dissipation variations measured for systems containing either 17 layers, with PDADMAC as the outermost layer, or 16 layers, being PSS the last layer, when the bulk solution is exchanged from water to NaCl solutions of increasing ionic strength, 0.5 M and 1 M, and then to water again.

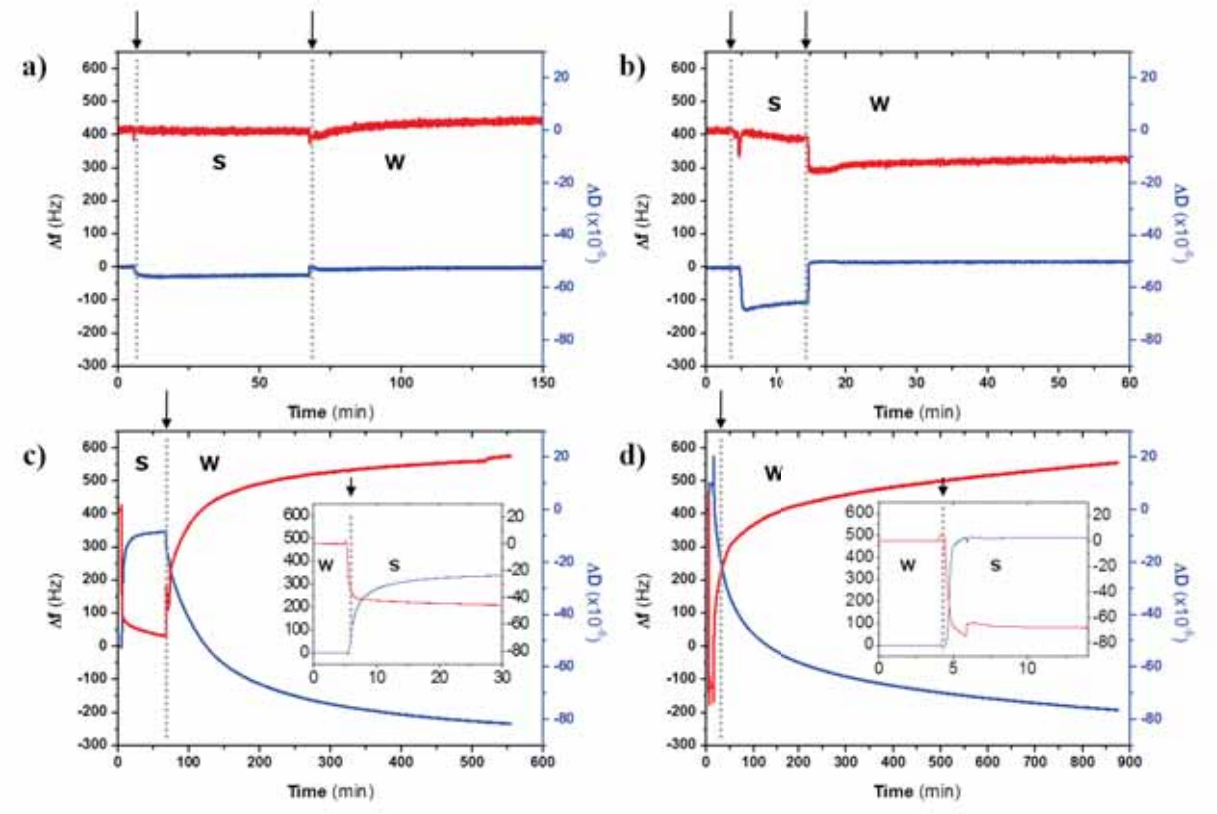

Figure 19 Frequency and dissipation changes for PEMs of PDADMAC/PSS of 16 layers (final PSS layer) exposed to (a) 0.5 M NaCl and (b) 1 M NaCl and of 17 layers (final PDADMAC layer) exposed to (c) 0.5 M NaCl and (d) 1 M NaCl. Arrows indicate the injection of salt solutions (s) or water (w) into the chamber. The insets in (c) and (d) figures enlarge the region comprising the change from water to NaCl.

For PEMs of 16 layers capped with PSS [Fig. 19(a, b)], the salt solution yields a negative shift in the frequency and shows almost no shift in the dissipation. The extent of the frequency change may be indicative of the exchange of water for a denser salt solution inside the PEM in agreement with Figure 18. In contrast, for PEMs with PDADMAC as last layer [Fig. 19(c, d)] a positive shift in the frequency, indicative of a mass loss, is shown. When the PEM was exposed to 0.5 M NaCl increases in the frequency of around 350 Hz were observed, meaning that about 6.3 μg/cm2 of water are lost; upon treatment with 1 M NaCl frequency shows an increase of 500

Hz corresponding to a loss of 9.0 μg/cm2 of water. In terms of thickness, this exchange results in a decrease of around the 25% and the 35% of the PEM height, respectively, far above the values reported for other systems, which follow a reversible swelling upon pH, ionic strength, temperature, or electrical currents.[16–20] Surprisingly, the final washing with water brings the frequency, in a slow re-hydration process of 8–10 h, to much lower values than the original starting point. The characteristics of the rehydration process of the PEM suggest a hydrogel or sponge-like behavior along the re-swelling procedure, where more water than the amount entrapped before the collapse is soaked. After such re-swelling in water, the increases in water content after treatment with 0.5 M and 1 M NaCl represent a net profit of about 70% and 40%, respectively, in comparison to the amount of water released. This is also reflected in film thicknesses for both systems around a 15% higher than the pretreated initial state. The treatment with salt may result in the annealing of the layers and in a better conformational arrangement of the chains, which provide the film the capacity to soak more water. The large variations in positive values of the frequency are accompanied with reversible variations in the dissipation of -50 ($x10^{-6}$) ΔD for 0.5 M NaCl and -80 ($x10^{-6}$) ΔD for 1 M NaCl. A decrease in dissipation implies a change in the mechanical properties of the film, towards a more rigid and compact arrangement of the polymer chains, where viscoelastic character is lost. Then, a PDADMAC/PSS PEM of 17 layers assembled in 0.5 M NaCl with PDADMAC as last layer shows a unique capacity to hydrate and swell when the NaCl solution is exchanged for water. Because of the interpenetration which is known to take place in the assembly of PDADMAC/PSS systems such osmotical response is likely to be restricted to those layers of the PEM affected by the polymeric diffusion. Free charges should be present in these layers. It

seems that PDADMAC has more freedom to change conformation and soak water than PSS in the PEM. Nevertheless, it could also be that the swelling/deswelling involves the whole PEM and it is blocked when PSS is the last layer, although charges in the interior of the PEM are almost fully compensated and no free charges remaining would be expected. The swelling at low ionic strength has been previously explained as a consequence of the top PDADMAC layer in the film, which is behaving as a free polyelectrolyte in solution. Because of the so called interdigitation effect, this PDADMAC layer can reach up to four four layers below the top[21]. This makes Zone III of the PEM increasing, which is the one sensitive to the ionic strength. Hence, at low ionic strength, the polymer chains will be less coiled, they will expand and the layer will consequently swell.

2.2.2. Effect of the nature of the counterions in PEM structure

To further explore the role of the ionic species on PDADMAC/PSS and PAH/PSS multilayer structures, Cl^- counterions in the PEMs were replaced by ions at the extremes of the Hofmeister series, such as ClO_4^- and $H_2PO_4^-$, which can have a specific interaction either with PDADMAC or with PAH, respectively.

For instance, a PDADMAC/PSS multilayer of 11 total layers was assembled in a quartz microbalance with dissipation (QCM-D), with intermediate water washings, and subsequently exposed to a 0.2 mol/L $LiClO_4$ solution. As explained above, ClO_4^- is a chaotropic anion, with a much larger volume than the Cl^- anions employed so far, and which is known for presenting a high hydrophobicity. Furthermore, ClO_4^- has been reported to have a high affinity towards

quaternary ammonium groups[22]. Then, the exposure of the ion to the PEM provokes an irreversible increase in frequency values of approximately 90 Hz which can be interpreted as a decrease in the multilayer mass (Figure 20).

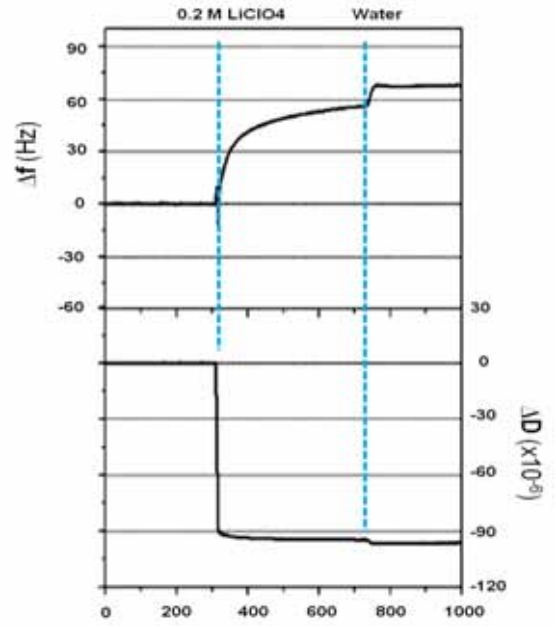

Figure 20 Changes in frequency (top) and dissipation (below) after $LiClO_4$ treatment on a multilayered system PDADMAC/PSS.

Since the last deposited layer of PDADMAC induced a 350 Hz variation in the frequency of oscillation of the crystal, the material lost from the multilayer corresponded to almost one-fourth of a layer of PDADMAC. It is also noticeable that after the salt treatment and water washing the different overtones split. This is indicative of a vertical change in the density of the material and perhaps less densely packed last layers. On the contrary, dissipation values, which can be related to the mechanical properties of the film, decreased after $LiClO_4$ treatment. This can be understood from the loss of polymers, which is almost half of the total assembled mass. It is important to highlight that repetition of same experiment with PSS-capped films (data not

shown) yielded no significant changes in the frequency and demonstrated that such response upon treatment with ClO_4^- can only be afforded for PEMs with PDADMAC as top layer.

To confirm the hypothesis of the mass removal, AFM measurements were performed on planar PDADMAC/PSS multilayers presenting PDADMAC as the topmost layer prior to (Figure 21a) and after treatment with ClO_4^- (Figure 21b).

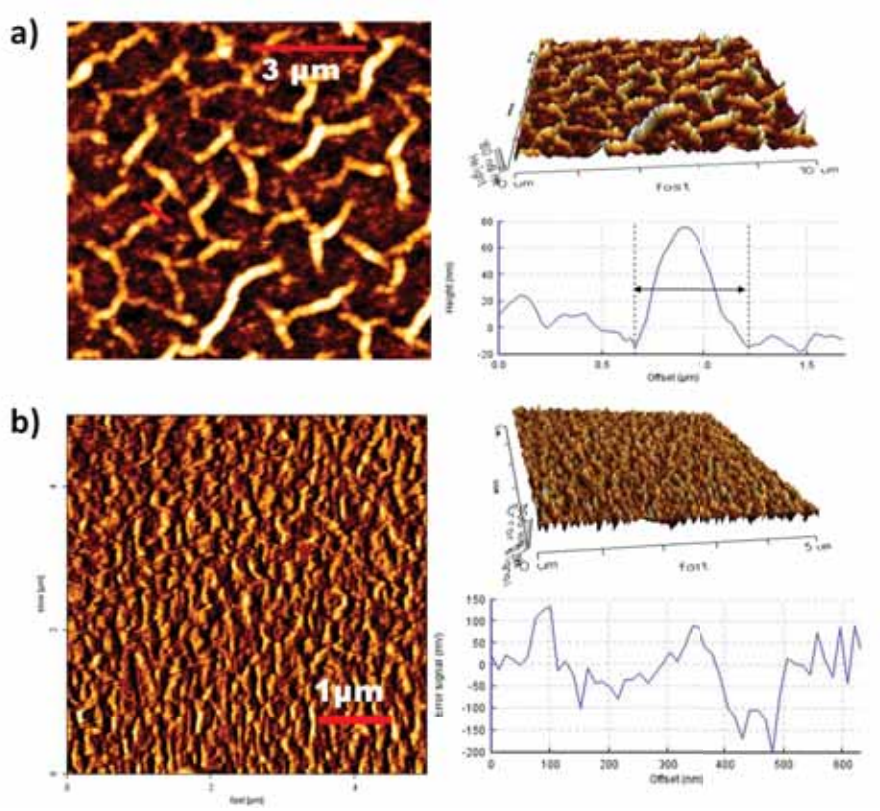

Figure 21 (a) AFM micrographs of PDADMAC/PSS 13 multilayered system before $LiClO_4$ treatment. (b) AFM micrographs of PDADMAC/PSS 13 multilayered system after $LiClO_4$ treatment.

Initially, the PDADMAC/PSS multilayer assembled, with 13 layers in total, showed a very high surface roughness in the presence of NaCl counterions. However, after treatment with 1 mol/L $LiClO_4$ (Figure 14b), the surface became flatter and much more homogeneous. The AFM image

is, indeed, very similar to the situation where PSS is the topmost layer (image not shown), which leads to conclude that PDADMAC has been removed from the surface either completely or partially. If so, this would be an evidence for the strong interaction of PDADMAC with perchlorate, which leads to film decomposition by replacing PSS with perchlorate.

In order to further determine how PEMs are influenced by ions appearing in the other extreme of the Hofmeister series, a shift to a cosmotropic salt such as KH_2PO_4 was done. Since it is known that the phosphate groups can interact with primary amines through hydrogen bonding. [23, 24-25] PAH/PSS multilayers presenting PAH as the topmost layer become the best example to repeat the QCM-D measurements (Figure 22). Such situation, however, does not take place in the case of PDADMAC due to the quaternary nature of the amino group that disables the formation of H-O-H bridges.

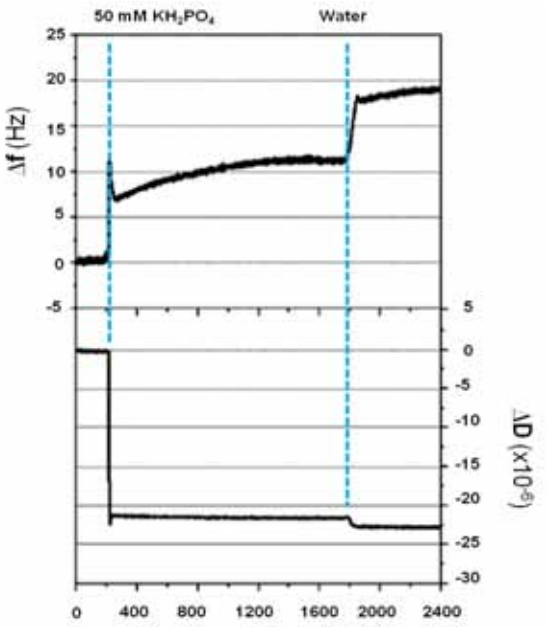

Figure 22 Frequency (top) and dissipation (below) changes for an 11 layer PAH/PSS film after treatment with 50 mM KH_2PO_4 and washing with water.

Figure 22 shows the changes in frequency of a PSS/PAH multilayer system consisting of 11 layers after exposure to 0.05 mol/L KH_2PO_4 and subsequent washing with water. A partial mass removal can be deducted in the presence of phosphate ions from a net increase in frequency toward positive values of around 9 Hz, while the frequency increase on the system after the deposition of the 11th layer of PAH was approximately 15 Hz. While an increase of the phosphate concentration had no effect, lower phosphate concentrations showed a slight frequency decrease indicating a mass increase, which is probably related to phosphate binding without desorption of PAH.

2.2.3. Electrophoretic behavior of Polyelectrolyte Multilayers

Measurement of the electrophoretic mobility becomes then a useful technique to complement QCM-D and AFM measurements showed above for the interaction between PEMs and different salts. The results obtained in the previous sections suggest that the charge density of the multilayers can be affected upon variations in the environmental ionic strength or the type of counterions. In this regard, PAH/PSS and PDADMAC/PSS coated silica particles, with either positive or negative outermost layers, were analyzed and compared by measurement of their ζ-potential.

The response in the ζ-potential as a function of ionic strength was measured for four different systems: PDADMAC/PSS and PAH/PSS multilayers with either 10 or 11 layer, which allow for comparison of the values obtained when having the polyanion or the polycation, respectively, on top of the film. The protocol followed was the same as for QCM-D measurements: colloidal samples were first exposed to solutions of increasing concentrations of NaCl, in order to determine the response of the spherical PEMs to an increasing ionic strength. Replacement of the Cl^- anions by ClO_4^- and $H_2PO_4^-$ was then done for a better understanding of those results showed in 1.2.2 section.

The results obtained for exposure of spherical PEMs composed of PAH/PSS polyelectrolyte pair to increasing ionic strength are shown in Figure 23.

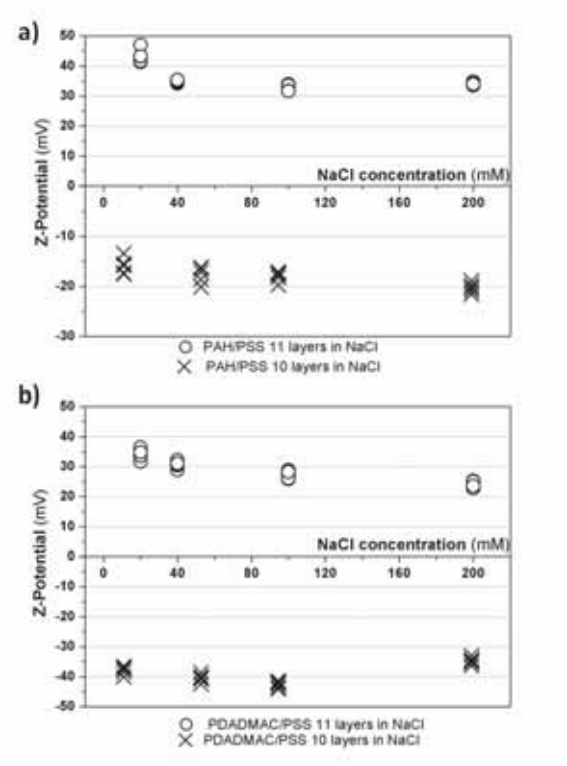

Figure 23 (a) ζ-Potential of PAH/PSS multilayered silica particles in the presence of NaCl as a function of the ionic strength for silica particles with 10 layers of PAH/PSS (with PSS as the outermost layer) and silica particles coated with 11 layers of PAH/PSS (with PAH as the outermost layer). (b) ζ-Potential of PDADMAC/PSS multilayered silica particles in the presence of NaCl as a function of the ionic strength for silica particles coated with 10 layers of PDADMAC/PSS (with PSS as the outermost layer) and 11 layers of PDADMAC/PSS (with PDADMAC as the outermost layer).

From Figure 23 it is noticeable that the value of the ζ-potential remains almost constant when the concentration of NaCl varies from 20 to 200 mM, around 30 mV for PAH/PSS multilayers (PAH as the outermost layer) and -15 to -20 for the PAH/PSS multilayers (PSS as the outermost layer). In a similar fashion, the PDADMAC/PSS coated particles show a ζ-potential of +30 and -40 mV for multilayers presenting PDADMAC and PSS as the outermost layer, respectively. Theoretically, instead of such constant trend, a 3-fold decrease would be expected because ζ-potential $\sim \Gamma^{1/2}$, but the soft and charged nature of the LbL film apparently permits the

reorganization of the polymer molecules in response to the increase of the ionic strength up to maximum values of 200 mM employed here.[26-27] The surface behaves more like a surface with constant potential rather than with constant charge. There are various possibilities of how this apparent charge regulation can be achieved. For example, if PAH is the top layer, increasing ionic strength results in a decrease in the pH near the layer surface. This should result in an increase of the protonation of PAH, and the surface charge should increase. However, the observed range of ζ -potential changes seems much too small to account for a substantial change in protonation. The pH cannot influence the degree of charge of PDADMAC or PSS around neutral or weakly acidic conditions. Therefore, we believe a more general mechanism than the change of the state of dissociation/protonation is at work. The effective surface charge density from the experimental values of the ζ-potential of Figure 23 was calculated applying equation 8:[27]

$$\sigma(c,\zeta) = \sqrt{8kT\varepsilon\varepsilon_0}\,\sinh\left(\frac{Ze_o\zeta}{2kT}\right) \quad (8)$$

where σ is the surface charge density, ζ is the zeta potential, k is the Boltzmann constant, T is the absolute temperature, ε is the relative permittivity, $\varepsilon 0$ is the dielectric constant, n is the number of ions per unit volume, c is the salt concentration, $e0$ is the charge of the electron, and z is the valence of the symmetric electrolyte (NaCl, z = 1). The influence of the curvature of the particles can be neglected, since the Debye length for the lowest ionic strength is still 50 times smaller than the particle radius.

In Figure 24a, the charge of PAH/PSS coated silica particles with 11 polyelectrolyte layers is presented as a function of the ionic strength. A linear increase of the electrophoretically effective charge density with ionic strength is observed.

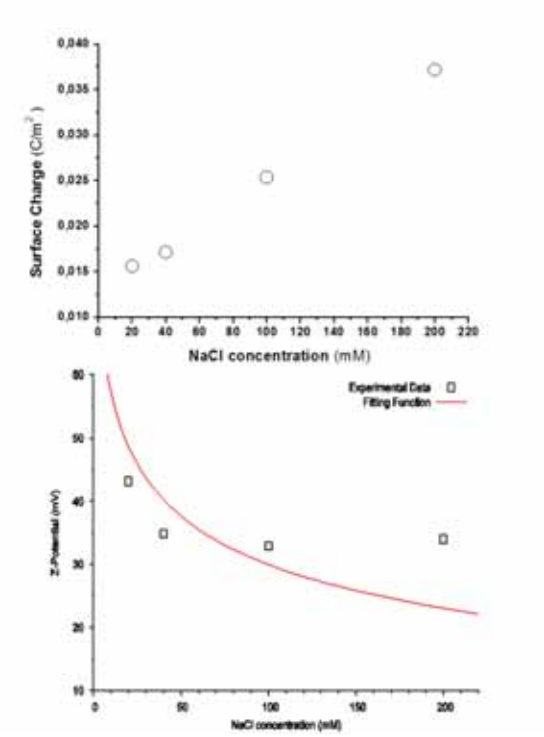

Figure 24. (a) Particle surface charge density as function of the ionic strength in NaCl calculated from the experimental ζ-potential values for silica particles coated with PAH/PSS 11 layers. (b) Comparison between experimental values of ζ-potential in NaCl (PAH/PSS 11 layers) and the theoretical potential function (constant charge model). The curve represents the "best" fit yielding a surface charge density of 0.019 C/m^2.

The failure of the constant charge model is obvious. The best fit according to constant charge density of the particles (equation 9) is widely off the experimental ζ-potential values (Figure 24b):

$$\zeta(c,\sigma) = \frac{2kT}{Ze_0} a\sinh\left(\frac{\sigma}{\sqrt{8kT\varepsilon\varepsilon_0}}\right) \quad (9)$$

Our conclusion was that in the case of polyelectrolyte multilayers the ζ-potential as a function of ionic strength follows a much weaker trend than expected for hard and smooth surfaces with constant charge density. The data of Figures 23 and 24, which show the response of the ζ-potential with NaCl, will be regarded as the reference for purely ionic concentration induced effects and will be compared with the specific effects of particular salts considered further below in this section.

In Figure 25, the changes of the ζ-potential for the four multilayer coatings considered in Figure 23 are plotted but in the presence of $LiClO_4$ instead of NaCl. The salt concentrations used are the same as those for NaCl ranging from 0.02 to 0.2 mol/L.

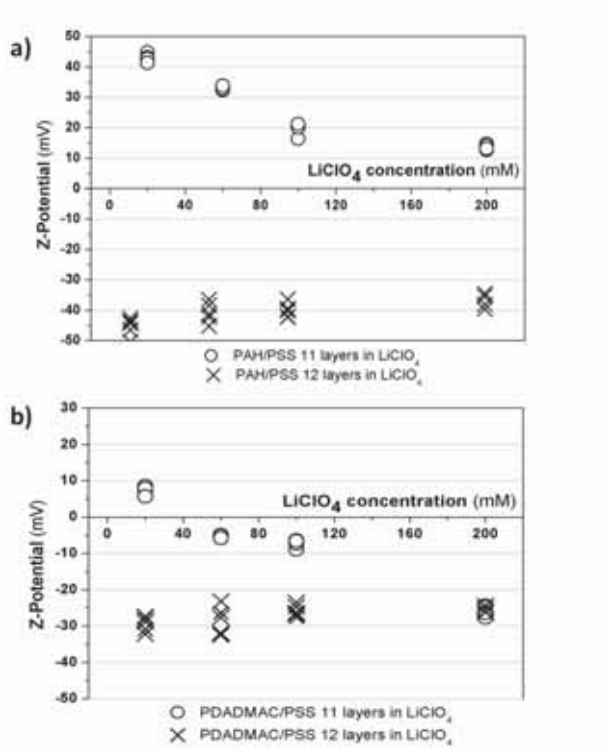

Figure 25 ζ-Potential of (a) PAH/PSS and (b) PDADMAC/PSS LbL silica particles in the presence of $LiClO_4$ as a function of the ionic strength.

For PSS as the outermost layer, both in combination with either PAH or PDADMAC, the ζ-potential remains almost constant over the concentration range from 0.02 to 0.2 mol/L and it can be considered to behave quite similar to the reference case of NaCl. For particles with PAH as the top layer, the ζ -potential curves show a different behavior from that observed in NaCl. The ζ -potential decreases more steeply with increasing salt concentration with variations of 5-10 mV between two immediate concentrations, from an initial value of + 50 mV for 0.02 mol/L $LiClO_4$ to approximately +10 mV in 0.2 mol/L $LiClO_4$. In the case of PDADMAC being the top layer, the ζ-potential shows a quite surprising behavior. At low ionic strength, the ζ-potential is slightly positive, but then the ζ-potential reverses and remains almost constant at negative values with further increase of the ionic strength. It is obvious that the interaction between the amino groups of both PAH and PDADMAC with ClO_4^- is responsible for this remarkable behavior.

As Figure 26 shows, for PAH being the top layer in $LiClO_4$, the surface charge density does not show a pronounced increase with increasing ionic strength. Indeed, the ζ-potential data can be reasonably well fitted with a model of constant charge, pointing toward the absence of the above-mentioned charge density regulation behavior observed in NaCl. To understand these data and those of PDADMAC, we have to make a few considerations.

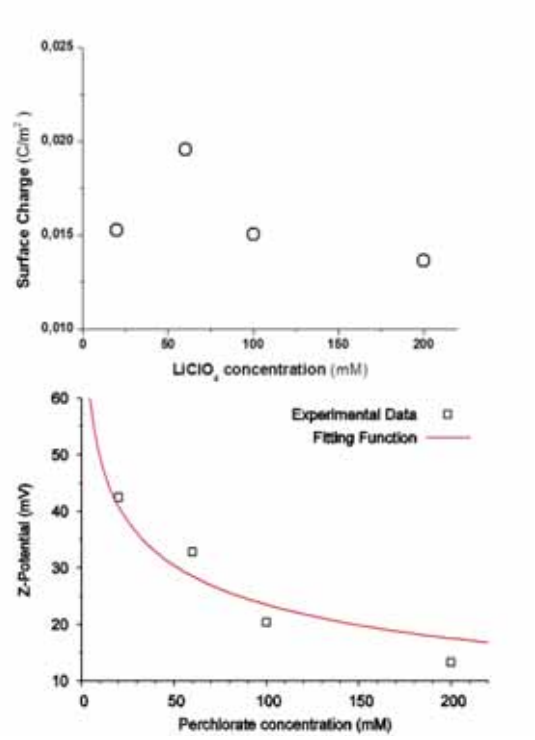

Figure 26 (a) Particle surface charge density as function of the ionic strength in $LiClO_4$ calculated from the experimental ζ-potential values for particles with PAH/PSS 11 layers (PAH is the top layer). (b) Comparison between experimental values of ζ-potential in $LiClO_4$ and the theoretical potential function calculated as the best fit from the calculated surface charge values for particles coated with PAH/PSS 11 layers. The best fit yields a surface charge density of 0.016 C/m^2.

Specific interactions between polyelectrolytes bearing quaternary ammonium groups and ClO_4^- reported for other systems[22] , as commented above, reflects in a change of hydration state of the monomers towards a more hydrophobic state when the counterions are replaced by ClO_4^- species. It could thus be that the screening of the quaternary ammonium groups of PDADMAC by perchlorate could induce similar changes. ClO_4^- ions are chaotropic and are featured by having their charge distributed over a relative large volume; also, they do not match well with the water structure and have a pronounced affinity for non-structured water over structured water. Besides, quaternary amines induce the formation of less structured water in their vicinity,

since they cannot form hydrogen bonds with water molecules. On the contrary, primary amines, as in the case of PAH, form hydrogen bonds with water molecules and have thus a positive effect on the water structure. Hence, it is understandable that ClO_4^- ions have a stronger affinity for the quaternary amines than for primary ones. The explanation for the charge reversal in the case of PDADMAC is thus a strong binding of the perchlorate to the quaternary amines promoted not only by electrostatic but also by entropic effects on the solvent. It cannot be excluded that perchlorate may break some attachment sites between PSS and PDADMAC, thus rendering the surface more negative by changing the balance between positive and negative charges in the multilayer. In fact, it is striking that the negative ζ-potential reached at the highest concentration of $LiClO_4$ drops to around -30 mV.

In presence of KH_2PO_4, particles coated with PSS/PDADMAC multilayers presenting PDADMAC as the outermost layer always displayed positive values of ζ-potential (Figure 27b), which was almost constant over the interval of applied concentrations. Again, the colloids with PSS as the outermost layer exhibited a similar behavior as well (both with PAH and PDADMAC as layer constituents).

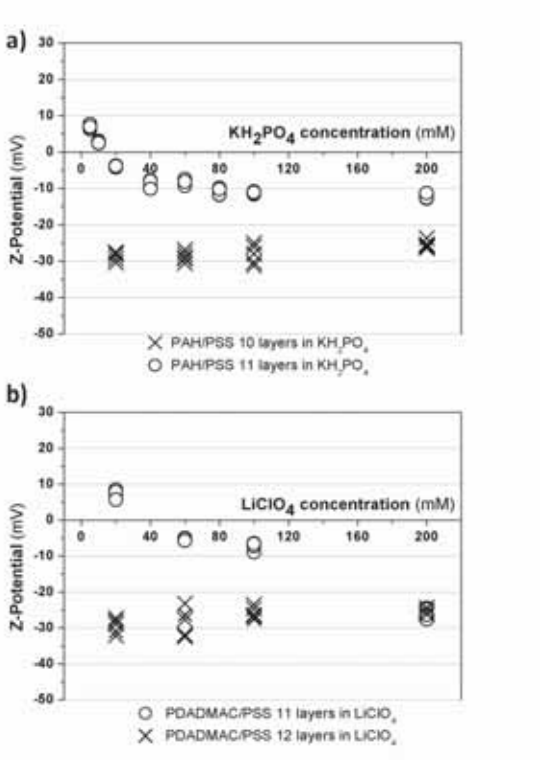

Figure 27 ζ-Potential of (a) PAH/PSS and (b) PDADMAC/PSS multilayered silica particles in the presence of KH_2PO_4 as a function of the ionic strength.

With PAH as the topmost layer, the ζ-potential value became, however, nearly zero at about 0.02 mol/L KH_2PO_4. At higher phosphate concentrations, the ζ-potential decreased toward even negative values of about -10 mV (Figure 27a). While phosphate groups can interact with primary amines through hydrogen bonding, conversely, hydrogen bonding interactions cannot take place with the quaternary amines. Phosphate anions thus are only able to screen the quaternary amine based surface charges as do the diffusive ion species, such as Cl^-. The recharging of the surface for PAH coated particles due to the interaction of $H_2PO_4^-$ with the amine groups of PAH can be explained as follows. Upon binding of the phosphate to NH_3^+, the charges are fully compensated, and the second OH of the phosphate groups may become deprotonated, forming a negative

charge at the amino-phosphate complex. Binding may also take place to uncharged amino groups through hydrogen bonding. It may also be that there is a compensation of the charges of the PAH by the phosphate and the few PSS charges in the top layer are partially responsible for the overall negative ζ-potential.

The reversibility of the changes observed in the ζ-potential was also tested through consecutive exchanges of the bulk solution. For instance, a potential of 28.8mV was originally measured for particles with PAH as the top layer in 0.1 M NaCl; after treatment with 0.1 M phosphate and dispersion in 0.1 M NaCl, the potential showed a value of 25 mV. The reversibility of the potential value clarifies the mass removal calculated from QCM-D results (Figure 22), which can be attributed to a water release induced by a densification of the layer, when forming phosphate-amine hydrogen bonds, and which can be inferred from the decrease of the ζ-potential with ionic strength. For PDADMAC coated particles, the potential in 0.1 NaCl was 14.8 mV; after treatment with perchlorate and dispersion in 0.1 M NaCl, the potential decreased to 5 mV. In the case of the PDADMAC coated particles, this reduction in the potential points to an irreversible change of the surface structure brought about by the interaction with perchlorate and confirms that shown by QCM-D and AFM measurements.

Finally, it is worth highlighting that for the case of PSS terminated films exposure to either $LiClO_4$ or KH_2PO_4, independently to the polycation taking part in the film, no significant effects were observed in the results from the ζ-potential when, respectively which is in agreement with QCM-D measurements.

2.3. Conclusions

This chapter has shown the effect that the nature of the counterion can have in the structure of PEMs. For instance, for PDADMAC/PSS multilayers with PDADMAC as top layer, variations in the ionic strength cause changes in thickness of >100 nm (~58%) and in the water content of about the 50%. The changes are reversible and the exchange of NaCl for water results in the re-swelling of the PEM to a thicker and more hydrated state. This behavior is comparable with the response of polyelectrolyte brushes and/or hydrogels to the ionic strength. When PSS is the top layer variations in the ionic strength up to 1 M NaCl do not induce changes in thickness and water content of the PEM. The choice of the last layer of the PEM provides then an easy option to tune the response of the PEM upon ionic strength variations.

The specific interaction between ClO_4^- and PDADMAC and $H_2PO_4^-$ and PAH in LbL multilayer systems has been also demonstrated. This interaction has a pronounced influence on the ζ-potential. Charge reversal takes place which is explained by the partial removal of polyelectrolytes from the top layer or charge compensation of the polyelectrolyte charge by the adsorbing ionic species. The driving forces for these interactions are ion specific. In one case (perchlorate/PDADMAC), entropic effects related to the solvent structure play a significant role. Phosphate, however, forms hydrogen bonds with primary amines.

2.4. References

(1) v. Klitzing, R.; Wong, J. E.; Jaeger, W.; Steitz, R. Curr. Opin. Colloid Interface Sci. 2004, 9(1-2), 158.

(2) Sukhorukov, G. B.; Schmitt, J.; Decher, G. Ber Bunsen-Ges 1996, 100, 948.

(3) Burke, S. E.; Barrett, C. J. Biomacromolecules 2003, 4, 1773.

(4) Mjahed, H.; Voegel, J.-C.; Senger, B.; Chassepot, A.; Rameau, A.; Ball, V.; Schaaf, P.; Boulmedais, F. Soft Matter 2009, 5, 2269.

(5) Wang, N.; Zhang, G.; Ji, S.; Qin, Z.; Liu, Z. J Membr Sci 2010, 354, 14.

(6) Dubas, S. T.; Schlenoff, J. B. Langmuir 2001, 17, 7725.

(7) Salomäki, M.; Kankare, J. Macromolecules 2008, 41, 4423.

(8) Miller, M. D.; Bruening, M. Chem Mater 2005, 17, 5375.

(9) Jiang, T.; Wu, J. J Phys Chem B 2008, 112, 7713.

(10) Tran, Y.; Auroy, P.; Lee, L.-T. Macromolecules 1999, 32, 8952.

(10) Jaber, J. A.; Schlenoff, J. B. Langmuir 2007, 23(2), 896.

(11) Salomäki, M.; Tervasmäki, P.; Areva, S.; Kankare, J. Langmuir 2004, 20(9), 3679.

(12) Hofmeister, F. Arch. Exp. Pathol. Pharmakol. 1888, 24(4-5), 247.

(13) Mermut, O.; Barret, C. J. J. Phys. Chem. B 2003, 107(11), 2525.

(14) Salomäki, M.; Laiho, T.; Kankare, J. Macromolecules 2004, 37(25), 9585.

(15) Kügler, R.; Schmitt, J.; Knoll, W. Macromol Chem Phys 2002, 203, 413.

(16) Glinel, K.; Déjugnat, C.; Prevot, M.; Schöler, B.; Schönhoff, M.; v. Klitzing, R. Colloids Surf A: Physicochem Eng Aspects 2007, 303, 3.

(17) Grieshaber, D.; Vörös, J.; Zambelli, T.; Ball, V.; Schaaf, P.; Voegel, J.-C.; Boulmedais, F. Langmuir 2008, 24, 13668.

(18) Schmidt, D. J.; Cebeci, F. C.; Kalcioglu, Z. I.; Wyman, S. G.; Ortiz, C.; Van Vliet, K. J.; Hammond, P. T. ACS Nano 2009, 3, 2207.

(19) Zahn, R.; Vörös, J.; Zambelli, T. Curr Opin Interface Sci 2010, 15, 427.

(20) Caruso, F.; Lichtenfeld, H.; Donath, E.; Möhwald, H. Macromolecules 1999, 32, 2317.

(21) Azzaroni, O.; Moya, S.; Farhan, T.; Brown, A. A.; Huck, W. T. S. Macromolecules 2005, 38(24), 10192.

(22) Fischlechner, M.; Zaulig, M.; Meyer, S.; Estrela-Lopis, I.;Cuellar, L.; Irigoyen, J.; Pescador, P.; Brumen, M.; Messner, P.;Moya S.; Donath, E. Soft Matter 2008, 4, 2245.

(23) Kovacevic, D.; van der Burgh, S.; de Keizer, A.; Cohen Stuart, M. A. J. Phys Chem. B 2003, 107, 7998.

(24) Kioussis, D. R.; Wheaton, F. W.; Kofinas, P. Aquat. Eng. 2000, 23, 315.

(25) Ibarz, G.; Dähne, L.; Donath, E.; Möhwald, H. AdV. Mater. 2001, 13(17), 1324.

(26) Donath, E.; Walther, D.; Shilov, V. N.; Knippel, E.; Budde, A.; Lowack, K.; Helm, C. A.; Möhwald, H. Langmuir 2007, 13(20), 5294.

Chapter 3:

Interaction of PEMs with surfactants

3.1. Introduction

PEMs are very stable, and, in general, resist high and low pH and temperature, conditions of high ionic strength and the action of surfactants.[1, 2] Indeed, for multilayer removal, relatively harsh conditions have to be applied. Standard treatments usually involve a TL1 (water:ammonia: hydrogen peroxide 5:1:1 at 85ºC) cleaning procedures or combined UV ozone oxidative radiation and bath ultrasonication in soapy solutions. There are, however, situations where it is desirable to dissolve the PEMs or just to remove a certain number of layers under mild conditions. For instance, when a controlled de-protection of a surface is intended because coating is worn and does not longer fulfill its function, or when a capsule wall has to be decomposed to release its content. In these cases controlled decomposition of the PEM coat under conditions not harming the support or the core would be a desirable option. This could be the case, for example, of a filtration membrane based on PEMs.[3-4] When the surface is no more functional due to foulant action, PEMs could be stripped off and afterwards replaced by fresh polyelectrolytes to regenerate the film.

Polyelectrolyte complexes and surfactants have many practical and industrial applications in detergency or as part of formulations in cosmetics, paints, and even food products.[5-7] Also, the interaction of surfactants with biological polyelectrolytes like DNA or proteins is a very important tool in the preparation, analysis, and encapsulation of biopolymers.[8-10] The interaction of polyelectrolytes with surfactants raises, from a physicochemical point of view, issues related to colloidal stability, conformational freedom of macromolecules, ordering in self-assembled

systems, etc.[11-14] Polyelectrolyte-surfactant complexes (PSC) themselves represent interesting self-assembled structures ranging from bead-like structures to polymer decorated elongated micelles/rods, nanoparticles, or surfactant bilayers,[15-20] controlled by electrostatic, hydrophobic, and entropic forces. The surfactants may determine the degree of order and the spatial arrangement of the polyelectrolyte molecules.[21-23] Polyelectrolyte-surfactant assemblies are applied in nanotechnology for the functionalization of surfaces,[24-25] for tuning surface wettabilities,[26] and for incorporation of antimicrobial agents.[27] PSC can be used as carriers for non-charged species, such as organic dyes and nanoparticles.[28] In most studies, PSC have been formed in solution from free polyelectrolyte molecules. Nevertheless, the interaction of surfactants with polyelectrolyte multilayer films has been investigated more seldom.[26, 28-29]

In this chapter, the interaction of the cationic surfactant N-tetradecyl trimethyl ammonium bromide (TTAB)[8, 30–31] at concentrations below and over the critical micellar concentration (CMC) with PEMs composed either of PSS together with PAH, or of PDADMAC with PSS is investigated by means of QCM-D technique. Such interaction takes place through the electrostatic interaction between the positive charge of the TTAB and the negatively charged PSS in the multilayer. The different response of PDADMAC/PSS and PAH/PSS multilayer films with regard to their stability to TTAB would be thus related to the strength of the amine-sulfonate interaction between polycation and polyanion. It will be shown that while poly(allyl amine hydrochloride) (PAH)/PSS films remain stable in the presence of TTAB, PDADMAC/PSS multilayers can be removed in a controlled manner. Then, the choice of the polyelectrolyte pair to form the multilayer makes possible to employ the interaction between the

surfactant and the polyelectrolyte for the selectively stripping off of individual polyelectrolyte layers.

Furthermore, the competition that takes place between the cationic surfactant, on one hand, and the polycation interacting with the polyanion, on the other hand, is an interesting issue to be analyzed that may depend on a variety of parameters. How the interaction between the two oppositely charged polyions is affected by the interfering surfactant is an unexplored subject. In the present section, polyelectrolyte complexes (PEC) produced by mixing polycations with polyanions are investigated both in solution and in the dry state. Bearing in mind the similarity of the PE multilayers with PE complexes, complexes of PDADMAC/PSS and PAH/PSS were used to study the interaction between PSS and TTAB, in the presence of the two mentioned polycations, by means of Raman microscopy and attenuated total reflection Fourier-transform infrared spectroscopy (ATR-FTIR). FTIR had already been successfully used to study the role of H-bridges and binding mechanisms in phospholipid/PE complexes.[32] Spectroscopic studies allow getting insight into the molecular mechanism, binding sites, and stoichiometry of the interaction in PSC. The role of the water and hydrogen bonds between the polycations and polyanions for the stability of polyelectrolyte complexes is also analyzed.

To conclude, at the final section of this chapter, how the PEMs will respond in the presence of TTAB when the PSS is facing PAH on one side and PDADMAC on the other side will be addressed. Combined or *hybrid* multilayers containing a first block of PAH/PSS, of variable thickness, and a second block formed by PDADMAC/PSS layers were assembled and exposed to TTAB in concentrations below and over the CMC. It will be shown that the presence of

PAH/PSS layers stabilize the PDADMAC/PSS on top, preventing it partially from removal. Such PEM composed of two blocks, where the block on top could be removed, would also be an interesting system to fabricate due to the multiple possible applications.

3.2. Results and discussion

3.2.1. Controlled stripping of PEMs

The growth of PEMs fabricated by means of the alternative assembly of PDADMAC and PSS, and of PAH and PSS, up to 9 total layers, was in situ monitored by means of QCM-D. The assembly was carried out by applying water rinses between each layer deposited. Thereby, the total change in frequency for the PAH/PSS film added up to approximately 140 Hz, while for a PDADMAC/PSS system with the same number of layers, the total change in frequency was about 220 Hz (data not shown). The optical mass and water content values corresponding to both systems can be obtained from figures 4 and 9, respectively, as shown in Chapter I.

PDADMAC/PSS and PAH/PSS multilayers were then exposed to solutions of TTAB of different concentrations, either below the CMC (0.1, 0.5 and 1 mmol/L), or above the CMC (5, 10 and 100 mmol/L) which were flushed over the PEMs in the QCM-D chamber. The frequency changes for 9 layers of PDADMAC/PSS with PDADMAC as the top layer caused by exposure to TTAB are shown in Figure 28a.

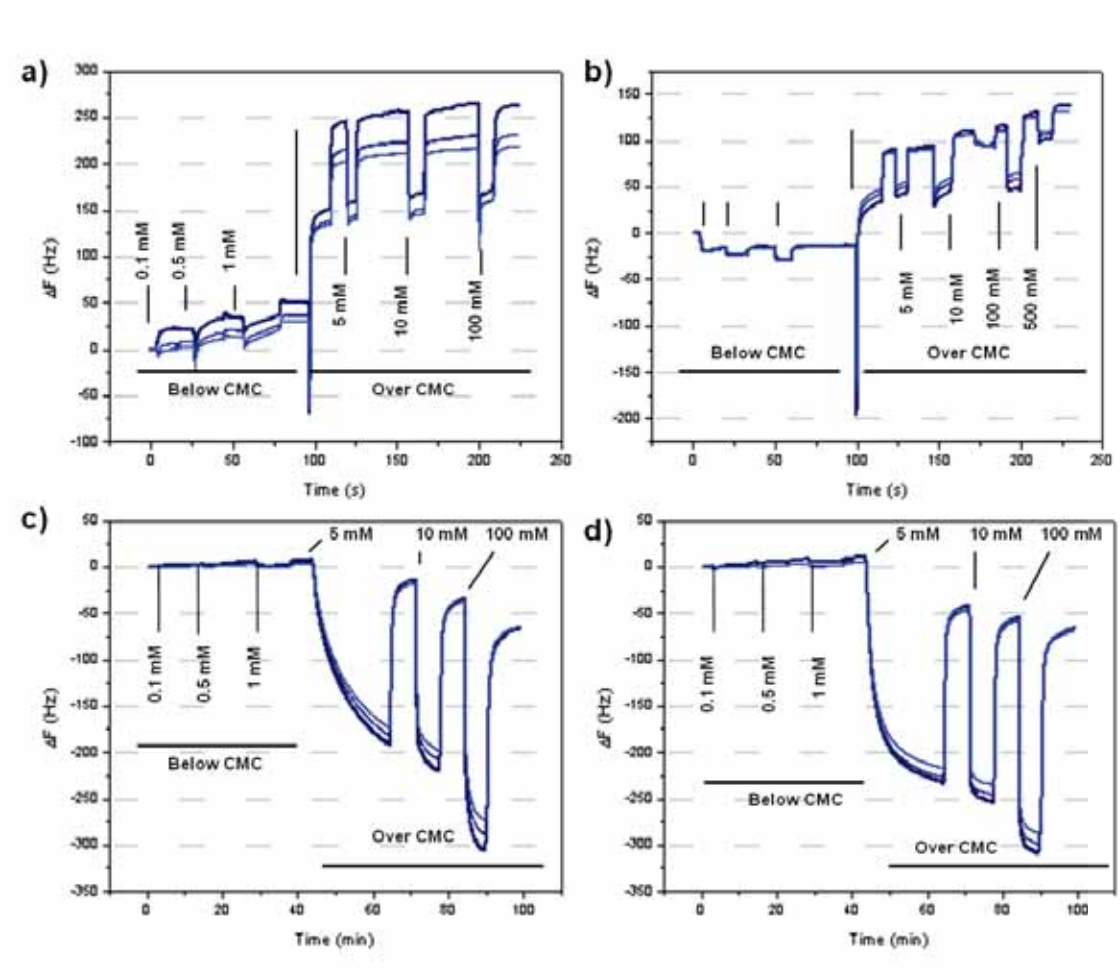

Figure 28 Frequency changes (3rd, 5th and 9th overtones) in presence of TTAB for a) 9 layers PDADMAC/PSS, b) 8 layers PDADMAC/PSS, c) 9 layers PAH/PSS, d) 8 layers PAH/PSS. In each figure concentrations below and above the CMC are indicated.

For the treatment with solutions below the CMC, positive frequency shifts from 20 Hz to 40 Hz can be observed. However, over the CMC the frequency shift is positive and corresponds to a value of 280 Hz which approximately compensates the frequency decrement resulting from the original deposition of the 9 layers. It can thus be concluded that the interaction with the surfactant at concentrations above the CMC has caused the removal of almost the entire PEM. In the case of PDADMAC/PSS multilayers containing 8 layers in total (Figure 28b), where PSS is

placed on top, the frequency shift corresponded to 140 Hz at the highest surfactant concentration of 100 mmol/L TTAB. This frequency change is consistent with a partial removal of the PEM which is attributed to a partially blocked access of TTAB to PDADMAC. It is noticeable that below the CMC the frequency decreased by approximately 20 Hz, corresponding to an increase of the deposited mass on the surface. This mass increase is explained by electrostatic interaction of the positively charged TTAB with the sulfonate groups of PSS. On the contrary, the interaction of PEMs composed of 9 or 8 layers of PAH/PSS with TTAB, as can be seen in Figure 28(c) and 28(d), respectively, resulted in a strong decrease of the frequency for TTAB concentrations above the CMC. This significant frequency decrease can be explained by deposition of TTAB micelles on top of PEMs. Flushing with water removed the micelles to a large extent, indicating relatively weak attachment of most of the adsorbed TTAB. Below the CMC the frequency remained almost constant.

The effect of TTAB on PAH/PSS multilayers thus differs considerably from the pattern of interaction with PDADMAC/PSS, indicating a stronger interaction between PAH and PSS than between PDADMAC and PSS. In the latter case, the positive TTAB, when interacting with the PSS in the multilayer, may substitute the PDADMAC quaternary ammonium group of the formed ionic pair between PDADMAC and PSS, which finally leads results in the removal of both PDADMAC and PSS. The fact that the removal of the PEMs by TTAB occurred only at concentrations above its CMC also deserves closer attention.

3.2.2. Spectroscopic analysis on the interaction

The spectroscopic Raman and IR studies of polyelectrolyte complexes interacting with TTAB will provide new insights in the interaction between PAH and PSS as well as between PDADMAC and PSS, and the interaction of the polyanion with TTAB quaternary ammonium surfactant. Infrared (IR) and Raman spectroscopy have both proved to be powerful tools to probe salt−polymer and polymer-polymer interactions by providing information in band positions, intensities, and band shapes through exploration of spectral changes of the characteristic functional groups in the polyelectrolytes. [33, 34]

The use of Raman spectroscopy allows for a rapid and nondestructive method which enables quantitative analysis of molecular interactions and *in situ* detection. An important advantage of Raman spectroscopy over FT-IR is that water does not cause interference and, consequently, Raman spectroscopy is more suitable for analyzing molecules in aqueous/humid environments (see *Materials and methods* section).

3.2.2.1. Stoichiometric composition of PE-PE complexes

As explained above, the quaternary ammonium surfactant TTAB can be expected to compete with polycations for the PSS binding sites. The number of free sulfonate groups and groups taking part in the interaction with the polycations depends in a straightforward way on the initial stoichiometric ratio of the complex forming constituents. The similarity of the PE multilayers with PE complexes, allows the measurement of complexes of PDADMAC/PSS and PAH/PSS by

Raman Spectroscopy to study the interactions between polyanion and polycation. Hence, complexes of PAH/PSS and PDADMAC/PSS were prepared at different molar ratios in 0.5 M NaCl. Stable complexes can exist only if one of the constituents has been added with a concentration in excess; otherwise, flocculation cannot be controlled. Because the competitive interaction with TTAB was in the focus of our interest, PSS was added in excess to obtain stable negatively charged polyelectrolyte complexes. In all subsequent experiments, the polyelectrolyte complexes were formed by mixing PSS with PAH in a ratio of either 3:1 or 5:1 (monomer/monomer), respectively. Because the stoichiometry of the formed complexes may not be identical to the applied monomer ratios, we first determined the stoichiometry of the complexes from analyzing the respective Raman spectra. The soluble excess of PSS, which has not been utilized for complex formation, was largely removed by the applied centrifugation/washing cycles while the complexes were retained and subsequently dried. The respective vibration spectra of PSS, PAH, PDADMAC, and the complexes of PAH/PSS and PDADMAC/PSS were recorded afterward. The spectra of PSS and PAH/PSS weighted on the integral intensity of the PSS aromatic band are shown in Figure 29a.

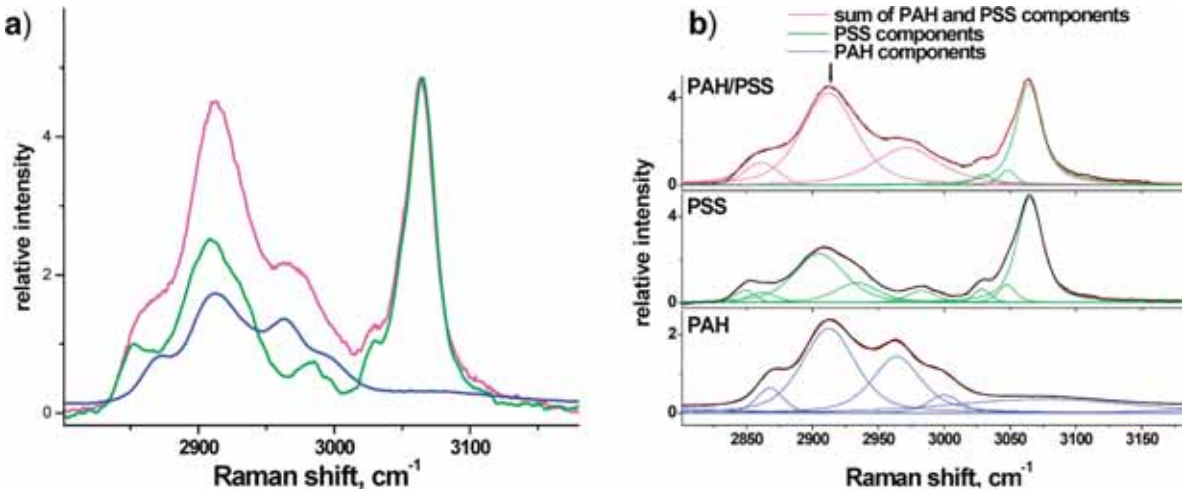

Figure 29 (a) Raman spectra of PAH/PSS (red), PSS (green), and their difference (blue) almost coinciding with the PAH spectrum. (b) Decomposition of the Raman spectra of PAH/PSS complexes and of PSS and PAH into components. The black line refers to the respective recorded spectra; the colored lines denote the fits, respectively.

The spectrum of the complex can thus be considered to be largely a superposition of its constituents. The spectra of the individual dry polyelectrolytes can be used to deconvolute the spectrum of the PAH/PSS complex. The contribution of the respective PAH and PSS components to the aliphatic band integral intensity with its center at $\nu_{as}{}^{CH2} = 2905$ cm^{-1} denoted by an arrow in Figure 29b was calculated from the spectrum decomposition. The Voigt function was used for fitting the spectra. It was found that the intensity ratio of the PAH and PSS CH_2 vibration bands is very close to 1:1. Therefore, it can be concluded that the stoichiometric ratio of the complexes was n_{PAH}:n_{PSS} = 1:2 [monomer/monomer], because PAH has two CH_2 groups per monomer, while PSS has only one CH_2 group per monomer. Almost identical spectra were obtained for the mixture of PAH and PSS regardless of whether the initial mixing ratio was 1:5 or 1:3. The stoichiometry of the complexes was thus independent of the initial proportions of polycations and polyanions, provided PSS was added in sufficient excess. The stoichiometry of

the PDADMAC/PSS complexes was obtained in the same way as for PAH/PSS. Figure 30 shows the spectra decomposition of the PDADMAC/PSS complexes and the spectra of the two components: PDADMAC and PSS.

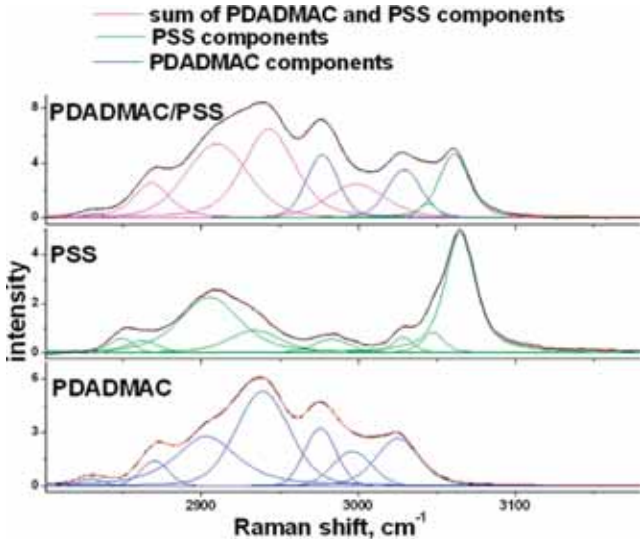

Figure 30 Raman spectral decomposition of PDADMAC/PSS complexes and their components. Black and colored lines denote the recorded spectra and their fits, respectively.

The ratio of PDADMAC to PSS was $n_{PDADMAC}$:n_{PSS} = 1:2,3 [monomer/monomer]. The stoichiometry of the complexes may depend on the conformational freedom of the polymers and on how well polycations and polyanions entangle together. Those charges, which are not compensated by the charges of the oppositely charged polyelectrolyte species, will be compensated by small counterions. The complexes formed with an excess of PSS can thus be visualized as being close to neutral in their interior, but negatively charged at their outer surface. These negatively charged sulfonic acid groups will serve as the binding sites for TTAB.

3.2.2.2. PSS-TTAB complexes

Prior to the study of the interaction between the complex and the surfactant, an analysis over the interaction between the quaternary salt and the polyanion is required as a reference.

The Raman spectra of TTAB in solution and the dry state are presented in Figure 31. The figure provides information on the C-C skeleton vibration in the frequency regime between 1040 and 1160 cm^{-1} and the C-H stretching modes of methylene and methyl groups in the range between 2700 and 3100 cm^{-1}.

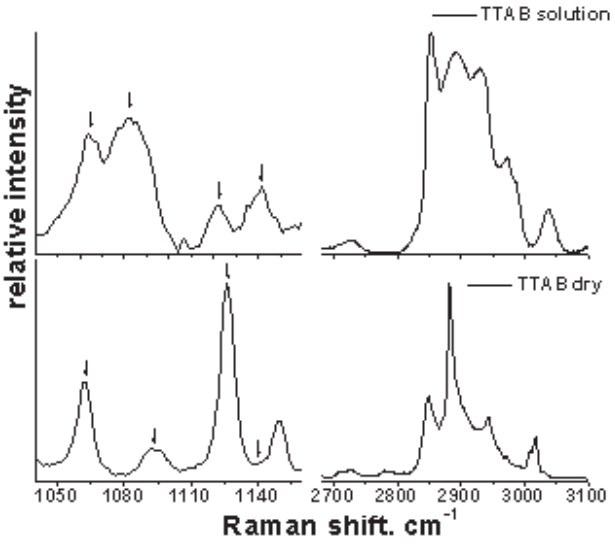

Figure 31 Raman spectra of TTAB in aqueous solution (top) and dry state (bottom).

The spectra of TTAB in solution reflect a typical micelle structure.[35] In the micellar phase, Raman spectra are dominated by broad bands similar to what is observed in hydrocarbon liquids.[36] The broad bands centered around 2890 and 2930 cm^{-1} are two Fermi resonance bands between the asymmetric CH_2 stretching band (2882 cm^{-1} for crystalline phase) and CH_2 bending overtones (2 × 1441 cm^{-1} and 2 × 1465 cm^{-1}). On the contrary, in the crystalline phase, the spectral bands of dry TTAB become sharp lines. In the C-C skeleton frequency region, the arrow marked bands (Figure 3) carry information about the conformation of the alkyl chain. The C-C stretching modes 1064 and 1123 cm^{-1} are assigned to the trans configuration of the alkyl chain, while C-C modes 1088 and 1140 cm^{-1} are responsible for *gauche* conformers.[36-37] The alkyl chains in the micelles exhibit a coiled liquid-like configuration with a similar amount of C-C bonds in trans and *gauche* conformation.[37] A strong reduction of the gauche conformers is observed in Figure 31 for the dry TTAB, indicating that the surfactant molecules arrange in a crystal lattice.

As explained above, TTAB forms complexes with PSS. Then, the Raman spectra of PSS/TTAB complexes were measured at different TTAB mole fractions in PSC. The spectra of dry TTAB/PSS complexes for TTAB percentages ranging from 0% to 67% are plotted in Figure 32a. Centrifugation/washing cycles were used to remove unbound TTAB micelles from the complexes. While in the dry state free TTAB is in a crystalline state, a coiled liquid-like phase was observed for bound TTAB in dry PSC. The spectra were normalized using the PSS band at 1600 cm^{-1} ($\nu(CCH)_{ringquadrant}$) as the reference band, because it does not overlap with the spectra of TTAB.

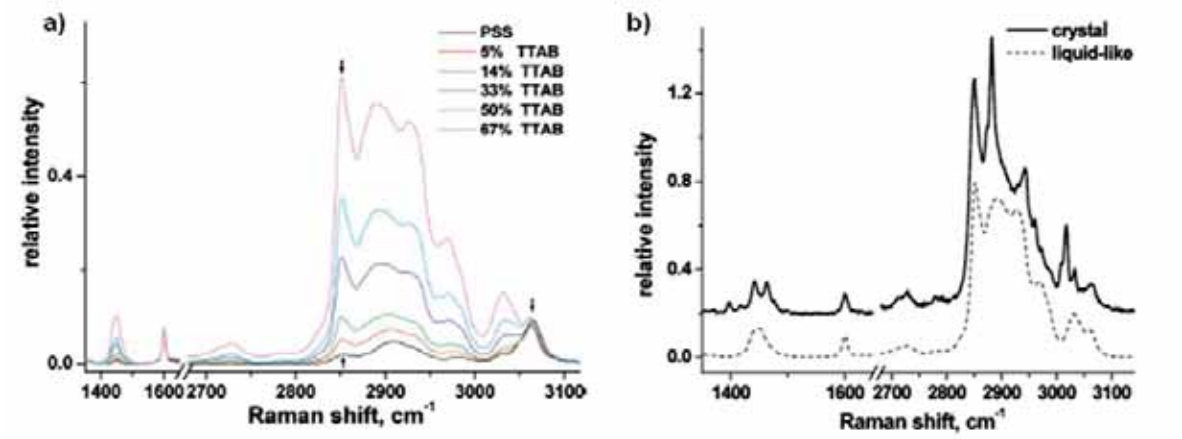

Figure 32 (a) Raman spectra of dry PSS/TTAB complexes at different surfactant mole fractions. (b) Phase transition of the PSS-bound TTAB from liquid-like to crystal phase at a surfactant mole fraction of 67%.

The increase in the intensity of the TTAB band, ν_s(CH2)) 2850 cm^{-1}, with increasing surfactant mole fraction can be clearly observed in Figure 32a. At a TTAB mole fraction of 67% in PSC, which corresponds to 2 TTAB molecules per 1 PSS monomer, a transition from a coiled liquid-like alkyl chain configuration of the PSS associated surfactant to a crystalline phase was detected (Figure 32b). The presence of a phase transition follows from the splitting into several peaks of the bands corresponding to the CH bending region (around 1450 cm^{-1}) and the appearance of sharp peaks in the stretching region. The two bands, a *trans* band at 1064 cm^{-1} and *gauche* band at 1088 cm^{-1}, were chosen to estimate the decrease of *gauche* conformers of PSS-bound surfactant at the phase transition since these bands do not overlap with PSS bands. The ratio of the integral intensity of the chosen bands for bound TTAB corresponds to that of free TTAB in both phases. It can be thus concluded that the coverage of PSS by TTAB becomes saturated at this molar ratio. One can assume that a following increase of the TTAB mole fraction in the

complexes leads to the growth of the crystalline phase of surfactant, which is not associated with PSS. From these considerations follows that two TTAB molecules bind to every sulfonic acid group of the side chain of PSS. One TTAB molecule compensates with its quaternary ammonium group the negative charge of the sulfonate group. If the second TTAB molecule would also interact with its head group with the sulfonate group, the resulting complex would be rather hydrophobic. This situation would be also unfavorable from an electrostatic point of view. Therefore, it can be proposed that the second TTAB molecule associates with its chain to the chain of the already bound first TTAB molecule in an anti-parallel fashion. A scheme of the proposed arrangement of PSS and TTAB molecules is shown in Figure 33.

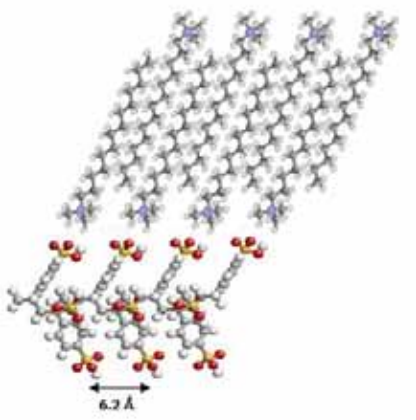

Figure 33 Side-view of the PSS/TTAB complexes. The red, yellow, blue, gray, and light gray balls correspond to O, S, N, C, and H atoms, respectively.

The hypothesis of two molecules of surfactant per monomer of sulfonic acid is confirmed by molecular considerations since the distance between two sulfonic acid side chains along the axis

of the molecule has been calculated to be about 6.2 Å.[38] Such a distance would be sufficient to accommodate two TTAB molecules.

The spectra of the TTAB/PSS complexes have been decomposed to separate the contribution of TTAB from PSS. Three bands denoted in Figure 32a by arrows, the symmetric CH2 stretching band of TTAB at 2850 cm^{-1}, and the corresponding band of PSS located at 2853 cm^{-1}, as well as the aromatic PSS band at 3064 cm^{-1}, were selected for calculating the TTAB content in the PSC. The contribution of the symmetric CH2 stretching components from PSS and TTAB cannot be separated. Therefore, the sum of both was used in the following calculation of the relative contribution of TTAB (*I*rel(TTAB)) to the spectra of the complex:

$$I_{rel}(TTAB) = \frac{\left[I_{TTAB}(\nu_s(CH_2)) + I_{PSS}(\nu_s(CH_2))\right]}{\left[I_{PSS}(\nu_{aromatic}(CH))\right]} = A + \frac{I_{TTAB}(\nu_s(CH_2))}{I_{PSS}(\nu_{aromatic}(CH))} \quad (10)$$

where A is a constant and $I_{TTAB}(\nu_s(CH_2))$, $I_{PSS}(\nu_s(CH_2))$, and $I_{PSS}(\nu_{aromatic}(CH))$ are integral intensities of symmetric CH2 stretching components from TTAB, PSS, and the aromatic band of PSS, respectively. The relative TTAB intensity was plotted as a function of the TTAB mole fraction in the complexes in Figure 34.

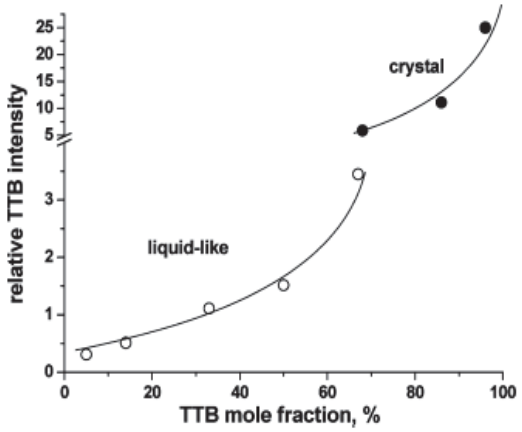

Figure 34 Relative TTAB intensity as a function of the TTAB mole fraction for the two phases: liquid-like (○) and crystal (●).

Two different branches can be observed in the plot depending on the phase state of TTAB: one at high TTAB mole fractions corresponding to the crystal phase and one related to the liquid-like phase at lower TTAB contents. This curves will be used further below as calibration curves for the quantification of the amount of TTAB bound to PSS/PDADMAC and PSS/PAH complexes. This is possible because the binding of TTAB to the complexes occurs only with PSS.

3.2.2.3. Interaction between TTAB and PE Complexes

TTAB was added to PAH/PSS and PDADMAC/PSS complexes at different concentrations given below as molar ratios of TTAB per PSS monomers in complexes: molar ratio (r) = n^{TTAB}:n^{PSS} [molecule:monomer]. Centrifugation/washing cycles were again used to remove unbound TTAB. Figure 35 presents the spectra of dry PAH/PSS complexes with TTAB at different relative molar ratios, K, of TTAB. K is defined as the relative molar ratio

$$K_i = \frac{r_i}{r_{\max}} = \frac{n_i^{TTAB}}{n_{\max}^{TTAB}}, \quad (11)$$

where the index “max” denotes the maximum surfactant concentration used in the experiment. *K* is a normalized molar ratio, which describes the increase of the surfactant mole fraction from *K*= 0, corresponding to polyelectrolyte complexes without surfactant, to *K*= 1, corresponding to the maximum surfactant concentration. The spectra of the PSC were normalized using the PSS band at 1600 cm^{-1}.

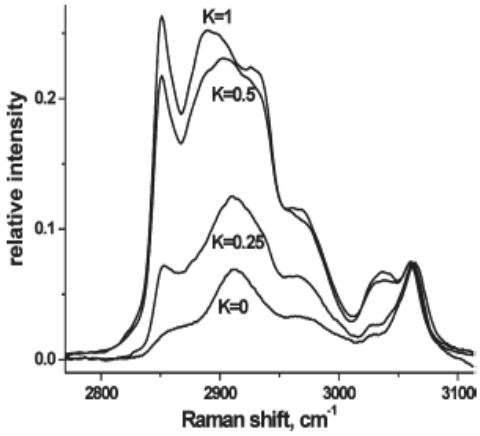

Figure 35 Raman spectra of dry PAH/PSS complexes with TTAB at different surfactant molar factors, *K*. Value *K* = 0 corresponds to PAH/PSS complexes without TTAB.

Figure 35 shows that the integral intensity of the surfactant band *v*s(CH2) = 2850 cm^{-1} steeply grows with increasing TTAB molar factor up to a *K* value of 0.5. Further increasing the TTAB concentration up to *K* = 1 increased the intensity of the CH2 stretching band only slightly. From such behavior can be deducted that the amount of bound TTAB molecules to the polyelectrolyte complexes saturates with an increasing molar ratio of TTAB to PSS in the complex.

Figure236 shows the spectra in the C-H stretching region for the two different PE complexes with and without TTAB.

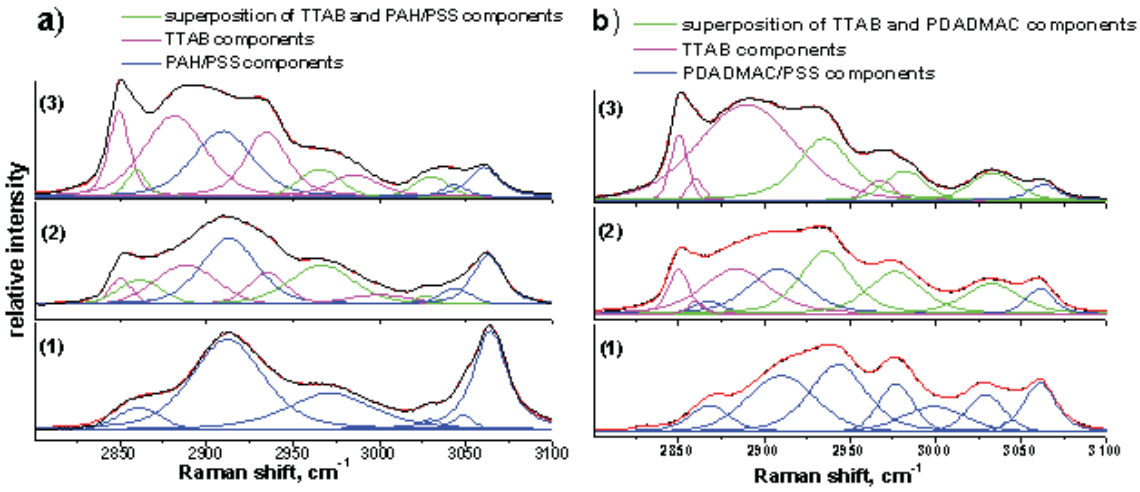

Figure 36 (a) Raman spectra of PAH/PSS without (1) and with surfactant at TTAB molar fractions of 25% (2) and 53% (3); (b) Raman spectra of PDADMAC/PSS without (1) and with surfactant at TTAB molar fractions of 33% (2) and 66% (3). The black and red lines denote the recorded spectra and their fits, respectively. The green bands are the superposition of TTAB and PE complexes spectral components, which have the same spectral location.

The mole fraction of TTAB bound to the PSS in PE complexes has been determined using the spectral decomposition and the calibration curve provided in Figure 34. It is noticeable that the TTAB band intensity at $\nu_s(CH_2)$ = 2850 cm^{-1} grows while the $\nu_{aromatic}(CH)$ = 3064 cm^{-1} band of PSS decreases with increasing TTAB molar fractions. The saturation of the surfactant binding for the two complexes, PAH/PSS and PDADMAC/PSS, is quantified in Figure 37. It displays the fraction of TTAB bound to the polyelectrolyte complexes as a function of the TTAB molar factor.

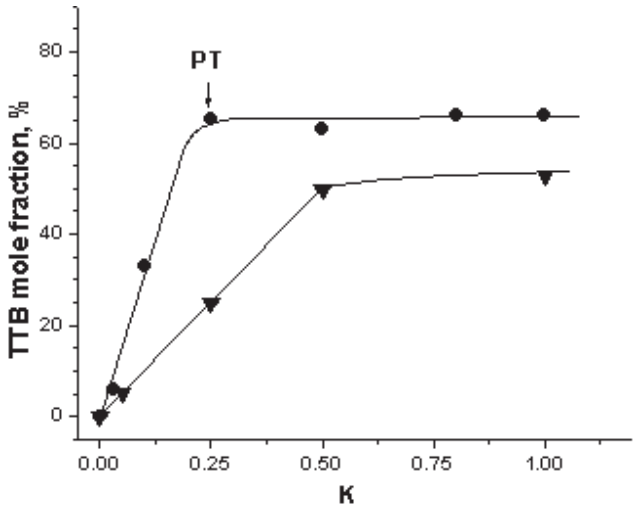

Figure 37 Saturation of surfactant binding to PSS in PAH/PSS (▲) and PDADMAC/PSS (●) complexes. The phase transition region is indicated by the arrow for PDADMAC/PSS complexes.

The most interesting finding is that the TTAB saturation on PSS in PAH/PSS and PDADMAC/PSS complexes was reached at molar fractions of 50% and 67%, respectively. A saturation value of 50% corresponds to one surfactant molecule per one PSS monomer in the PAH/PSS complex. Taking into account that the stoichiometry of the PAH/PSS complex was 1:2 and that the complex remains stable, it follows that only every second sulfonate group can serve as a potential binding site for TTAB. The surfactants bound to PSS in PAH/PSS complexes furthermore reveal a coiled liquid-like spectrum but a phase transition does not occur. For the PDADMAC/PSS complex, the situation is quite different. The TTAB molar fraction reaches a plateau at 67%, which corresponds to the binding of two surfactant molecules to each PSS monomer. As in the complex with PDADMAC roughly every second sulfonate group is utilized for the binding of PDADMAC, this would mean that about 4 TTAB molecules bind to a free PSS monomer in the complex. Therefore, the only possibility to explain the binding ratio is that the PDADMAC/PSS complexes become disassembled by TTAB and the observed 2:1 ratio

corresponds to binding of TTAB to free PSS (Figure 33). Furthermore, when the surfactant threshold is reached (see arrow in Figure 37), a phase transition to the crystalline phase occurs. This corresponds to the same TTAB mole fraction of about 67% as in TTAB/PSS complexes. The spectral features of surfactant bands in the crystalline phase are identical to those of TTAB/PSS complexes (Figure 32b). This similar behavior provides further evidence for the disassembling effect of TTAB, when interacting with PDADMAC/PSS complexes.

Because, on the contrary, PAH/PSS complexes remained stable, it can be concluded that the interaction of TTAB with PSS is stronger than the interaction of PSS with PDADMAC, but weaker than the interaction of PSS with PAH. This finding is consistent with the observation that TTAB is able to decompose polyelectrolyte multilayers composed of PDADMAC/PSS but not those consisting of PAH/PSS (see section 3.2.1). The head groups of the TTAB are quaternary amines, being the same as the charged sites in PDADMAC. Consequently, the electrostatic part of the interaction between TTAB and the sulfonic acid groups in PSS has to be similar in strength to the interaction of latter with the quaternary amines of PDADMAC. In this case, sterical considerations may play an additional role for the dissembling. The comparatively small TTAB may possibly get direct access to each monomer of the PSS, while the PDADMAC/PSS interaction may suffer from conformational constraints. PAH/PSS complexes remained stable upon addition of TTAB, which confirms data obtained by measurements with polyelectrolyte multilayers explained above. The PAH charges are provided by primary amines, which interact with the sulfonic acid groups. This interaction is obviously stronger than that with the quaternary amines of TTAB. This is consistent with the behavior of PE multilayers, where it has been evidenced that the PAH/PSS multilayers have a stronger interlayer interaction than

PDADMAC/PSS multilayers.[39-40] The question, however, remains: why the interaction of primary amines with the sulfonic acid is stronger than that of the quaternary amines with the sulfonic acid? To better understand the nature of these interactions, the influence of water on the TTAB-polyelectrolyte interaction should be studied in a more systematic way.

3.2.2.4. Role of Water

The stronger affinity between primary amines born in the repeating units PAH chains and sulfonate groups from negatively charged PSS insinuate the existence of binding forces of different nature to those barely electrostatic. In this regard, FTIR has already been proved as a useful tool to study the role of hydrogen-bridges and binding mechanisms in systems involving polyelectrolyte complexes[32] through analysis of the band position of those groups driving the electrostatic interaction and the appearance of red shifts upon molecule assembly, which are unequivocal indications of the presence of hydrogen bonds.

Since the sulfonate group of the PSS is sensible to humidity, its vibrational band responses can be analyzed by ATR-FTIR at different humidities, as shown in Figure 38.The assignments for the different vibration modes of the sulfonate group, $\nu_s(SO_3^-)$, $\nu_{as}(SO_3^-)$ and $\nu(SO_2)$, can be then compared to values predicted by literature.[41-43]

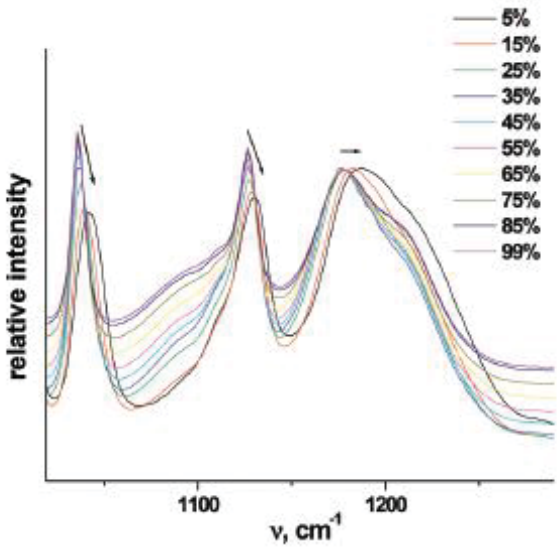

Figure 38 ATR-FTIR humidity scans of PSS decreasing the relative humidity from 99% to 5%.

Decreasing the water content induced a blue shift of the vibrational bands $\nu_{as}(SO_3^-)$ from 1177 to 1187 cm^{-1}, $\nu_s(SO_3^-)$ from 1039 to 1045 cm^{-1}, and $\nu(SO_2)$ from 1128 to 1133 cm^{-1}. The arrows denote the blue shift in Figure 38. This is the typical dehydration behavior of groups that are forming hydrogen bonds with water. The same blue shift upon dehydration was seen when the Raman spectrum of the dry state was compared to the spectrum in solution.

In Figure 39 the maxima of the Raman $\nu(SO_2)$ and the $\nu_s(SO_3^-)$ vibrations bands in the dry state have been plotted as a function of the mole fraction of TTAB for mixtures of TTAB with PSS, PSS/PAH, and PSS/PDADMAC complexes.

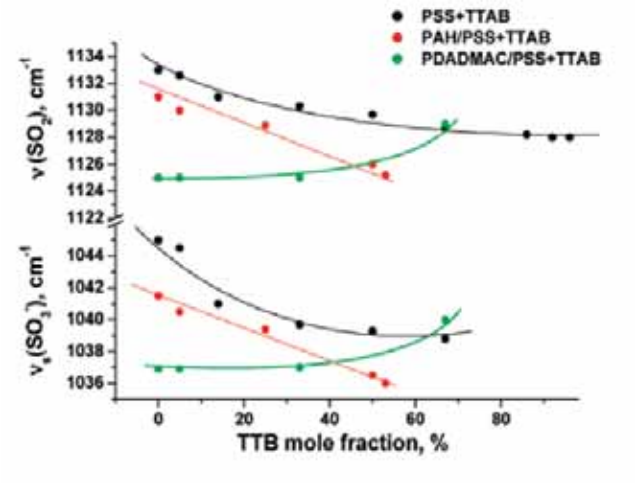

Figure 39 Maxima of the vibrational frequencies corresponding to the sulfonate groups as a function of TTAB mole fraction for PE complexes with surfactant recorded by Raman in dehydrated state.

The major finding in the plot above was that the addition of TTAB reverses the characteristic dehydration-induced blue shift of PSS. For example, in the case of PAH/PSS complexes, the blue shifting even becomes overcompensated. On the other hand, PDADMAC/PSS complexes in the presence of low to medium fractions of TTAB keep vibrational frequencies in almost constant values, but at saturation molar fractions of about 67%, the frequency increased to values corresponding to the case of free PSS, which is again associated with the disassembly of the complex by TTAB. In Figure 40 the values of the $\nu(SO_2)$ and $\nu_s(SO_3^-)$ for PSS, PSS/PDADMAC, PSS/PAH, alone, or with TTAB (saturation region) are compared for the dry and the fully hydrated state.

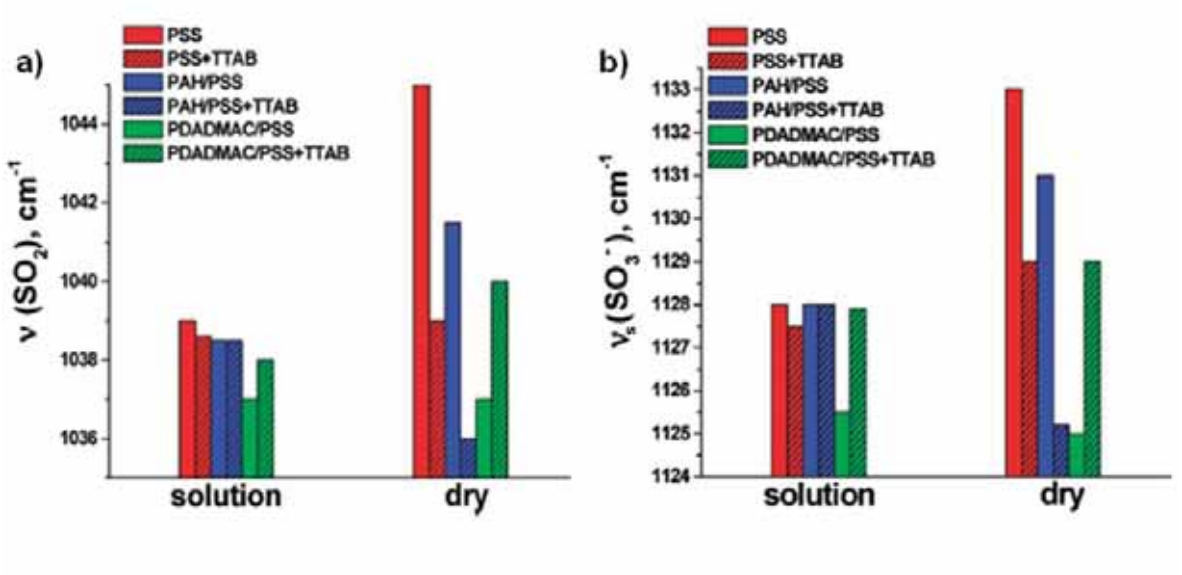

Figure 40 The sulfonate frequencies bar diagram in hydrated and dehydrated states for PSS and its complexes with polycations, in the presence and absence of TTAB. The surfactant mole fraction was 67% where saturation occurs.

A frequency decrease with the growing surfactant concentration can be observed for PSS and PAH/PSS complexes. In case of dry PSS/TTAB complexes, it is remarkable that they display the same frequency as if the complex would be in the hydrated state, $\nu_s(SO_3^-)$ = 1039 cm^{-1} and $\nu(SO_2)$ = 1128 cm^{-1}. Therefore, it can be concluded that the quaternary ammonium ion from the surfactant carrying three methyl groups excluded water from the sulfonate group, rendering its frequency independent of the state of hydration.

Then, Figure 40 allows for comparison of the degree of dehydration of the different complexes. For the PAH/PSS complex, the dehydration effect resulted remarkably smaller than for PSS alone. Therefore, it is supposed that the binding of PAH and PSS removes some water from the sulfonate group by forming hydrogen bonds between the primary amines and the oxygens of the sulfonate. This extra interaction on top of the electrostatic interaction may contribute to the

exceptional stability of the PAH/PSS interaction sites. This would be a remarkable point, because the PAH/PSS multilayer system is one of the most studied multilayers and has been considered as the characteristic example for electrostatic interaction as the basis for multilayer assembly. Another interesting finding is that in the presence of TTAB in PAH/PSS complexes, the observed vibrational frequencies of the sulfonate groups in the dehydrated state are lower than in the hydrated state. This behavior is opposite to the one observed for the complex without TTAB. It is supposed that the interaction of TTAB with PSS removes water from sulfonate groups. This may cause a change in the conformation of the PAH/PSS complex, because the sulfonic acid groups become more hydrophobic, when the sulfonic acid charge is compensated by TTAB. It is possible that as a result of these conformation changes certain topological restrictions are overcome, and some sulfonate groups may get closer to the primary amino groups of the PAH. This situation could result in the formation of additional hydrogen bonds between the amino groups of PAH and sulfonic acid groups, which have not been close enough to each other before surfactant addition. This would explain the comparatively small frequency in the dry state. The addition of TTAB thus would induce a stronger interaction between PAH and PSS.

From Figure 40 it can also be seen that for PADMAC/PSS complexes, the dehydration had no effect on the vibration frequencies of the sulfonate groups. The quaternary ammonium ion carries three methyl groups generating a hydrophobic environment for the sulfonic acid groups. It is thus quite conceivable that the quaternary amine replaced water molecules from the sulfonate group and prevents the formation of hydrogen bonds. Therefore, the vibrational properties of the

sulfonate group in the PSS/PDADMAC complex become independent of the state of hydration. This behavior is very similar to the interaction of PSS with TTAB as discussed further above.

3.2.3. Interaction of TTAB with hybrid multilayers.

While PAH/PSS interaction has been proved to remain unaltered upon exposure to TTAB surfactant, PDADMAC/PSS bonding, on the contrary, is disrupted. Then, what would happen in the case of PSS "sandwiched" between a PAH layer and a layer of PDADMAC? Would this make possible to control/limit somehow the degree of removal for a multilayer treated by the cationic surfactant? The idea of building a PEM composed of an initial block of PAH/PSS and a second block of PDADMAC/PSS, which could be removed, would be regarded as a very interesting system attending to its potential applications. For instance, the combination of PAH/PSS and PDADMAC/PSS blocks could be extremely useful in those cases when the membrane is no longer functional due to foulants actions and has to be removed. In such a case the top layer could be removed without dismantling the whole membrane and hence the removed layers could be easily replaced by new and foulant-free layers of PDADMAC/PSS.

QCM-D was employed to follow in situ the assembly of hybrid PEMs composed of a first block of PAH/PSS with a second block of PDADMAC/PSS on top of it. Two different hybrid systems, based on the number of PAH/PSS layers acting as support, were assembled: first, one PEM based on a single PAH/PSS bilayer followed by deposition of PDADMAC/PSS layers and, as

comparison, a second system where the build-up starts by assembling two PAH/PSS bilayers and then several PDADMAC/PSS layers. For the hybrid PEM containing a single bilayer of PAH/ PSS (Fig. 41a), the total frequency variation measured after the assembly was -440 Hz, which corresponds to a total mass, including the mass of trapped water, of 7.9 μg/cm^2 as obtained by Sauerbrey equation.

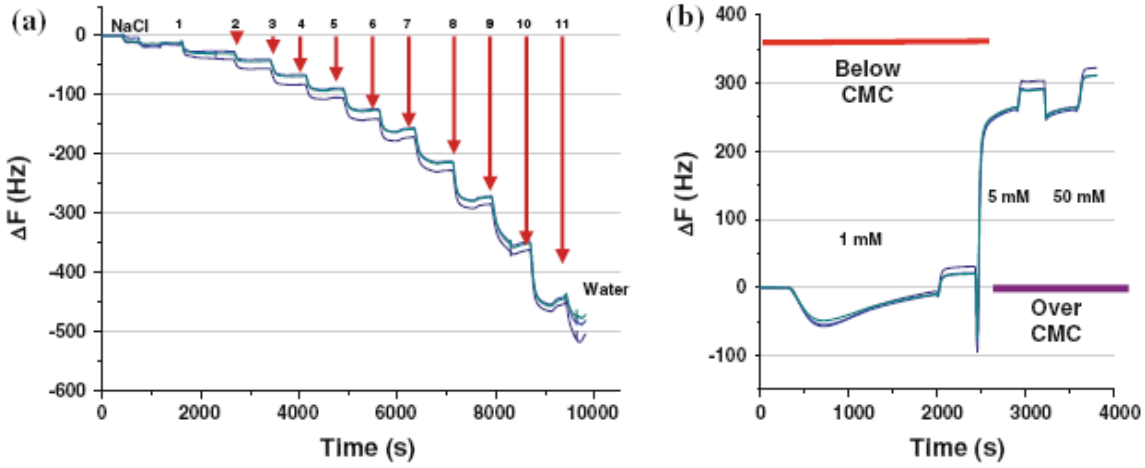

Figure 41 Frequency changes as measured by QCM-D of the 3rd, 5th, and 7th frequency overtones for (PAH/PSS)/(PDADMAC/PSS)$_4$/PDADMAC multilayer system: (a) frequency changes during the assembly of the PEM. (b) Frequency changes during TTAB treatment.

Figure 41b shows the response of this multilayer when flushing through the chamber TTAB solutions of concentrations going from below to over the CMC. While the treatment with 1 mM TTAB did not show any specific response, exposure to 5 mM TTAB induced a sudden frequency increase of about 290 Hz due to a mass loss on the surface. Increasing TTAB concentration led to a final shift of +310 Hz, which corresponds to a mass desorption of 5.7 ± 0.1 μg/cm^2. This meant that all the layers from the 7th to the 11th are completely erased or, in other words, that two-thirds of the mass deposited during the assembly were removed from the PEM. The mass of

the remaining layers corresponds to the initial PAH/PSS bilayer and a PDADMAC/PSS polyelectrolyte bilayer. If we compare this result to that from sole PDADMAC/PSS layers, we can see how the presence of PAH/PSS bilayer below the removable layers makes them more stable than in the previous case. If, instead of nine layers of PDADMAC/PSS, the assembly proceeded until two, four, or six layers, the amount of polyelectrolyte removed was none, or just a bilayer or two bilayers, respectively (data not shown). The PDADMAC/PSS layer directly on top of PAH/PSS seems not to be removable in any case.

To study how the thickness of the PAH/PSS multilayer affects the stability of the PDADMAC/PSS on top, a thicker initial block based on a double bilayer of PAH/PSS was assembled followed again by deposition of a PDADMAC/PSS block on top up to 11 layers. Figure 42 shows the response upon surfactant treatment measured by QCM-D.

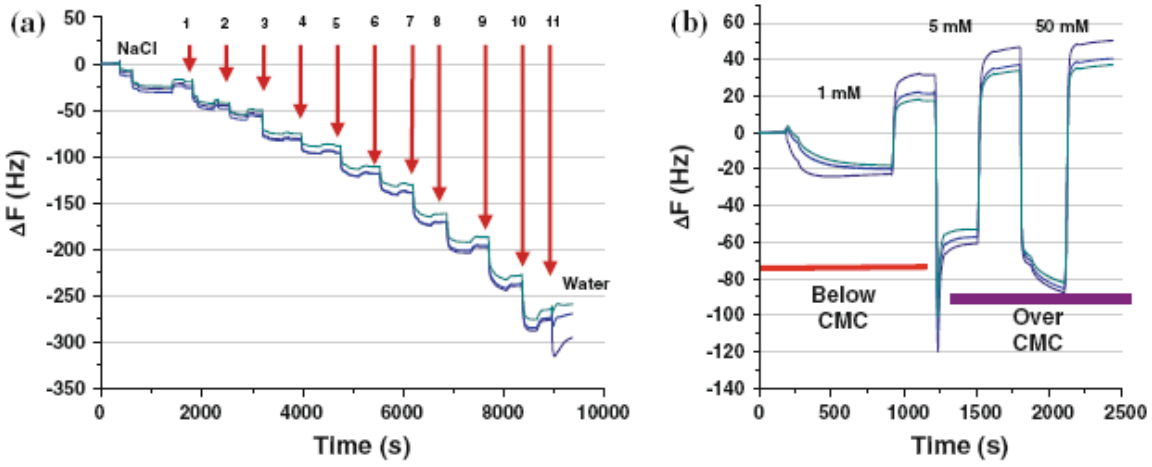

Figure 42 Frequency changes as measured by QCM-D of the 3rd, 5th, and 7th frequency overtones for $(PAH/PSS)_2/(PDADMAC/PSS)_3/PDADMAC$ multilayer system: (a) frequency changes during the assembly of the PEM. (b) Frequency changes during TTAB treatment.

As shown in Fig. 42a, the build-up of this PEM resulted in a total frequency variation of -260 Hz or, after conversion by Sauerbrey, a deposited wet mass of 4.7 μg/cm^2. Since in this case a bilayer of PDADMAC/PSS has been replaced by another PAH/PSS, the PDADMAC/PSS multilayer was thinner and with almost a 40% less of wet mass than the value measured for the first PEM studied. This mass difference corresponds to the last PDMAC/PSS layers, which show a high water content. However, the main result came from the treatment with the surfactant solutions (Fig. 42b). The treatment of this PEM with TTAB resulted in a smaller mass loss than the one observed for the system with a single bilayer of PAH/PSS. In this case, the change in frequency reached +20 Hz when the concentration employed is 1 mM TTAB, and for the maximum value over the CMC, 50 mM, the frequency measured reached +50 Hz. This shift corresponds to the loss of only the last two layers of the PEM. Conversion of this frequency by Sauerbrey to wet mass shows that 0.9 ± 0.1 μg/cm^2 were removed. It means that only 19.2% of the total mass was peeled off from the surface, while in the previously assembled PEM there was a loss of around 65% of the mass. Thickness variations stemming from treatment of both di-block PEMs with TTAB were studied by ellipsometry, as shown in Fig. 43.

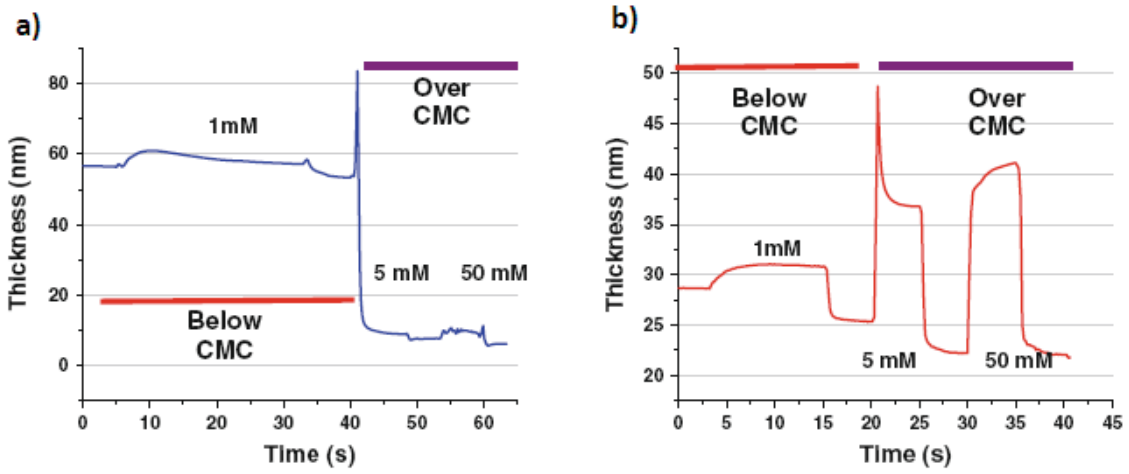

Figure 43 Ellipsometric film thickness variations in real time of PEMs containing a PAH/PSS bilayer (a) or a PAH/PSS double bilayer (b), when exposed to increasing concentrations of TTAB.

Figure 43a clearly shows that working below the CMC causes only a loss in thickness of 5 nm for the system built on top of a (PAH/PSS) bilayer. Once the CMC is exceeded, this shrinkage becomes dramatic for the film and minimum thickness values below 10 nm are reached. For the system based on a double bilayer of PAH/PSS (Fig. 43b), a smaller decrease can be observed. Thickness changed from an initial thickness of 29 nm to a final value of around 22 nm after exposure to high concentration surfactant solutions. Therefore, the assembly of PAH/PSS below the PDADMAC/PSS multilayer and the thickness of the PAH/PSS have a direct influence on the number of layers of PDADMAC/PSS that can be stripped off. Since the interaction with TTAB with PAH does not induce layer degradation, it is very likely that there is an intermixing of the layers of PAH and PDADMAC. This mixing of the layers must occur for the first layers assembled on top of the PAH/PSS. It is more pronounced when the PAH/PSS film is thicker since only the PDADMAC/PSS bilayer on the very top of the film is erased in those conditions.

It is known that there could be a certain degree of mixing of the layers during polyelectrolyte assembly and that the PEMs are not as stratified as it could be expected [44, 45]. Our results with QCM-D hint that this is the case and also to what extent mixing could be happening. For the 4-layer PAH/PSS system, the mixing of the layer can be such that the next 4–5 layers of PDADMAC/PSS are stable against the action of TTAB. The intermixing of the layers must reinforce the stability of the PDADMAC/PSS film inducing a sort of cross-linking of the layers.

3.3. Conclusions

The specific nature of the interaction of a quaternary ionic surfactant with polyelectrolyte multilayers has been highlighted. Choosing a proper composition for the PEMs it becomes possible to strip off the multilayer by applying a TTAB surfactant solution. The removal depends strongly on the nature of the layer. PAH/PSS multilayers remains stable while PDADMAC/PSS multilayers can be removed in a controlled manner. Below the CMC PDADMAC/PSS multilayers either lose material, if PDADMAC was the top layer, or TTAB adsorption occurs, if PSS is the last layer. Above the CMC in either case, the layer can be stripped off. PEMs of PAH/PSS and PDADMAC/PSS sequentially assembled have also been exposed to solutions of the quaternary ammonium surfactant TTAB below and over the CMC. Results show that a single bilayer of PAH/PSS as basement reduces the removal of the PDADMAC/PSS layers assembled on top of PAH/PSS directly to that bilayer. When the initial PAH/PSS multilayer incorporates a second bilayer, the extent of the stabilization seen for the previous system reaches almost the entire multilayer and only those PDADMAC/PSS layers in the outermost positions can be erased.

Additionally, spectroscopic studies of polyelectrolyte complexes have provided new insights in the interaction between PAH and PSS as well as between PDADMAC and PSS. The stoichiometry of both PSS/PAH complexes and PSS/PDADMAC complexes has been calculated from deconvolution of their spectra in the individual contribution of each dry polyelectrolyte, which allows obtaining final polycation/polyanion monomer ratios of 1:2 and 1:2.3, respectively. FTIR measurements performed at different humidities show that the dry PSS/PAH complexes

display the $\nu(SO_2)$ and $\nu s(SO_3^-)$ bands at positions that are indicative of the presence of hydrogen bonds between PSS and PAH. Such importance of hydrogen bonds for the PAH/PSS assembly had been underestimated in the past since it may account for the exceptional stability of multilayers of PAH/PSS. It may further be an important factor influencing the permeability, the mechanics, and other properties of PAH/PSS multilayers and capsules.

3.4. References

(1) Shiratori, S. S.; Rubner, M. F. Macromolecules 2000, 33, 4213.

(2) Mauser, T.; Dejugnat, C.; Sukhorukov, G. B. Macromol. Rapid Commun. 2004, 25, 1781.

(3) Malaisamy, R.; Bruening, M. L. Langmuir 2005, 21, 10587.

(4) Hong, S. U.; Malaisamy, R.; Bruening, M. L. Langmuir 2007, 23, 1716.

(5) Langevin, D. Adv. Colloid Interface Sci. 2001, 467, 89.

(6) Langevin, D. Adv. Colloid Interface Sci. 2009, 170, 147.

(7) Antonietti, M.; Thünemann, A. Curr. Opin. Colloid Interface Sci. 1996, 1, 667.

(8) Sabaté, R.; Estelrich, J. Int. J. Biol. Macromol. 2001, 28, 151.

(9) Grueso, E.; Roldan, E.; Sanchez, F. J. Phys. Chem. B 2009, 113, 8319.

(10) Mitra, D.; Bhattacharya, S. C.; Moulik, S. P. J. Phys. Chem. B 2008, 112, 6609.

(11) Winnik, F.; Regismond, S. T. A.; Picullel, L.; Lindman, B.; Karlstrom, G.; Zana, R. Polymer Surfactant Systems; Dekker: New York, 1998; Vol. 77, pp 65-142, 267-316, 409.

(12) Mantzaridis, C.; Mountrichas, G.; Pispas, S. J. Phys. Chem. B 2009, 113, 7064.

(13) Norman, J.; Lynch, I.; Piculell, L. J. Phys. Chem. B 2007, 111, 8402.

(14) Picullel, L.; Lindman, B. Adv. Colloid Interface Sci. 1992, 41, 149.

(15) Taylor, D. J. F.; Thomas, R. K.; Penfold, J. Adv. Colloid Interface Sci. 2007, 132, 69.

(16) Staples, E.; Tucker, I.; Penfold, J.; Warren, N.; Thomas, R. K.; Taylor, D. J. F. Langmuir 2002, 18, 5147.

(17) Campbell, R. A.; Ash, P. A.; Bain, C. D. Langmuir 2007, 23, 3242.

(18) Nizri, G.; Magdassi, S. J. Colloid Interface Sci. 2005, 291, 169.

(19) Vaknin, D.; Dahlke, S.; Travesset, A.; Nizri, G.; Magdassi, S. Phys. Rev. Lett. 2004, 93, 218302.

(20) Nizri, G.; Lagerge, S.; Kamyshny, A.; Major, D. T.; Magdassi, S. J. Colloid Interface Sci. 2008, 320, 74.

(21) Sasaki, S. J. Phys. Chem. B 2007, 111, 8453.

(22) Sokolov, E. L.; Yeh, F.; Khokhlov, A.; Chu, B. Langmuir 1996, 12, 6229.

(23) Nizri, G.; Makarsky, A.; Magdassi, S.; Talmon, Y. Langmuir 2009, 25, 1980.

(24) Zhang, M. N.; Su, L.; Mao, L. Q. Carbon 2006, 44, 276.

(25) Liu, Y.; Jiang, W.; Li, S.; Li, F. Appl. Surf. Sci. 2009, 255, 7999.

(26) Döbbelin, M.; Arias, G.; Loinaz, L.; Llarena, I.; Mecerreyes, D.; Moya, S. E. Macromol. Rapid Commun. 2008, 29, 871.

(27) Dvoracek, C. M.; Sukhonosova, G.; Benedik, M. J.; Grunlan, J. C. Langmuir 2009, 25, 10322.

(28) Liu, X.; Zhou, L.; Geng, W.; Sun, J. Langmuir 2008, 24, 12986.

(29) Samokhina, L.; Schrinner, M.; Ballauff, M. Langmuir 2007, 23, 3615.

(30) Backlund, S.; Bergenstål, B.; Molander, O.; Wärnheim, T. J. Colloid Interface Sci. 1989, 131, 393.

(31) Zana, R. Langmuir 1996, 12, 1208.

(32) Estrela-Lopis, I.; Leporatti, S.; Clemens, D.; Donath, E. Soft Matter 2009, 5, 214.

(33) Hong, L.; Shi, L.; Tang, X. Macromolecules 2003, 36, 4989.

(34) Dootz, R.; Nie, J.; Du, B.; Herminghaus, S.; Pfohl, T. Langmuir 2006, 22, 1735.

(35) Kalyanasundaram, K.; Thomas, J. K. J. Phys. Chem. 1976, 80, 1462.

(36) Snyder, R. G. J. Chem. Phys. 1967, 47, 1316.

(37) Haramagatti, C. R.; Islamov, A.; Gibhardt, H.; Gorski, N.; Kuklin, A.; Eckold, G. Phys. Chem. Chem. Phys. 2006, 8, 994.

(38) Donath, E.; Walther, D.; Shilov, V. N.; Knippel, E.; Budde, A.; Lowack, K.; Helm, C. A.; Möhwald, H. Langmuir 2007, 13(20), 5294.

(39) Picart, C.; Senger, B.; Sengupta, K.; Dubreuil, F.; Fery, A. Colloids Surf., A 2007, 303, 30.

(40) Gao, C.; Donath, E.; Moya, S.; Dudnik, V.; Möhwald, H. Eur. Phys. J. E 2001, 5, 21.

(41) Gao, C.; Leporatti, S.; Moya, S.; Donath, E.; Möhwald, H. Langmuir 2001, 17, 3491.

(42) Whittington, D.; Milar, I. R. J. Appl. Chem. 1968, 18, 122.

(43) Grumelli, D.; Bonazzola, C.; Calvo, E. J. Electrochem. Commun. 2006, 8, 1353.

(44) Edwards, H. G. M.; Brown, D. R.; Dale, J. R.; Plant, S. J. Mol. Struct. 2001, 595, 111.

(45) Liu, G.; Zhao, J.; Sun, Q.; Zhang, G. J. Phys. Chem. B 2008, 112, 3333.

(46) Guzman, E.; Ritacco, H.; Rubio, J. E. F.; Rubio, R. G.; Ortega, F. Soft Matter 2009, 5, 2130.

Section II:
Polyelectrolyte Brushes

Introduction

In the Overview section at the beginning of this thesis, it has been already mentioned how the anchoring of polymeric chains to the substrate surface can take place either by physisorption or by covalent chemical attachment.[1–3] Nevertheless, the latter is often preferred as it overcomes some of the disadvantages of physisorption, including solvent and thermal instabilities.

In this regard, polymer brushes are presented as monolayers of polymer chains tethered by one end to the surface while the other end of the chain remains free. [4-8] Polyelectrolyte brushes can be basically obtained through two different strategies: The *grafting-to* approach, on one hand, involves the experimentally simple process of tethering pre-synthesized, end-functionalized polymer chains to a suitable substrate. This technique, however, often leads to low grafting density and low film thickness due to sterical repulsions stemming from previously adsorbed polymer chains. On the other hand, the *grafting-from* method overcomes the shortcomings of the grafting-to approach, and yields densely packed polymer brushes through surface-initiated polymerization. In such a dense-package situation repulsive segment interactions take place between surface-tethered polymer chains and the only way those interactions can be relieved would be by a chain extension (swelling) normal to the substrate surface. [9-11]

The grafting method is compatible with a wide range of polymerization chemistries, including anionic [12], cationic,[13] plasma induced,[14] condensation,[15] photochemical,[16] electrochemical,[157] controlled radical polymerization,[18–20] and ring-opening metathesis polymerization (ROMP),[21] For the work presented in this chapter, brushes were synthesized by a grafting from approach

through activation of the surface and subsequent polymerization following an Atom-Transfer Radical Polymerization (ATRP). ATRP is defined as a Controlled or Living radical polymerization (L/CRP) technique, which represents an interesting alternative to traditional free radical polymerization by allowing for excellent control over molecular microstructure to produce tailor made polymers.[22] It basically differs from other controlled/ "living" polymerization techniques in the use of a reversible metal-catalyzed atom transfer to generate the propagating radicals. [19] The catalyst, commonly copper (I), reactivates the addition product, and the activation-addition-deactivation cycle can be, therefore, repeated until all of the unsaturated substrate present is consumed, resulting in a chain-growth polymerization. Fig. 44 shows a schematic view of the polymerization process, which could be described as follows: alkyl halides present in the initiator molecules react with Cu (I) in a concerted fashion by bridged transition-state intermediates and form a coordination cage consisting of a higher oxidation state metal and a radical. The radical quickly diffuses out of the cage and reacts with monomer (propagates). After a certain time, the radical abstracts an halogen atom from the transition metal at a higher oxidation state (X-Cu(II)), reforming the dormant alkyl halide. The number of monomer units added during one activation step (n) depends on the concentration of monomer, the employment of a certain amount of Cu (II) as deactivator and on the relative values of the rate constants of deactivation (kd) and propagation (kp). Mechanism of the ATRP allows for the preparation of polymers with low polydispersities (Mw/Mn < 1.1), predetermined degrees of polymerization, and controlled end functionalities. [23]

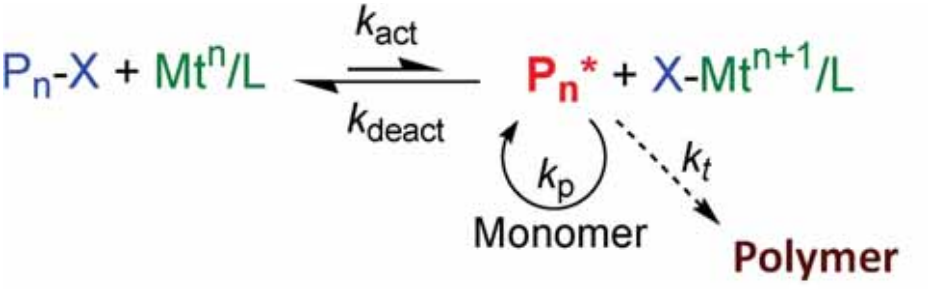

Figure 44. Schematic view of the general mechanism for the Atom Transfer Radical Polymerization process.

ATRP method is applicable to a wide range of monomers, including styrenes, acrylates, methacrylates, substituted acrylamides, and acrylonitrile. Among the important characteristics featuring ATRP would be worth a mention the low polydispersity obtained for the growing chains, as commented above, the possibility to operate in an aqueous environment and, as will be shown further in this thesis, the capability for re-activation of the process in order to synthesize block co-polymers. Because of the tethering effect, the properties of the polymers in a brush can be quite different from those corresponding to free polyelectrolytes in an aqueous solution. Nevertheless, the polymer chains forming the brush retain some conformational freedom.

The term 'polyelectrolyte brushes' is defined in the case of brushes formed by polymer chains bearing an electrolyte group in their repeating units. Polyelectrolyte brushes constitute a new class of material which has recently received considerable interest. The strong segment–segment repulsions and the electrostatic interactions present in such systems bring about completely new physical properties of such monolayers compared to those consisting of either non-stretched or non-charged polymer chains. Polyelectrolyte brushes are well known responsive systems that display changes in chain conformation, upon variations in environmental conditions such as the nature of the solvent, temperature, the pH or the ionic strength, depending on their chemical

composition [24-28]. Conformational changes result in variations in the film thickness and in the packing of the chains. For instance, positively charged Poly (Methacryloyloxy Ethyl Trimethyl Ammonium Chloride) (PMETAC) and poly-anionic Poly (potassium Sulfo Propyl Methacrylate) (PSPM) are two widely studied polyelectrolyte brushes [29-30] which fit into the description given above. For both systems the collapse upon an increase in the ionic strength is a consequence of the screening of charges in the brush, and the initial structure would be recovered after an exchange to a high solvation state.

Poly(*N*-isopropyl acrylamide) (PNIPAAm)brushes are a different example of hydrated brushes with a responsive behavior.[31-32] The chains of PNIPAAm do not have charges but the PNIPAAm monomers are stabilized in water by hydrogen bonding. PNIPAAm is a thermally responsive polymer that undergoes a conformational change above its lower critical solution temperature (LCST) of 32 °C. Below the LCST value, the polymer is hydrophilic and the amides in the pendant group of the NIPAM monomers form hydrogen bonds in the aqueous media with surrounding water molecules. This interaction helps to stabilize the chains and leads the film to be in a swollen state. When the temperature is risen over the LCST, the amide-water hydrogen bonds of PNIPAAm are disrupted, which causes the collapse of the brush. The hydrogen bonds are then replaced by new intra-molecular hydrogen bonding between neighbouring amide groups.

Such conformational changes normally follow a controllable and reversible process since brushes recover their original height once the initial conditions are re-established. This turns polyelectrolyte brushes into a robust method for surface modification with a wide range of

mechanical and chemical properties that, in addition, introduces the possibility to make a "smart" or responsive surface based on conformational changes in the polymer backbones. [33] In regard to their responsive behavior, a range of unique properties can be exploited with a spectrum of applications in the areas of surface wettability,[34] micro/nanofluidics and electronics,[35–39] mechanical actuation and chemical sensing,[40-48] biocompatibility and biotribology,[49-53] controlled drug release, cell growth and separation,[54-59] and micro/nanomaterials fabrication.[60–65] Applications of stimulus-responsive polymer brushes have also received considerable attention in biomedical related fields and have recently been reviewed by several groups.[66–68]

This section describes a comparative study between three common systems in the field of responsive polymers: ionic strength-responsive Poly (methacryloyloxy ethyl trimethyl ammonium chloride) (PMETAC) and Poly (potassium sulfopropyl methacrylate) (PSPM), and thermally responsive Poly (N-Isopropyl Acryl Amide) (PNIPAAm). The study will address some basic questions regarding the growth of such systems, both forming an individual entity and a copolymer brush, such as the amount of water retained during the assembly or how the properties of the brushes are affected by the density of initiator molecules on the surface. In addition, the amount of water lost during the reversible shrinkage displayed triggered by changes in the ionic strength or temperature will be calculated. The last part of the section will also describe the use of these polymer brushes as templates for the LbL assembly of PEMs to form hybrid supramolecular structures in three dimensions.

References

(1) Brittain, W. J.; Minko, S. *J. Polym. Sci. A Polym. Chem.* 2007, 45, 3505.

(2) Edmondson, S.; Osborne, V. L.; Huck, W. T. S. *Chem. Soc. Rev.* 2004, 33, 14.

(3) Zhou, F.; Huck, W. T. S. *Phys. Chem. Chem. Phys.* 2006, 8, 3815.

(4) Ballauff, M; Borisov, O. *Curr. Opin. Colloid Interface Sci.* 2006, 11, 316.

(5) Boyes, S. G.; Granville, A. M.; Baum, M; Akgun, B.; Mirous, B. K.; Brittain, W. J. *Surf. Sci.* 2004, 570, 1.

(6) Tran, Y.; Auroy, P.; Lee. L-T. *Macromolecules* 1999, 32, 8952.

(7) Huck, W. T. S. *Mater. Today* 2008, 11, 24.

(8) Advincula, R. C.; Brittain, W. J.; Caster, K. C.; Rühe, J. *Polymer Brushes: Synthesis, Characterization, Applications*; Wiley-VCH: Weinheim (Germany), 2004.

(9) Halperin, A.; Tirrell, M.; Lodge, T. P. *Adv. Polym. Sci.* 1992, 100, 31.

(10) Zhao, B.; Brittain, W. J. *Prog. Polym. Sci.* 2000, 25, 677.

(11) Milner, S. T.; Witten, T. A.; Cates, M. E. *Macromolecules* 1988, 21, 2610.

(12) Jordan, R.; Ulman, A.; Kang, J. F.; Rafailovich, M. H.; Sokolov, J. *J. Am. Chem. Soc.* 1999, 121, 1016.

(13) Ingall, M. D. K.; Honeyman, C. H.; Mercure, J. V.; Bianconi, P. A.; Kunz, R. R. *J. Am. Chem. Soc.* 1999, 121, 3607.

(14) Chen, W.; Fadeev, A. Y.; Hsieh, M. C.; Oner, D.; Youngblood, J.; McCarthy, T. J. *Langmuir* 1999, 15, 3395.

(15) Husemann, M.; Mecerreyes, D.; Hawker, C.J.; Hedrick, J. L.; Shah, R.; Abbott, N. L. *Angew. Chem. Int. Ed.* 1999, 38, 647.

(16) Prucker, O.; Naumann, C.A.; Ruhe, J.; Knoll, W.; Frank, C. W. *J. Am. Chem. Soc.* 1999, 121, 8766.

(17) Gurtner, C.; Wun, A. W.; Sailor, M. *Angew. Chem. Int. Ed.* 1999, 38, 1966.

(18) Matyjaszewski, K.; Xia, J. H. *Chem. Rev.* 2001, 101, 2921.

(19) Patten, T. E.; Matyjaszewski, K. *Acc. Chem. Res.* 1999, 32, 895.

(20) Matyjaszewski, K.; Dong, H. C.; Jakubowski, W.; Pietrasik, J.; Kusumo, A. *Langmuir* 2007, 23, 4528.

(21) Grubbs, R. H.; Chang, S. *Tetrahedron* 1998, 54, 4413.

(22) Chan, N.; Cunningham, M. F.; Hutchinson, R. A. *Macromol. Chem. Phys.* 2008, 209, 1797.

(23) Matyjaszewski, K. *Macromolecules* 1998**,** 31, 4710.

(24) Chen, T.; Ferris, R.; Zhang, J.; Ducker, R.; Zauscher, S. *Prog. Polym. Sci.* 2010, 35, 94.

(25) Zhou, F.; Hu, H.; Yu, B.; Osborne, V. L.; Huck, W. T. S.; Liu, W. *Anal. Chem.* 2007, 79, 176.

(26) Brown, A. A.; Azzaroni, O.; Huck, W. T. S. *Langmuir* 2009, 25, 1744.

(27) Laloyaux, X.; Fautré, E.; Blin, T.; Purohit, V.; Leprince, J.; Jouenne, T.; Jonas, A.M.; Glinel, K. *Adv. Mater.* 2010, 22 (44), 5024.

(28) Mi, L.; Bernards, M.T.; Cheng, G.; Yu, Q.; Jiang, S. *Biomaterials* 2010, 31 (10), 2919.

(29) Kobayashi, M.; Terada, M.; Terayama, Y.; Kikuchi, M.; Takahara, A. *Macromolecules* 2010, 43, 8409.

(30) Masci, G.; Bontempo, D.; Tiso, N.; Diociaiuti, M.; Mannina, L.; Capitani, D.; Crescenzi, V. *Macromolecules* 2004, 37, 4464.

(31) Liu, G.; Zhang, G. *J. Phys. Chem. B* 2005, 109, 743.

(32) Liu, R.; De Leonardis, P.; Tirelli, N.; Saunders, B. R. *J. Colloid Interface Sci.* 2009, 340, 166.

(33) Zhou, F.; Zheng, Z.; Yu, B.; Liu, W.; Huck, W. T.S. *J. Am. Chem. Soc.* 2006, 128, 16253.

(34) Jonas, A. M.; Hu, Z. J.; Glinel, K.; Huck, W. T. S. *Macromolecules* 2008, 41, 6859.

(35) Ionov, L.; Houbenov, N.; Sidorenko, A.; Stamm, M.; Minko, S. *Adv. Funct. Mater.* 2006, 16, 1153.

(36) Seino, M.; Yokomachi, K.; Hayakawa, T.; Kikuchi, R.; Kakimoto, M.; Horiuchi, S. *Polymer* 2006, 47, 1946.

(37) Pinto, J. C.; Whiting, G. L.; Khodabakhsh, S.; Torre, L.; Rodriguez, A. B.; Dalglish, R. M.; et al. *Adv Funct Mater* 2008, 18, 36.

(38) Lokuge, I.; Wang, X.; Bohn, P. W. *Langmuir* 2007, 23, 305.

(39) Whiting, G. L.; Snaith, H. J.; Khodabakhsh, S.; Andreasen, J. W.; Breiby, D.; Nielsen, M. M. et al. *Nano Lett* 2006**,** 6, 573.

(40) Ryan, A. J.; Crook, C. J.; Howse, J. R.; Topham, P.; Geoghegan, M.; Martin, S. J. et al. *J. Macromol. Sci. Phys.* 2005, B44, 1103.

(41) Abu-Lail, N. I.; Kaholek, M.; LaMattina, B.; Clark, R. L.; Zauscher, S. *Sens. Actuators B* 2006, 114, 371.

(42) Mitsuishi, M.; Koishikawa, Y.; Tanaka, H.; Sato, E.; Mikayama, T.; Matsui, J. et al. *Langmuir* 2007, 23, 7472.

(43) Gupta, S.; Agrawal, M.; Uhlmann, P.; Simon, F.; Oertel, U.; Stamm, M. *Macromolecules* 2008, 41, 8152.

(44) Li, L.; Li, J.; Lukehart, C. M. *Sens. Actuators B* 2008, 130, 783.

(45) Zhou, F.; Biesheuvel, P. M.; Chol, E. Y.; Shu, W.; Poetes, R.; Steiner, U. et al. *Nano Lett.* 2008, 8, 725.

(46) Yu, K.; Wang, H. F.; Han, Y. C. *Langmuir* 2007, 23, 8957.

(47) Anraku, Y.; Takahashi, Y.; Kitano, H.; Hakari, M. *Colloid Polym. Sci.* 2007, 57, 61.

(48) Tokareva, I.; Minko, S.; Fendler, J. H.; Hutter, E. *J. Am. Chem. Soc.* 2004,126, 15950.

(49) Alarcon, C. D. H.; Farhan, T.; Osborne, V. L.; Huck, W. T. S.; Alexander, C. *J. Mater. Chem.* 2005, 15, 2089.

(50) Cho, W. K.; Kong, B. Y.; Choi, I. S. *Langmuir* 2007, 23, 5678.

(51) LeMieux, M. C.; Lin, Y. H.; Cuong, P. D.; Ahn, H. S.; Zubarev, E. R.; Tsukruk, V. V. *Adv. Funct. Mater.* 2005, 15, 1529.

(52) Pei, X. W.; Xia,Y. Q.; Liu, W. M.; Yu, B.; Hao, J. C. *J. Polym. Sci. A Polym. Chem.* 2008, 46, 7225.

(53) Xu, F. J.; Li, H. Z.; Li, J.; Teo, Y. H. E.; Zhu, C. X.; Kang, E. T. et al. *Biosens. Bioelectron.* 2008, 24, 773.

(54) Lue, S. J.; Hsu, J. J.; Wei, T. C. *J. Membr. Sci.* 2008, 321, 146.

(55) Nagase, K.; Kobayashi, J.; Kikuchi, A.; Akiyama, Y.; Kanazawa, H.; Okano, T. *Biomacromolecules* 2008, 9, 1340.

(56) Bayramoglu, G.; Ekici, G.; Besirli, N.; Arica, M. Y. *Colloid Polym. Sci.* 2007, 310, 68.

(57) Jain, P.; Sun, L.; Dai, J. H.; Baker, G. L.; Bruening, M. L. *Biomacromolecules* 2007, 8, 3102.

(58) Kusumo, A.; Bombalski, L.; Lin, Q.; Matyjaszewski, K.; Schneider, J. W.; Tilton, R. D. *Langmuir* 2007, 23, 4448.

(59) Zhang, Z.; Chen, S. F.; Jiang, S. Y. *Biomacromolecules* 2006, 7, 3311.

(60) Lu, Y.; Mei, Y.; Schrinner, M.; Ballauff, M.; Moller, M. W. *J. Phys. Chem. C* 2007, 111, 7676.

(61) Schrinner, M.; Proch, S.; Mei, Y.; Kempe, R.; Miyajima, N.; Ballauff, M. *Adv. Mater.* 2008, 20, 1928.

(62) Shkilnyy, A.; Friedrich, A.; Tiersch, B.; Schone, S.; Fechner, M.; Koetz, J. et al. *Langmuir* 2008, 24, 2102.

(63) Tugulu, S.; Harms, M.; Fricke, M.; Volkmer, D.; Klok, H. A. *Angew. Chem. Int. Ed.* 2006, 45, 7458.

(64) Saleh, N.; Sarbu, T.; Sirk, K.; Lowry, G. V.; Matyjaszewski, K.; Tilton, R. D. *Langmuir* 2005, 21, 9873.

(65) Edmondson, S.; Huck, W. T. S. *Adv. Mater.* 2004, 16, 1327.

(66) Alarcon, C. D. H.; Pennadam, S.; Alexander, C. *Chem. Soc. Rev.* 2005, 34, 276.

(67) Jeong, B.; Gutowska, A. *Trends Biotechnol.* 2002, 20, 305.

(68) Gil, E. S.; Hudson, S. A. *Prog. Polym. Sci.* 2004, 29, 1173.

Chapter 4:

Assembly and water content of PE brushes

4.1. Introduction

The importance of quantifying the water content of supramolecular polyelectrolyte structures has already been highlighted in chapter 1. As explained there, polyelectrolytes are charged molecules bearing hydrated monomers. In addition, in a brush the polyelectrolytes chains can trap water either between each single, randomly coiled, polyelectrolyte chain or between neighbouring chains forming the brush. Although the growth of polyelectrolyte brushes has been extensively described in literature[1-4], less has been reported about their water content.

The combination of spectroscopic ellipsometry and QCM-D in a single device will be employed, in a similar fashion as already explained for the case of PEMs, to study both the growth and the water content of polyelectrolyte brushes.

Brushes were synthesized following an ATRP polymerization from gold surfaces, which go under covalent modification an initiator thiol such as the ω-Mercaptoundecyl bromoisobutyrate thiol prior to polymerization.[5]. The growth of polymer chains from initiator molecules results in the formation of dense polymer brushes. Indeed, the number of growing chains will be, in principle, determined by the number of initiator present on the surface. Besides that, initiator density can be varied by incorporating a non initiating thiol in the solution from which the thiol monolayer is formed and will thus impact the growth of the chains forming the brush. Decreasing the density of initiators will reduce the number of polymer chains but, at the same time, the formed chains will have more lateral space to grow.

The length of the chains and the space between chains are additional factors with a direct influence on the water content of the brush. The longer the chains the more water will be associated to them. On the other hand, the higher the chain density in the brush the less space between them that can be filled with free water. Jones et al.[2] showed that the initiator density on a gold surface can be varied by deposition of thiols from mixed solutions of initiator ω-mercaptoundecyl bromoisobutyrate thiol, and of 1-undecanethiol as blank thiol. Although the actual initiator concentration in the monolayer may not be exactly that of the solution, taking into account the differences in size of the thiols and the probably different kinetics of assembly of the two thiols employed, the method has been shown to work effectively to vary the initiator concentration[6].

In this chapter the growth, through ATRP from monolayers of polymerization-initiating molecules grafted on gold surfaces, and the water content of polyelectrolyte brushes composed of either Poly (methacryloyloxy ethyl trimethyl ammonium chloride) (PMETAC) or Poly (potassium sulfo propyl methacrylate) (PSPM) and of polymer brushes composed of Poly (N-Isopropyl Acrylamide) (PNIPAAm) will be analyzed and compared by means of the combination of QCM-D and ellipsometry in a single device. In the case of PSPM brushes, the synthesis was performed both in presence and absence of reaction-inhibitor Cu (II) in the polymerization. The addition of the inhibitor in solution is done with the scope of gaining control over chain polydispersity.

Also, in order to analyze the effect that the initiator grafting density has in the final structure formed, brushes composed of either PMETAC or PSPM were synthesized from a wide range of

initiator/blank mixtures and their respective thicknesses and water contents were compared. Additionally, since ATRP offers the possibility to re-activate the polymerization process and can be employed for the formation of block copolymers. In case of polyelectrolyte brushes such reactivation can be employed to produce multi-responsive di-block copolymer which could include a first brush bearing, for instance, thermally-responsive groups (PNIPAAm) and a second brush on top formed by ionic-responsive monomers (PSPM) in the same structure. The same analysis done for one-block brushes, as described above, can then be extended to di-block copolymer brushes. Water content and polymer mass can be measured after each polymerization step. This will allow us to determine the polymer mass of each block in the copolymer.

4.2. Results and discussion

4.2.1. Synthesis of PMETAC, PSPM and PNIPAAm brushes

Figure 45 illustrates the "in situ" growth of a PMETAC brush monitored by the QCM-D/ellipsometry combined technique from a 100 % monolayer of thiol initiator. The thiol monolayer was previously assembled on top of the gold coated QCM-D sensor (data not shown).

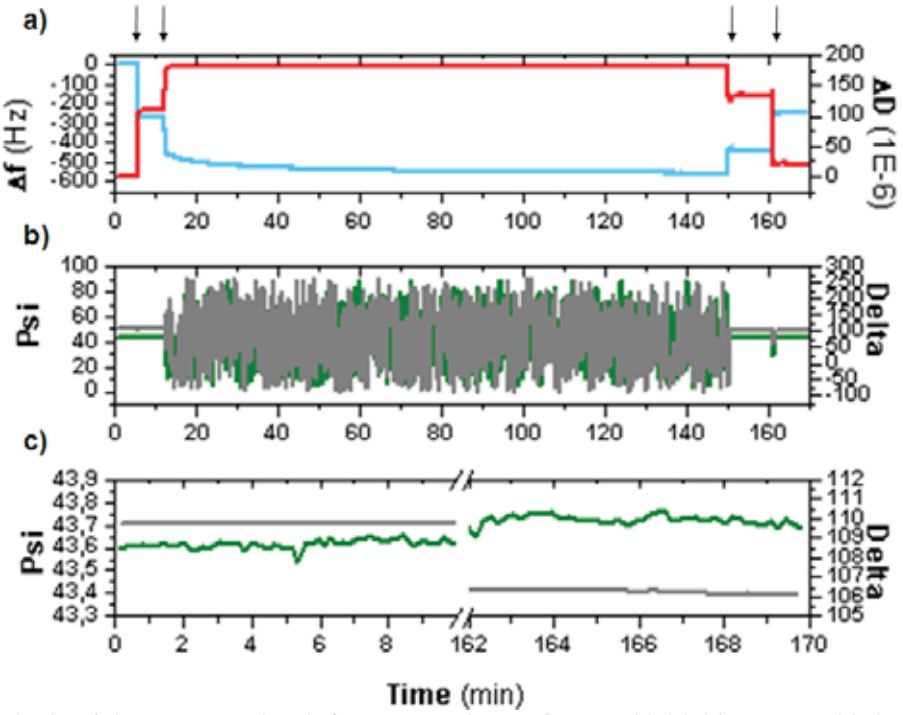

Figure 45 Synthesis of the PMETAC brush from a monolayer of 100% thiol initiator assembled on top of a gold surface followed *in situ* by the combined QCM-D/ellipsometry device. (a) QCM-D response, i.e., Δf and ΔD *vs.* time for a selected overtone ($i = 3$). (b) Ellipsometric response, i.e., Ψ and Δ *vs.* time for a selected wavelength ($\lambda = 632.5$ nm). (c) Magnification of the ellipsometric response at the pre- and post-polymerization states. The starting time of each solution injected is indicated by solid *arrows*.

The variations in the acoustic parameters, frequency and dissipation, as recorded by the QCM-D device are shown in Fig. 45a. While frequency follows a continuous decrease along the

polymerization, which is indicative of the progressive mass growth on top of the sensor, the dissipation reaches higher values as the polymerization progresses, pointing out the formation of a film with a certain viscoelastic character. The relation of the values of dissipation and frequency shown by the brush during the synthesis ($\Delta D/-\Delta f = 0.154\times10^{-6} < 0.2\times10^{-6}$) make it possible the use of the Sauerbrey equation to calculate the total film mass (including solvent), m_{QCM}.

The polymer mass, m_{opt}, was obtained from the fitting of the real-time variation of ψ and Δ, shown in Fig 45b, measured during the synthesis of the PMETAC brush. The dense colour mixture formed by METAC monomer, CuCl and 2, 2'-bipyridyl employed for the polymerization blocks the light path through the QCM-D chamber. As a consequence of the blocking of the light path the signal reaching the detector is totally lost. As it can be seen in Fig. 45b, psi and delta turn into noise as polymerization takes place, and only after a consecutive rinse with DMF/water and pure water at the end of the polymerization the monomer solution is swept away and the optical parameters can be detected again. For a better interpretation of the ellipsometric data, these were re-plotted in Fig. 45c excluding the region where the signal is blocked. In this way the starting point and the final point of the polymerization can be easily compared to determine the total amount of polymer grown.

The synthesis of PSPM and PNIPAAm brushes from 100% of initiator density was followed in the same way as for PMETAC. For comparison the in-situ monitoring of a PSPM brush in the absence of Cu (II) is also depicted in Figure 46.

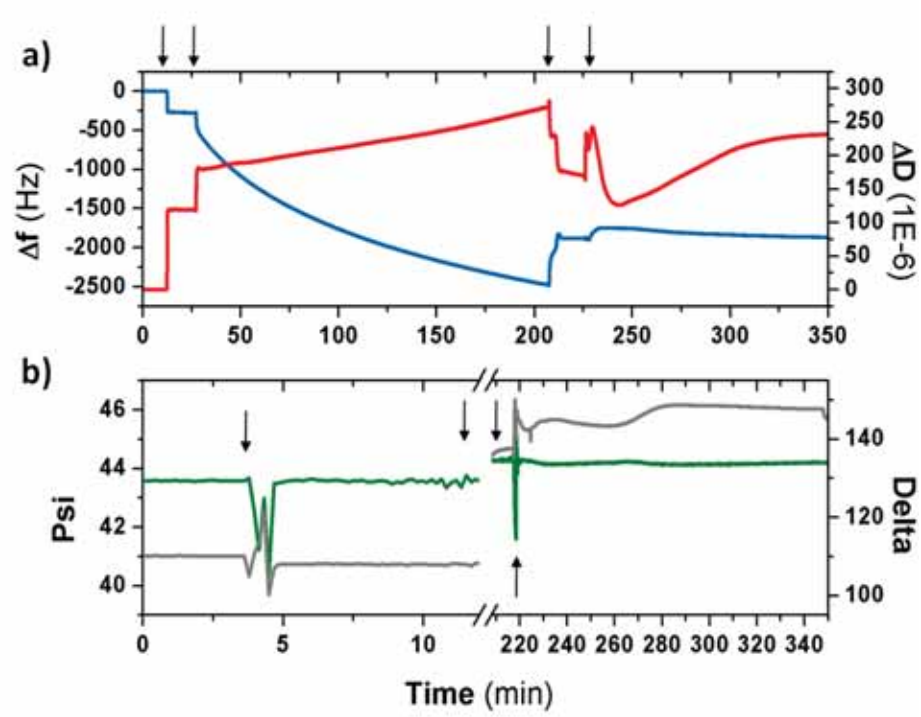

Figure 46 Synthesis of the PSPM *free* brush from a monolayer of 100% thiol initiator assembled on top of a gold surface followed *in situ* by the combined QCM-D/ellipsometry device. (a) QCM-D response, i.e., Δ*f* and Δ*D vs.* time for a selected overtone (*i* = 3). (b) Magnification of the ellipsometric response, Ψ and Δ *vs.* time for a selected wavelength (λ = 632.5 nm) at the pre- and post-polymerization states. The starting time of each solution injected is indicated by solid *arrows*.

To have a clearer view over the systems built, the data obtained with both the acoustic and optical techniques were converted into mass values as done for PEMs. The values of m_{opt} and m_{QCM} and the acoustic thickness (d_{QCM}) at the end of polymerization (after thorough rinses with DMF/water and water), and the brush hydration calculated can be compared for PMETAC, PSPM, PSPM (4:1), and PNIPAAm brushes as shown in Figure 47.

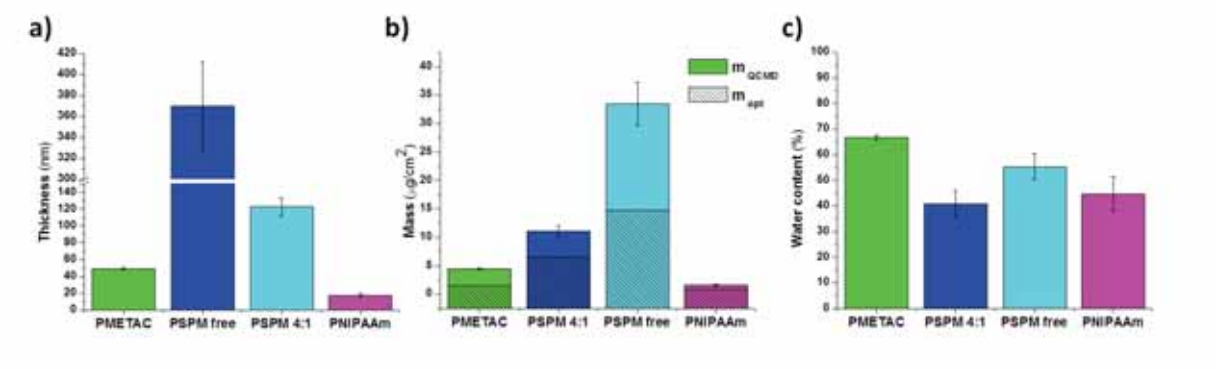

Figure 47(a) acoustic thickness (b) m_{QCMD} (*coloured columns*) and m_{opt} (dashed *columns*), (c) hydration of PMETAC / PSPM (4:1) / PSPM (free growth) / PNIPAAm brushes.

Figure 47a shows the thickness of the different brushes synthesized, all for a same polymerization time of 4 h. From the studied polymer brushes PNIPAAm was the most difficult to polymerize, resulting in film of only 16 nm at the end of the process. The synthesis of PMETAC brushes resulted in a film of approximately 45 nm, and PSPM brushes, both freely polymerized and with inhibitor, yielded thicknesses of 132 and 370 nm, respectively. The high efficiency in the growth of PSPM is due to, the negative charge of the sulfopropyl methacrylate, which favors the radical polymerization because of its charge-donor character. The positive charge of the METAC monomer tends, on the other hand, to destabilize the free radical. As a consequence the ATRP polymerization becomes less effective.

In Fig. 47b the acoustic and optical masses have been plotted for the different polymers under study. The values of m_{QCMD} are always higher than those of m_{opt}, because of the amount of associated water. As PNIPAAm showed the lowest m_{opt}, it yielded, consequently, the lowest m_{QCMD} as well. The PSPM brush grown freely, in the absence of inhibitor Cu (II) shows the

highest optical mass among the studied brushes, 14.8 μg/cm^2, and a total mass (water included) of almost 20 μg/cm^2.

Applying Equation 5 (see Materials and methods), the water content or hydration of the brush was calculated from the values of m_{QCMD} and m_{opt}. The water content is then represented as percentage of total mass in Fig. 47c for each of the brushes. For PMETAC brushes, the water content was the highest observed, around the 65 %. On the contrary, the lowest hydration, a 40%, corresponded to the growth-limited (4:1) PSPM brushes, while short-chained PNIPAAm brushes showed water content of the 45%. In case of the freely grown PSPM brushes synthesized with ATRP-inhibiting $CuCl_2$, water represented approximately the 55% of their total mass. Although the free synthesized PSPM forms the thickest brush and has the highest dry mass its water content is lower than, for instance, that of PMETAC. These results are somehow surprising because one would think that increasing the mass of the brush the number of hydrated monomers will increase proportionally and, consequently, more water will be present. Besides, the quaternary amines in PMETAC should be more hydrophobic since its charge appears protected by the methyl groups than the sulfonate groups of PSPM, which can additionally form hydrogen bonding with the water, but results do not show so. There are some other factors affecting the final water content. To understand why the PMETAC is the more hydrated of the three polyelectrolyte brushes studied it must be kept in mind that the water in the brush is not only the water associated to the pendant groups of the monomers of the brush, but also water which is entrapped between the polymer chains. The use of Cu (II) when polymerizing PSPM ensures a narrow molecular weight polydispersity for the chains of the brush. The brush is, therefore, more compact than that synthesized in the absence of $CuCl_2$. In the case of the freely

grown PSPM or PMETAC some of the chains grow to a larger extent than others, and promote the existence of regions in the brush with different polymer density. In these conditions, the chains lose some of their packing degree and the amount of water entrapped between the chains is higher than for the (4:1) Cu (I)/Cu (II) PSPM brush, where the chains probably tend to be better packed. In the case of the PMETAC, which does not grow as well as PSPM, the chain polydispersity and the presence of regions of different density of polymer may be more pronounced than in PSPM and the percentage of water entrapped is therefore higher.

4.2.2. Effect of the ATRP initiator grafting density

To determine how the number of initiator molecules attached to the surface can affect the final structure and water content of the brush synthesized the same type of analysis as the one described in the previous point was repeated for PMETAC and PSPM brushes grown via ATRP from different initiator grafting densities. For these studies, the monolayer of thiol initiators is formed on the gold-coated quartz sensor from solutions of ω-mercaptoundecyl bromo isobutyrate (thiol initiator) and 1-undecanethiol 98% (blank thiol) in different ratios.

4.2.2.1. Synthesis of PMETAC brushes

Figure 48 shows the calculated values for m_{opt} and m_{QCM} and the acoustic thickness (d_{QCM}), at the end of the polymerization of PMETAC brushes, as a function of the initiator density in the hybrid monolayer of thiols grafted on the surface, from 1 % initiator thiol to 100%.

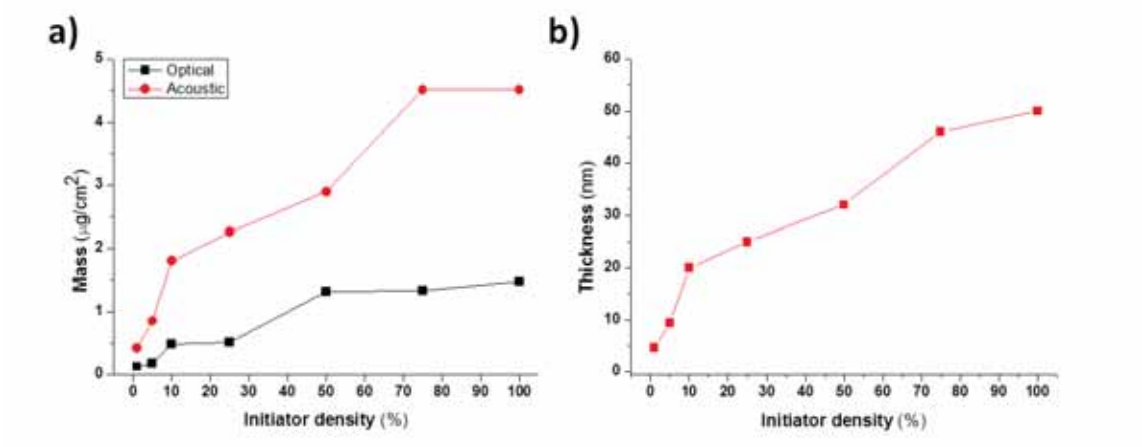

Figure 48 (a) m_{QCMD} (circles) and m_{opt} (squares), and (b) acoustic thickness values obtained for PMETAC brush assembly from different initiator/blank thiol ratios.

From Fig. 48a it can be immediately observed the difference between the acoustic and optical masses and their divergence, which becomes more pronounced as the percentage of initiator density on the surface is increased. This is indicative of proportionally higher content of water in the brush as the percentage of initiator density is increased. Another interesting observation from this figure is that the optical mass of the brushes varies very slightly for initiator densities over the 50%. Indeed, when starting from 50 % initiator the final polymer mass reached is 1.32 μg/cm^2, while for a brush grown from 100% it reaches 1.47 μg/cm^2. On the contrary, both the acoustic mass and the acoustic thickness increase, respectively, from 2.89 μg/cm^2 and 30 nm to 4.51 μg/cm^2 and 50 nm. For brushes with 75 % as initiator density an intermediate value of thickness of 46 nm is observed but the optical mass is 1.33 μg/cm^2, which is only slightly higher than for the 50 % initiator brush. This dichotomy between thickness increases of over the 50% and very slight changes in the polymer mass reflects a different arrangement of the polyelectrolyte chains in the brush with increasing percentage of initiator. When growing from

50 % initiator the brush has more lateral space to occupy since the number of surrounding/neighboring chains is lower and therefore it can grow towards its lateral volume. An increase in the (initiator/blank) ratio of the thiol monolayer is reflected as an increase in the number of growing chains, and this will restrain the chains from occupying the lateral volume. Taking into account that the masses are so similar for the three highest initiator densities one would think that the polyelectrolyte chains are longer for the 50% initiator but at the same time they present a more coiled conformation since the thickness of the brush is smaller than for the 75% and 100 % cases. However, it must also be considered that how brush density changes with brush thickness in not know. It can be that at an initial state most of the initiator molecules will lead to a growing polymer chain but after a while the growth of a certain percentage of chains will be sterically limited. Hence the growing chain would not be accessed by the monomers, and then only few chains, with a certain space between them, could go on growing and protruding in the solution. Such behavior was already suggested by Cheng et al. for brushes with a high Cu(I)/Cu(II) ratio in the polymerization solution[7]. As for PMETAC brushes studied here the synthesis takes place in the absence of Cu (II), these systems could be considered as close to such consideration. According to the authors, a high Cu(I)/Cu(II) ratio leads to the formation of less dense, but higher molecular-weighted polymer brushes. The difference between optical mass and acoustic mass corresponds to the water content of the brush, which regards both hydration water or, in other words, water molecules associated to the charged monomers along the chain, but also to entrapped water, which is the water retained in the structure. Such discernment results very useful for a better understanding of the differences in acoustic mass observed for the analyzed systems. For instance, when passing from a 75% to a 100% initiator-grafted brush, the

optical mass values are so similar that we can assume that the hydration masses are pretty similar too. Therefore the differences observed in the acoustic mass are only due to water entrapped between neighboring polymer chains.

For initiator densities between 10% and 50 % the acoustic mass of the brush increases linearly. However, almost no difference results from the optical masses when passing from a 10 % to a 25 % initiator density of the PMETAC brush. This resembles the situation observed for the 100 % and 50 % initiator-grafting PMETAC brushes. Decreasing the number of polymerization initiators from 25% to 10% yields a similar polymer mass indicating the chains grow more coiled and occupy more lateral volume but at the same time they retain less water entrapped. Below the 10 % initiator both acoustic and optical masses drop significantly. For 5 % and 1 % initiator-grafted brushes the optical mass values are also very close to each other while the acoustic mass for 5 % is twice the one observed for 1 %. Fig. 48b shows the two linear trends followed by acoustic thickness values measured in the growth of the PMETAC brushes: a change in the initiator density from 1% to 10% makes the brush undergoing a remarkable thickness increase from 4.6 to 20 nm. For brushes grown from densities over 10 % the increase in thickness follows also a linear tendency although less steeply. Acoustic thicknesses of 25 nm, 32 nm, 46 nm and 50 nm are calculated for brushes grown from initiator densities of the 25%, 50%, 75% and 100%, respectively.

Both the water content of the brush and the number of water molecules per monomer in the system have been calculated from the acoustic and optical mass values presented above, as shown in Figure 49.

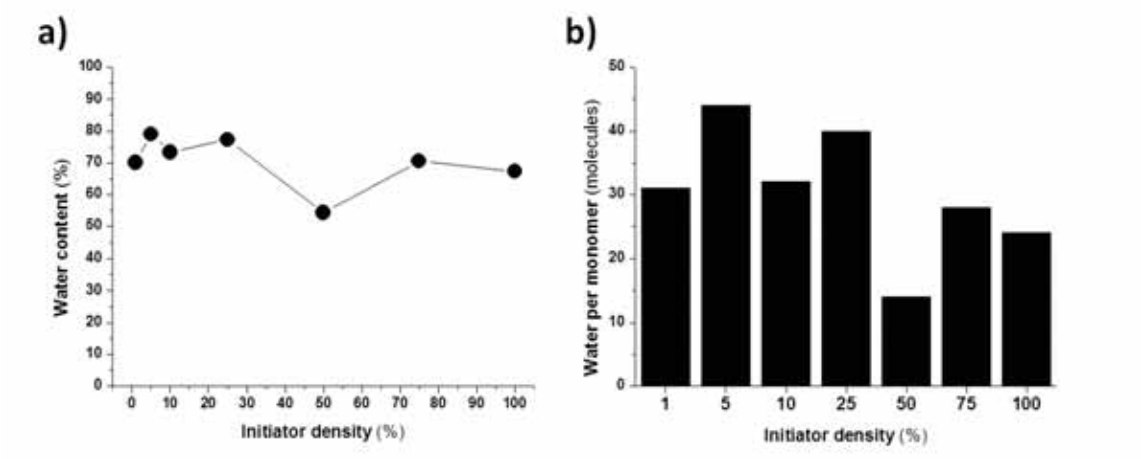

Figure 49 Water content (a) and number of water molecules per METAC monomer in the brush (b) as a function of the initiator grafting density on the surface.

Water content values in Fig. 49a range between 67% and a maximum of 79% for every grafting percentage employed except for the brush grown from 50% of initiator on the surface which yields a slightly lower hydration of around 55%. The relative limited variation in the hydration for the different percentages employed of initiator is indicating an almost constant value of hydration per monomer. If the hydration would be indeed constant it would mean that the amount of water molecules associated to each monomer is constant and independent of the density of the chains. The fact that hydration is not strictly constant is reflecting that, to a certain extent, hydration along the chain could change for the different packing in the brush monolayer. It is then worth distinguishing between water associated to the monomers forming a hydration cage and free water entrapped between the chains. Such differences in hydration for the different grafting densities are suggested to be mostly associated with the free water entrapped. Variations reach at most around the 10% of the total hydration, which implies that most of the water in the brush is water associated with the monomers and not freely entrapped water. In this regard, the

total water content values could be expressed in terms of water molecules per METAC monomer as shown by Fig. 49b. Water/monomer ratios of 27:1, 44:1, 32:1 and 40:1 were calculated for 1, 5, 10 and 25% of initiator-grafted brushes, respectively. Then, the value drops to 14 molecules per monomer for a brush grown from 50% of initiator and it rises back to 28:1 and 24:1 for the 75% and 100% initiator-grafted brushes.

4.2.2.2. Synthesis of PSPM brushes

The analysis presented above for PMETAC can be also extended to other polymers. The effect of varying the initiator density on the growth of the brush was studied for PSPM (4:1) and free-PSPM brushes assembled from monolayers of mixed initiator/blank thiols in different ratios. The results obtained for both systems are shown in Figure 50.

Comparison of Figures 50a and 50c shows how an increase in the initiator density leads to a progressive increase of the mass deposited in both systems, although the calculated values differ considerably from one case to the other as a results of working whether in the absence or in the presence of Cu (II). m_{QCMD} and m_{opt} values in Fig. 50c almost double those in Fig. 50a, regardless of the initiator grafted on the surface.

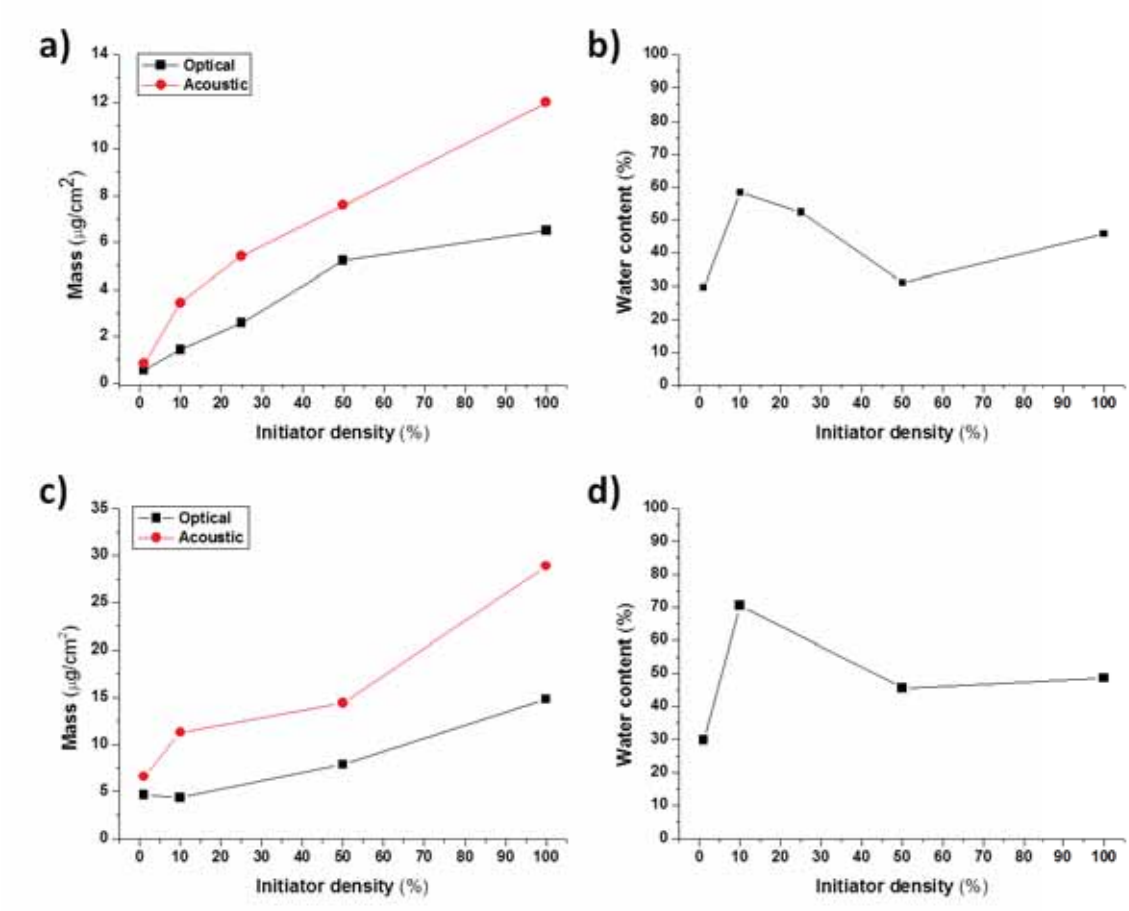

Figure 50 (a), (c) m_{QCMD} (circles) and m_{opt} (squares), and (b), (d) water content values obtained for PSPM (4:1) and free-PSPM brushes, respectively, assembled from different initiator/blank thiol ratios.

But still some common features can be found between free-PSPM and PSPM (4:1) brushes: for instance, while for initiator percentages between the 10 and the 50 % increases in m_{QCMD} and m_{opt} of both samples are observed to progress almost in parallel, working in grafting densities over the 50% makes acoustic and optical mass values to diverge. The water content of the brushes is shown in Figures 50b and 50c for PSPM with and without co catalyst. In both plots it can be observed that when shifting from a 1 % to a 10% of initiator on the surface we increase from contents of around the 30% up to the 60-70% of water in the structure. Over such grafting

densities hydration diminishes back down to a 30% and a 50% for PSPM (4:1) and free-PSPM brushes, respectively. For free PSPM brushes the content in water will remain constant even though the initiator density reaches the 100% of the surface coverage while for polydispersity-controlled PSPM (4:1) brushes hydration increases gradually up to the 50%. Both brushes show for the water content a very similar dependence on the density of initiators, which is different from the observed for PMETAC. The presence of a maximum of the water content around 10 % initiator is surprising but hints to the role of the entrapped water not associated with the monomers in the total water content. It is presumable that at this initiator density there will be significant space between the chains.

4.2.3. Synthesis of a di-block copolymer brush

This last section of chapter 4 regards the formation of multi-responsive supramolecular structures by reactivation of the ATRP process, which allows for the consecutive synthesis of a new block of polymers from the polymer chains of a preformed brush of different chemical composition. For this kind of di-block co-polymer brushes it is necessary the reactivation of the chains of the preformed brush. For reactivation the chains are exposed to an aqueous solution containing Cu (I) and 2, 2'-Bipyridyl, for a certain period of time, prior to the second polymerization step. Thus, a first block of thermally-responsive PNIPAAm was used for the polymerization of a PSPM-free block on top.

The QCM-D/ellipsometry set up allows for the quantification of the mass of each block in the brush. The polymer mass of the first block can be obtained before reinitiating the synthesis as

shown in 4.2.1. The mass of the second block is simply calculated from the total mass measured at the end of the second polymerization and the mass of the first block.

Figure 51 shows the results obtained for the acoustic thickness, m_{QCMD}/m_{opt} and for the water content right after the assembly of the two-block brush. For a proper comparison, the values obtained for a single PNIPAAm brush (see section 4.2.1) can be used as reference.

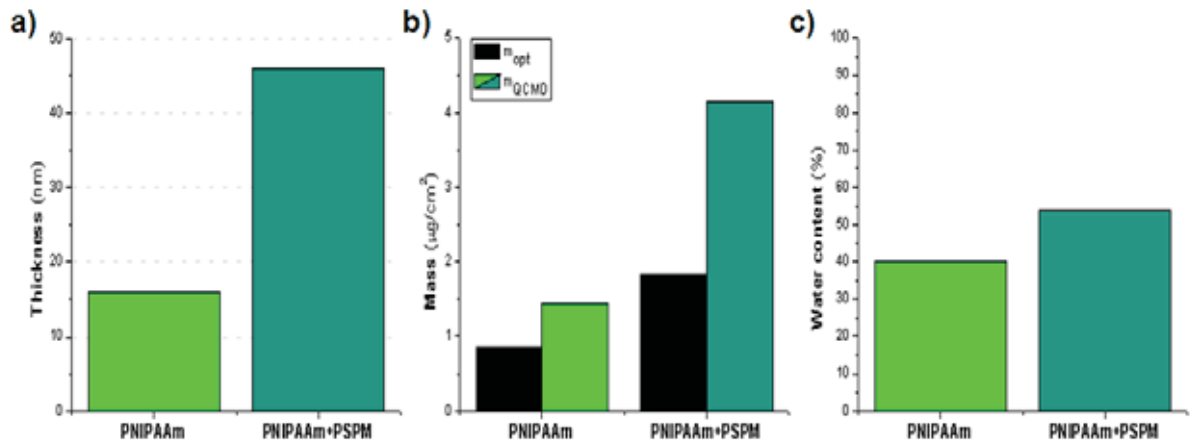

Figure 51 Comparison between the (a) acoustic thickness (b) m_{QCMD} (*coloured columns*) and m_{opt} (*black columns*) and (c) hydration values for PNIPAAm (green) and PNIPAAm / free-PSPM copolymer brushes (dark cyan).

Both optical and acoustically obtained parameters represented in Fig. 51 show a noticeable increase in their values. For instance, a variation in the thickness from 16 nm (first block) to 46 nm is measured for the copolymer brush as can be seen from Fig. 51a. These results differ significantly from those previously obtained for the assembly of a free-PSPM brush on top of planar gold surfaces, which showed thicknesses of around 360 nm. Such difference can be also observed for m_{opt} and m_{QCMD} values depicted in Fig. 51b since PSPM as copolymer shows variations in the optical mass of 1 µg/cm^2 and 2.7 µg/cm^2 in case of the acoustic mass, while PSPM assembled on gold yielded values more than 10 times higher. A reason for these

differences in the growth may be due to the limited number of active sites from which PSPM can start growing in the case of the PNIPAAm brush, significantly smaller than the density of active sites in the monolayer of thiol initiators. Although ATRP reactivation can be considered to be rather successful, a high percentage of PNIPAAm chains may still remain in a dormant state and, thus, PSPM grows to a much lesser degree. This has a direct impact on the lower film thickness values obtained. The lower the PSPM chain density the higher the lateral space the polymer can occupy and chains tend to acquire a more coiled, curly-like, structure instead of the fully extended chains as previously observed for higher densities.

When passing from a single block brush to a di-block structure the total aqueous content of the system is calculated to change from the initial 40 % calculated for PNIPAAm to a 56 % for the PNIPAAm/PSPM copolymer as shown in Fig. 43c. As the synthesis of each single block was followed in well-differentiated experiments, one would be able to discriminate between the respective contributions of each single component to the total water content of the structure being formed. Thereby, the individual contribution of the block of PSPM to both total acoustic (2.7 $\mu g/cm^2$) and optical (1 $\mu g/cm^2$) masses allows for the calculation of a hydration value of almost the 65 %. This value is around a 15% higher than the case of free-PSPM directly synthesized from a monolayer of thiols on gold and would confirm the assumption of the curly-like situation brought by a lower density of PSPM chains in the copolymer which is reflected in a higher capacity to entrap water in the structure.

4.3. Conclusions

This chapter has first described the growth of PMETAC, PSPM and PNIPAAm?? brushes via ATRP from monolayers of initiator thiols chemically bound to gold surfaces. The growth was followed by means of the combination of optical and acoustic techniques in a single device. Such combination allowed for simultaneous measurement of dry and wet masses of the brush and, therefore, to determine the water content of the brushes composed of each of the three polymers under study. Remarkably, PMETAC brushes show the highest hydration, of approximately the 65 % although they grow less efficiently than PSPM brushes. The content of water and hydration of PSPM brushes varies with the growing conditions. If the synthesis takes place in the presence of a co-catalyst, Cu (II), where the chain polydispersity is limited, the water content stays close to the 45%. On the contrary, Cu (II)-free PSPM brushes, which show a significantly higher film thickness, allow reaching a 49% of entrapped water in the structure.

The growth of PMETAC and PSPM brushes was also followed for samples grown from different densities of initiator thiols grafted on the gold surfaces, and the yield of polymerization and the water content of the brush were determined. Remarkably, PMETAC brushes grown from a wide range of initiator percentages (between 1% and 100%) show an almost constant content of water. This observation implies that the water associated to the monomers represents most of the water in the brush independently of the packing of the brush chains in the brush and the small differences in water content between the different brushes must be, thus, due to water entrapped in the structure of the brush. In case of PSPM brushes the study basically showed the effect of whether incorporating Cu (II) or not in the polymerization reaction at the same time that the grafting density was also varied. Surprisingly, calculation of the aqueous content for PSPM (4:1)

and free-PSPM brushes led to obtain almost the same values for the both of them at the different initiator densities employed. From a hydration of the 30% at 1% of initiator grafting, they passed to have around the 65% for an initiator density of the 10% and then, for a density of the 50%, a drop in the hydration occurred. Such a drop has a stronger effect on the brushes grown in the presence of Cu (II), which decreased down to the 31 %, rather than in freely grown PSPM, which drops its water content to the 45 %. But polymerization from a monolayer of initiator recovered the water content to higher water contents as those commented above.

In addition, the assembly of a multi-responsive copolymer brush composed of a first brush of PNIPAAm and a second block of PSPM on top has been achieved by reactivation of the ATRP process to originate a highly hydrated structure where a 56 % of the mass corresponds to water. However, the low percentage of polymerization sites being regenerated leads PSPM chains in the second block to present a more coiled conformation, in comparison to the situation where PSPM brushes are synthesizes from a surface, which affects considerably to thickness and water content values obtained.

4.4. References

(1) Kim, J.-B.; Bruening, M. L.; Baker, G. L. J. Am. Chem. Soc., 2000, 122, 7616–7617.

(2) Jones, D. M.; Huck, W. T. S. Adv. Mater. 2001, 13, 1256-1259.

(3) Topham, P. D.; Howse, J. R.; Crook, C .J.; Parnell, A. J.; Geoghegan, M.; Jones, R. A. L.; Ryan, A. J. Polymer Int. 2006, 55, 808-815.

(4) Parnell, A. J.; Martin, S. J.; Dang, C. C.; Geoghegan, M.; Jones, R. A. L.; Crook, C. J.; Howse, J. R.; Ryan, A. J. Polymer 2009, 50, 1005-1014.

(5) Shah, R.R.; Merreceyes, D.; Husemann, M.; Rees, I.; Abbott, N.L.; Hawker, C.J.; Hedrick, J.L. Macromolecules 2000, 33, 597-605.

(6) Dubacheva,G. V.; Van Der Heyden, A.; Dumy, P.; Kaftan, O.; Auzély-Velty, R.; Coche-Guerente,L.; Labbé, P. Langmuir 2010, 26, 13976–13986.

(7) Cheng, N.; Azzaroni, O.; Moya, S.; Huck, W. T. S. Macromol. Rapid Commun. 2006, 27, 1632-1636.

Chapter 5:

Quantification of the collapse of PE brushes

5.1. Introduction

The responsive character of polyelectrolyte brushes, moreover highly hydrated brushes, upon external stimuli has been already commented in a previous section. Such response, as explained, leads to changes in the conformation of the chains in the brush and is reflected as variations in the film thickness and in water content. The process is featured by its reversibility since the system can be taken back to the initial state through re-establishment of the initial environmental conditions.

As a consequence of the collapse not only the film thickness and packing of the chains are modified, but water is released from the brush, also in a reversible manner.[1] The variations in thickness in brushes during their collapse have been extensively studied, though less work has been done on quantifying the release of water associated to the collapse.[2-4] While film thickness can be rather directly obtained by means of standard techniques like Ellipsometry or AFM, the calculation of the water content after the collapse became a more difficult task to solve. The first approaches towards quantification of the water amount released by the brush regarded the use of the QCM-D technique, which allowed converting the monitored increases in the oscillation frequency of the quartz sensor into water mass loss. But at the same time the calculation of the water percentage being lost failed because the original content of water was not known and the water lost during collapse could not be compared with the total water amount initially contained in the brush. Nevertheless, as a consequence of the studies performed by means of combinative acoustic (QCM-D) and optical (Ellipsometry) measurements for the assembly of polyelectrolyte

brushes of different composition, the initial amount of water in the brush can be now known and, therefore, the percentage of water lost during the shrinkage of the polymer chains in response to external stimuli can be calculated as well.

This chapter will be then focused on the characterization of the water release induced by the collapse of the polymer chains upon different external stimuli: the use of an increasing ionic strength in the bulk solution or a change in the nature of the counterions for PMETAC and PSPM brushes, and the raising of the temperature over the LCST to provoke the shrinkage of PNIPAAm systems.

5.2. Results and discussion

5.2.1. Ionic strength-responsive systems

5.2.1.1. Shrinkage of PMETAC and PSPM brushes

The collapse with ionic strength was followed in situ by means of single QCM-D measurements for PMETAC, PSPM free and PSM (4:1) brushes (See Materials and Methods section) grown from a monolayer of initiator molecules grafted onto the surface. The frequency changes monitored were converted, by application of the Sauerbrey equation, to the corresponding mass loss values which have been plotted in Fig. 52a. For the calculation of the percentage lost (Fig. 44b) these mass values are compared to those previously shown in section 4.2.1. The variations in the film thickness, which actually originate the water loss, were also calculated by conversion of the frequency shifting values (Equation 2) for the three systems studied.

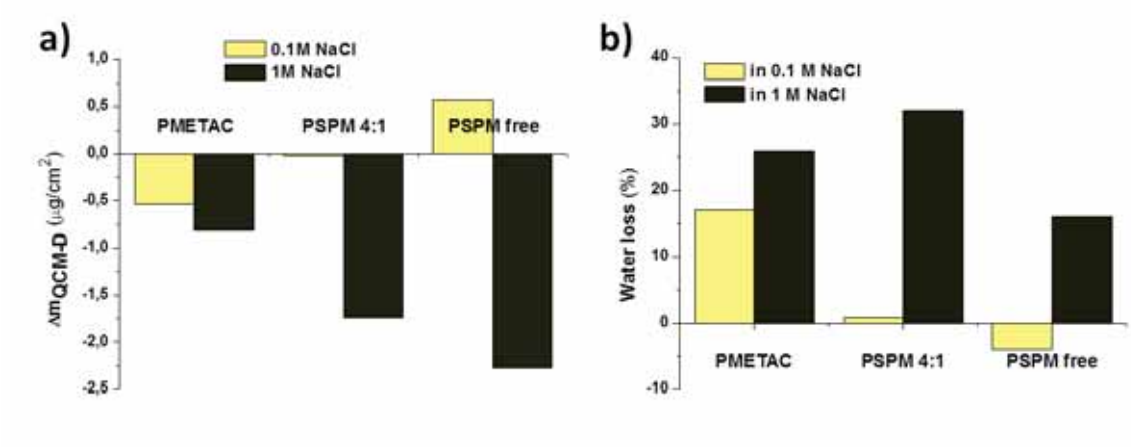

Figure 52 (a) m_{QCMD} variations and (b) water loss percentages obtained for PMETAC, and for (4:1) PSPM, and freely grown PSPM brushes by exposure to 0.1 M (light colored columns) or 1 M (dark colored columns) NaCl solutions.

At 100 mM and 1M NaCl, the water mass in the PMETAC film decreased in 0.56 and 0.78 µg/cm^2, respectively, as plotted in Fig. 44a. This mass difference only represents a 17% of the

initial aqueous content in the case of the lowest ionic strength employed and then the loss rises up to the 26% for the treatment with 1 M NaCl (Fig. 44b). It is remarkable how despite of the high percentage of entrapped water the structure only releases a fourth of the total amount. In terms of PMETAC brush thickness the height variation triggered by exposure to 0.1 M and 1 M NaCl solutions would be, respectively, of 6 and 10 nm.

For the (4:1) PSPM brush, there is a negligible loss of mass at 0.1 M NaCl, but then the brush releases over 1.7 $\mu g/cm^2$ of water, a 32% of its content, through a collapse of almost 20 nm when the ionic strength is increased to 1 M. In the case of freely grown PSPM brushes, exposure to 0.1 M NaCl and lower ionic strength (not shown) leads, surprisingly, to a mass increase in the brush. This behavior and the observation that there are no changes in the mass of the (4:1) PSPM are unexpected results and could be explained as a conformational change of those PSPM chains protruding from the brush towards solution as has been explained previously. In a soft ionic strength environment these chains can become more coiled and closer to the brush, instead of being as extended as in aqueous solution. If several of these chains would coil on top of the dense brush region, the distance between different protruding segments of chains will become smaller and the QCM-D could sense a sort of extra layer, which includes both the chains and that water entrapped in the coiled structure. As a consequence of this, QCM-D would sense the water between these chains and the mass of the brush would increase for the conditions of low ionic strength. An alternative explanation could be that if these protruding chains are very long, their mass is partially decoupled from the resonator and cannot be registered until the chains become coiled and closed to the surface with the low ionic strength. A combination of both suggested situations can take place as well. Nevertheless, when the NaCl concentration is increased to 1

M, the PSPM brushes return to behave as one would expect for this type of polyelectrolytes, and the brush collapses. In their collapse, freely grown PSPM brushes decrease their initial film thickness from 360 to 336 nm and release up to almost 3.0 μg/cm^2 of water. The lost of water for PSPM is more significant than for PMETAC, in absolute terms. But when the change in mass for free-PSPM is compared to the original water content calculated for the film (14.2 μg/cm^2) it results in a decrease of only the 16% of the total mass.

5.2.1.2. Effect of the initiator density in the water mass loss

As already seen in Chapter 4, the number of initiator molecules grafted on the surface had a direct impact on the final structure achieved for the brush and, by extension, on the amount of water that can be entrapped. Therefore, exposure of such systems may yield very different results depending on the initiator density used to build the film. Then, quantitative analysis on the amount of water released upon exposure to increasing ionic strengths was also extended to PMETAC brushes grown from different initiator densities, as plotted in Figure 53.

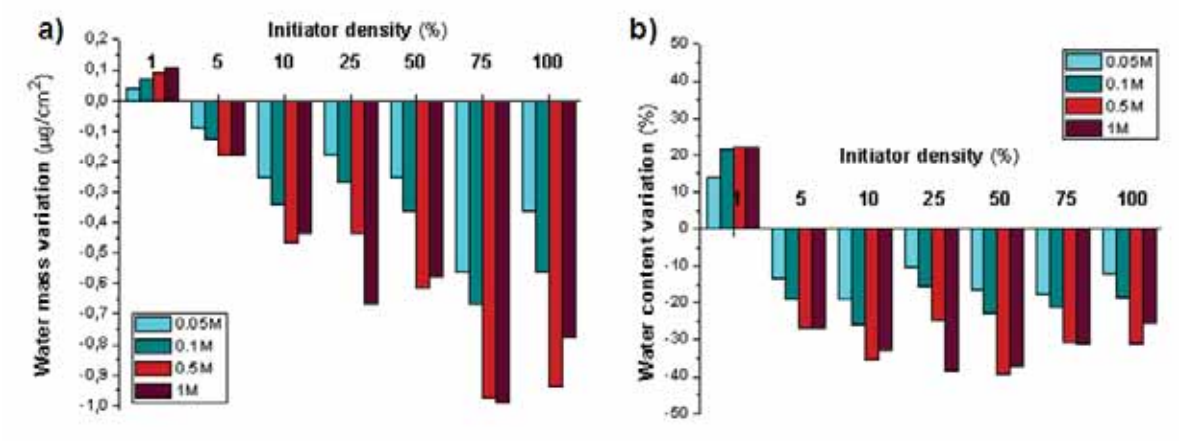

Figure 53 (a) water mass and (b) water content percentage variations derived from treatment of the PMETAC brushes with 0.05 M (cyan), 0.1 M (blue), 0.5 M (red) and 1 M (purple) NaCl solutions.

Fig. 53a compares the water mass shifts in PMETAC brushes of variable density of initiator obtained after treatment with 0.05, 0.1, 0.5 and 1 M NaCl solutions. Mass values were calculated from the frequency shifts monitored by the QCM-D by the Sauerbrey equation. In all the cases, the effect in the signal caused by varying the solution density was taken into account for the calculation and the frequency values stemming from it were subtracted. Exposure of the brush to salt solutions yielded negative changes in the mass, except for the PMETAC brush grown from 1% initiator, which shows a small positive shift. For brushes with initiator grafting percentages between 5% and 100% the changes in mass are bigger as the amount of initiator on the surface is increased. Also released mass variations are, as expected, smaller after exposure to solutions of lower ionic strength. For those brushes grown from 100% and 75% initiator densities 0.05 M and 0.1 M NaCl concentrations would drive to a loss of around 0.4-0.5 μg/cm^2 but at higher ionic strengths such as 0.5 and 1 M the brushes lose almost 1 μg/cm^2, which represents a 30% of the initial water content, as can be observed from Fig. 53c. The percentage of water lost reaches a

maximum of the 40% for the brushes grown from 50% and 25% initiator when treated with the NaCl solutions, and remains constant in values around the 30% for the rest of the samples under study. The behavior shown by the PMETAC brush with 1% initiator grafted can be probably due to water molecules carried by ions diffusing through the polymer chains. The fact that the maximal loss of water for all the studied brushes corresponds to a 40% of the total hydration of the brush means that the brush does not fully dehydrate exposing up to 1 M NaCl.

Figure 54 shows how such variations in water content can be also expressed in terms of water molecules per METAC monomer.

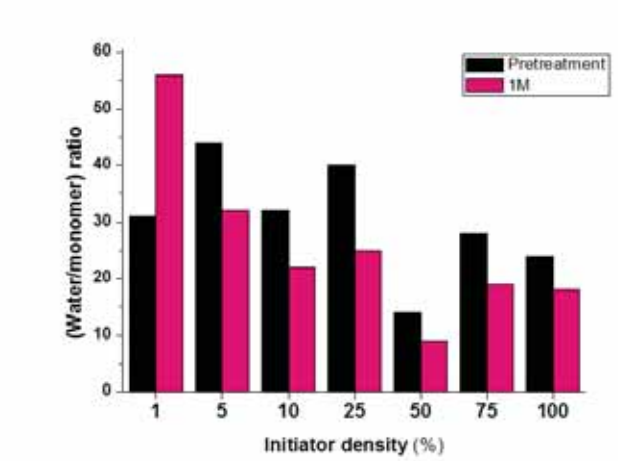

Figure 54 Water molecules per monomer of METAC at the initial/non-treated state (black columns) and after exposure upon 1 M NaCl (purple columns).

The treatment of 100% initiator-grafted brush with 1M NaCl, for instance, reflects in a decrease of this ratio from 24:1 to 18:1, while the opposite situation would take place for brushes grown from 1% initiator, where the number of water molecules changes from 31:1 to up to 56:1 upon exposure to the highest ionic strength. Only at 1% initiator the brush fails to accomplish a conformational change, which would induce a loss of water, upon an increase in the ionic strength of the bulk solution. This change in behavior is indicative of the polyelectrolyte chains

not having or having very little water entrapped that can be lost. Probably at this density of initiator the chains are extended, coating the surface and not forming a brush as this is understood.

Since polymer chains rearrange and become closer together, it can be assumed that the water being primarily lost during the brush collapse corresponds to entrapped water, especially for ionic strengths below 0.1 M, but at higher ionic strengths some dehydration of the monomers should take place as well.

5.2.1.3. Effect of the nature of the counterions

The effect of a counterion exchange in the hydration of the brush has been also studied. With this purpose, Cl^- counter-ions were replaced by ClO_4^-, a chaotropic anion according to Hofmeister's classification[5], which creates a more hydrophobic environment for the film and that has been already shown to have a pronounced influence on the water content of PMETAC brushes[1]. Then, exposure of a PMETAC brush grown from 100% to 0.05 M and 0.1 M $LiClO_4$ solutions was followed in situ by QCMD and the frequency changes observed were converted into mass values, as explained above. Treatment with both concentrations makes the brush releasing 1.65 $\mu g/cm^2$ of water, which represents about the 54% of the water initially entrapped. The difference between $LiClO_4$ and NaCl is clearly depicted in Fig. 55, which compares the percentage of water lost for the same PMETAC brush treated by both salts.

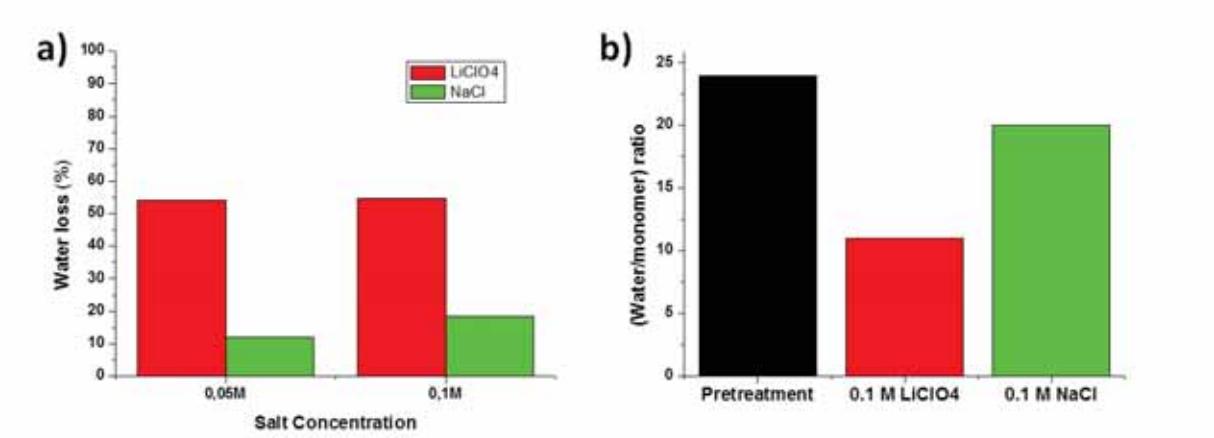

Figure 55 Water releases caused in a 100% initiator-grafted PMETAC brush by treatment with NaCl (green) and $LiClO_4$ (red) solutions with the same ionic strength. (a) Water percentage lost and (b) water molecules remaining per monomer of METAC.

While NaCl in those concentration ranges would only remove as much as the 18% of the water through the collapse originated, $LiClO_4$ provokes the release of almost three times more the amount of water. This means that the number of water molecules per METAC monomer remaining in the brush during the collapse (Fig. 55c), would decrease from 24:1 to 20:1 for the treatment with 0.1 M NaCl, and up to 11:1 for 0.1 M $LiClO_4$.

The high affinity ClO_4^- ions show for quaternary amines, as in PMETAC, is proved by the replacement of the Cl^- induced by the presence of ClO_4^- even at concentration as 0.05 M. These ClO_4^- ions, which are bulky and hold a diffuse charge, are less hydrated than Cl^-, and due to their chaotropic nature they tend to soak non structured water and create a more hydrophobic environment around the quaternary ammonium groups of METAC monomers.

5.2.2. Thermally-responsive brushes

For thermally-responsive PNIPAAm brushes the change in the water mass content was measured when the temperature of the system was taken from a value below the LCST, such as 23º C, at which polymer chains appear in a swollen state, to a value over the critical LCST such as 40º C, where the film is fully collapsed. As explained above, below the LCST value, the polymer is hydrophilic and the amides in the pendant group of the NIPAAm monomers form hydrogen bonds in the aqueous media with surrounding water molecules. This interaction helps to stabilize the chains and leads the film to be in a swollen state. When the temperature is risen over the LCST, the amide-water hydrogen bonds of PNIPAAm are disrupted and this causes the collapse of the brush. The collapse could be again followed in situ by means of QCM-D, since it permits applying a temperature increase/decrease cycle where the temperature increase took place gradually (5ºC/min) and the cycle-limiting temperatures were programmed to be kept for periods over 10 min, to ensure the total collapse/swelling of the brush.

Both acoustic thickness and water mass were calculated from the frequency response of the PNIPAAm brush when exposed to a temperature of 40º C, as depicted in Figure 56. These values obtained are also compared to those obtained in section 4.2.1 for the growth of the brush from 50% initiator density, which are used as reference values.

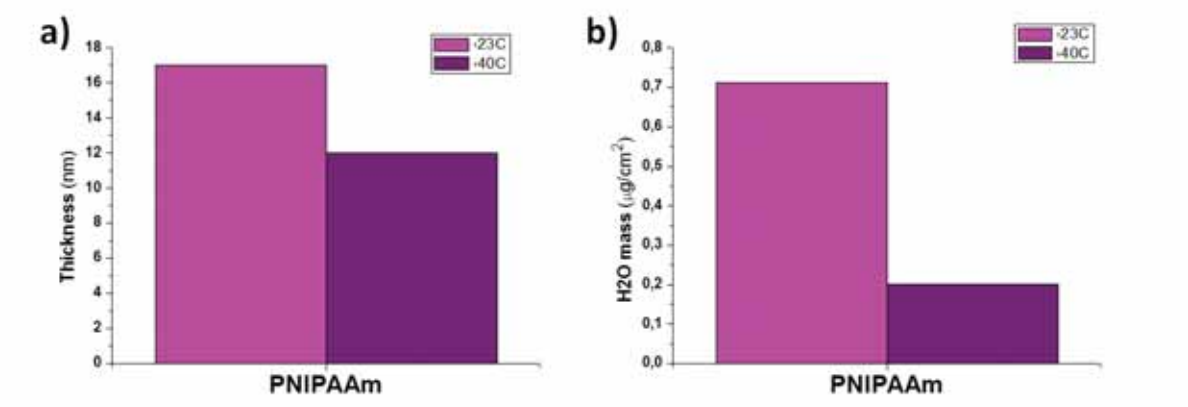

Figure 56 (a) film thickness and (b) water mass values calculated for a PNIPAAm brush when the environmental temperature is raised from 23ºC (pink) to 40ºC (purple).

From Fig. 56a it can be observed how, during the shrinkage, the film thickness for the PNIPAAm brush undergoes a decrease of 5 nm, from 16 to 11 nm. Such change could be initially considered not to be very dramatic, but then calculation of the water release associated to the collapse (Fig 8b) showed a water mass change from initial 0.58 μg/cm^2 to only 0.127 μg/cm^2. By taking into account the original hydration of the brush, such change in the mass means that almost the 80% of the initial water content of the brush is being removed. Decreasing back the temperature to 23ºC provoked rehydration of the brush.

None of the brushes studied so far in this chapter showed a complete dehydration during collapse. PNIPAAm brushes, which are not charged are the ones losing more water, an 80 % compared with a maximum loss of the 50 % at 1 M $LiClO_4$ and NaCl calculated for PMETAC and PSPM polyelectrolyte brushes, respectively. During the collapse with the temperature, the monomers of PNIPAAm break their hydrogen bonds with water and establish bonds among themselves, excluding water and becoming hydrophobic. Nevertheless, there may be some remaining water trapped between the collapsed chains. On the contrary, for the polyelectrolytes,

even at high ionic strength water can still be associated with the monomers because of their hydrophilic character.

5.2.3. Collapse of multi-responsive brushes

In section 4.2.3 it was already explained how one could go through consecutive ATRP of two different monomers to form a di-block copolymer. While the assembly of the first brush started from the initiator molecules grafted on the surface, the growth of the second block took place on top of the previous system through reactivation of the polymerization process. In this study the copolymer was composed of a first brush of thermally sensitive PNIPAAm with an ionic-strength responsive PSPM on top. A scheme of such multi-responsive activity is shown in Figure 57.

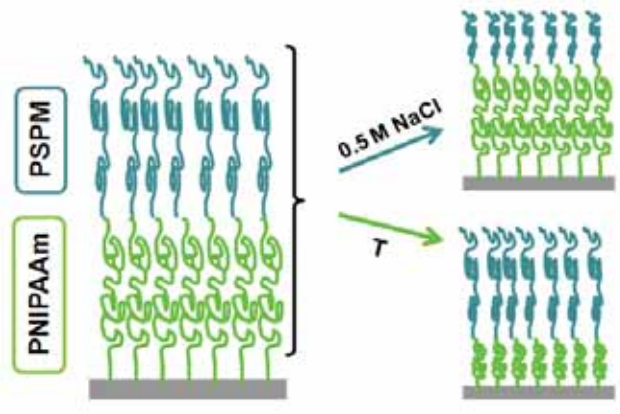

Figure 57 Schematic view of the responsive activity of a PNIPAAm/PSPM copolymer brush when exposed to a high ionic strength (up) or to an increase in the temperature above the LCST.

As the original water content of the copolymer, in general, and of the respective blocks, in particular, is already known the amount of water being released as a result of the induced collapse can be determined.

The copolymer brush was first exposed to a temperature increase/decrease cycle where the temperature oscillated between 23 and 40 ºC in a same fashion as explained above for a single block of PNIPAAm. In case of the PNIPAAm/PSPM copolymer brush the water lost calculated from the collapse now results to be of 0.235 $\mu g/cm^2$. By considering the system as a single entity such loss would be equivalent to the 10% of the initial water content of the film but in case of discriminating between individual contributions of each single block, it would represent the 40% of the water entrapped in the PNIPAAm block as measured before the growth of PSPM. From such results it is rather clear that the presence of the PSPM on top has ample effect on the shrinkage of PNIPAAm in comparison to the situation where PNIPAAm appeared as a single block, in which the brush was able to release the 80% of its aqueous content. Such collapse limitation may be explained by a decrease in the chain mobility for the PNIPAAm imposed by the synthesis of the block of PSPM.

In order to determine the water lost induced by an increase in the ionic strength, the copolymer brush was exposed to aqueous solutions of NaCl of increasing concentrations: 10, 50, 100 and 500 mM, which provoked a mass loss of 0.054, 0.343, 0.470 and 0.722 $\mu g/cm^2$, respectively. The maximum release induced, for the 500 mM NaCl solution, would represent the 41% of the total water entrapped by the PNIPAAm/PSPM system and around the 31% of the water associated to the block of PSPM, if considered individually. Comparison of this value to the percentage lost

for free-PSPM directly assembled from a gold surface shows that for the case of the PSPM in the copolymer the water percentage being released almost doubles that of the single brush. Such difference is explained by the curly-like structure that PSPM chains adopt when the synthesis is carried out from a preformed brush, as already seen in Chapter 4, as a consequence of the higher free lateral space brought by a bigger distance between polyelectrolyte chains. This situation, which already made the PSPM brush in the di-block copolymer being around a 15% more hydrated than that synthesized from a monolayer of thiol, can also contribute to a more pronounced chain collapse. This behavior is opposite to that observed above for the PNIPAAm block, especially because PNIPAAm chains are doubly restricted by the surface and the brush over them, while the PSPM chains still keep one of their ends free and exposed to the bulk.

Though the increase in the ionic strength of the bulk solution was considered in this case to affect solely to the block of PSPM, it should be taken into account that variations in the salt concentration can provoke dramatic changes in the properties of PNIPAAm brushes.[6] Such changes, which basically affect to the LCST temperature at which PNIPAAm undergoes chain shrinkage, have been reported to show a strong dependence on the nature of the counterions employed and their position in the Hofmeister series. In the particular case of NaCl, for instance, an increase in the salt concentration up to 1M has been proved to cause a decrease of the LCST value down to 26 ºC. Since in this work the working temperature was set at 23 ºC, the resulting decrease in the LCST still remained out of the range and did not affect to the water content. However, for higher working temperatures it would turn into a crucial issue and an additional water release should be calculated.

5.3. Conclusions

In this chapter, the percentage of water lost has been calculated for the collapse of responsive polymer brushes upon exposure either to high ionic strengths, as for PMETAC/PSPM systems, or to temperatures over the LCST, as shown for thermally-responsive PNIPAAm. On one hand, PMETAC and PSPM (4:1) polyelectrolyte brushes lost a maximum of around a 30 % of their water content at 1 M NaCl, and freely grown PSPM only released a 16% of its aqueous content upon treatment with the same ionic strength. The thermally-responsive PNIPAAm, on the other hand, showed a water release of the 80% of its water content at a temperature of 40º C.

Exposure of PMETAC brushes, grown from different initiator densities, to increasing ionic strengths of NaCl permits calculating the amount of water released at the osmotically originated collapse. From this treatment a removal of around the 30-40% of the water in the brush is observed for 0.5 and 1 M NaCl solutions while only a 10% is eliminated at ionic strengths below 0.1 M NaCl.

It has been also shown that exposure of a PMETAC brush grown from 100% to 0.05 M and 0.1 M solutions of chaotropic ClO_4 anions makes the brush releasing 1.65 $\mu g/cm^2$ of water, around the 54% of the water initially entrapped, almost three times more than the water release induced by the exposure to NaCl in the same conditions.

The amount of water released would mostly come from entrapped water but changes in the hydration of the monomers can take place as well in response to high ionic strengths. However, the total dehydration of the brush could not be reached in any case.

Finally, alternate exposure of PNIPAAm/PSPM multi-responsive brush to either an increase in the temperature over the LCST or high ionic strength solutions showed the selective response of the structure built. However, reactivity of each single block is clearly affected by the presence of a second brush. Indeed, for PNIPAAm: simultaneous tethering to the surface and the block on top limit the collapse of the chains upon temperature and thus the amount of water released (40%) is much lower than the one seen for a single PNIPAAm brush (78%). For the PSPM block on top, on the contrary, the curly-like structure allows for a more pronounced film collapse that originates a 31% of the water content to be released.

5.4. References

(1) Moya, S. E.; Azzaroni, O.; Farhan, T.; Osborne, V. L.; Huck, W. T. S. Angew. Chem. Int. Ed. 2005, 44, 4578 –4581.

(2) Lego, B.; Skene, W. G.; Giasson, S. Macromolecules 2010, 43, 4384-4393.

(3) Moya, S. E.; Azzaroni, O.; Kelby, t.; Donath, E.; Huck, W. T. S. J. Phys. Chem. B 2007, 111, 7034-7040.

(4) Parnell, A. J.; Martin, S. J.; Jones, R. A. L.; Vasilev, C.; Crook, C. J.; Ryan, A. J. Soft Matter 2009, 5, 296-299.

(5) Hofmeister, F. Arch. Exp. Pathol. Pharmakol. 1888, 24(4-5), 247–260.

(6) Zhang, Y.; Furyk, S.; Bergbreiter, D. E.; Cremer, P. S. J. Am. Chem. Soc. 2005, 127, 14505-14510

Chapter 6:

Hybrid LbL-Polyelectrolyte brush systems

6.1. Introduction

As already explained in Section I, polyelectrolyte multilayers built up by LbL process represent a simple pathway to fabricate a film with well controlled film thickness. However, the stability of the multilayered system in different environments is generally a cause of concern. The adhesion of the first layer to the surface poses, for instance, a problem which should not be neglected. Because the attachment of the first layer depends solely on the interaction of the polyelectrolyte with surface charges, the whole multilayer assembly can be desorbed by either changing the sign of the surface charge of the substrate or by addition of competing low molecular weight electrolytes which at some concentration can displace the polymer molecules in the first monolayer.[1]

In this regard, the use of a substrate in which a brush has been previously grown for the assembly of a polyelectrolyte multilayer on top arises as an optimal alternative to overcome the troublesome situation commented above.[2] Depending on the choice of the monomer an either positive or negative stable surface charge can be established and since the polyelectrolyte chains are covalently attached to the surface, they can only be removed from the surface by cleaving the chemical bonds that connect the polymer to the substrate. Besides, the assembly of the brushes can be easily controlled concerning layer thickness, graft density, charge density, and swelling behavior, and their use thus represents an interesting approach to prepare surfaces with well-defined structure and surface charge. The use of polyelectrolyte brushes as binding sites for the subsequent LbL deposition of charged polymer chain brings some other advantages: in addition to homogeneously coated surfaces, it is also possible to assemble brushes from patterned

substrates.[3] For instance, the soft lithographic technique of micro-contact printing (μCP) has proved to be an invaluable tool in the synthesis of such patterned polymeric coatings at the micrometric level.[4] The μCP technique allows for the formation of geometrically well-defined regions of grafted ATRP initiating molecules, as imposed by the topology of the stamp employed, from which polyelectrolyte brushes are grown. Subsequent formation of PEMs would thus only take place on top of those specific sites where brushes supply a certain surface charge. On the contrary, brush-free regions do not provide proper sites for electrostatic attachment of polyelectrolytes. Besides, the responsiveness of polyelectrolyte brushes implies that the hybrid brush/multilayer system also behaves as a smart surface which shows structural changes triggered by different external stimuli. Such responsive behavior can turn into something more complex if the PEM assembled on top is composed of PDADMAC and PSS polyelectrolyte pair, which would collapse upon exposure to increasing ionic strength (Chapter 2) or can become even more sophisticated if, instead of a single brush, a multi-responsive copolymer brush would be employed as substrate for the LbL deposition.

For a number of reasons, it can be expected that LbL adsorption on polyelectrolyte brushes differs considerably from the formation of multilayers on solid surfaces. One of the main differences would come from the fact that, contrarily to solid or liquid interfaces, which represent a more or less sharp boundary between different phases, brushes can be considered as fuzzy films with a thickness ranging from a few nanometers to hundreds of nanometers. A polyelectrolyte brush can be expected, for instance, to have a much higher adsorption capacity than a solid surface because of its much higher charge density provided by the three-dimensional charge distribution.[5] When during the LbL assembly oppositely charged polyelectrolytes are

interacting with the brush, they may become embedded between the polyelectrolyte chains in the interior of the brush, instead of adsorbing at the brush surface.[6] But such capability of the incoming bulk polyelectrolytes to diffuse through the brush will be undoubtedly related to the degree of compactness shown between the chains. It has been shown how several factors like the grafting density or the existence of regions in the brush with a different polymer density, as a result of a poor control over the chain polydispersity (see section 4.2.1), can affect the interactions with neighboring chains and thus lead to looser structures. The less compacted brush structure that first layers being deposited find, the deeper they will be able to penetrate into the brush. Diffusion may also have certain effect on the PE-PE electrostatic interactions driving the formation of the multilayers, mainly related to the sterical repulsions provoked by the brush chains. Then, taking all these considerations into account, it is more than likely that the final structural arrangement also differs considerably from that obtained after LbL assembly of polyelectrolytes on a planar SiO_2 substrate. Indeed, the assembly of these brush-LbL hybrid systems has been demonstrated to provoke the appearance of some interesting topological features as shown by some authors.[7]

Along this 6th chapter, the LBL deposition of oppositely charged polyelectrolytes conducted on polyelectrolyte brushes will be described. More specifically, the assembly of a multilayer composed of PDADMAC and PSS polyelectrolyte pair on top of negatively charged PSPM brushes was followed. Since assembly of PDADMAC/PSS systems on SiO_2 surfaces has been sufficiently described in previous chapters, those results obtained can be here taken as a reference for a proper comparison. While the use of acoustic QCM-D measurements permits quantifying the amount of polymer deposited, microscopy based techniques such as Atomic

force microscopy (AFM) and scanning electron microscopy (SEM) will become a useful tool for the characterization of the topology of films built in different experimental conditions.

6.2. Results and discussion

6.2.1. Fabrication of PE brush-PE multilayer complex systems

6.2.1.1. PDADMAC/PSS deposition on top of brushes

The alternate deposition of PDADMAC and PSS on top of PSPM brushes, grown from monolayers of initiator thiol, was followed in-situ by means of QCM-D. The growth of PSPM chains was carried out, as already seen in chapter 4, by following two different protocols which basically differed in the content of $CuCl_2$ in the polymerization. In absence of Cu (II) the polymer chains grow freely (PSPM free) while the presence of $CuCl_2$ in a well-defined proportion has been showed to help to control the final chain length polydispersity (PSPM 4:1). Working with different chain polydispersities will have a direct effect on the packing of the brush and, as a consequence, the way that PE layers are deposited may be varied.

First, three bilayers of (PDADMAC/PSS) were assembled on top of a freely grown PSPM brush, with 0.5 M NaCl rinses between each layer deposition, as depicted in Figure 58.

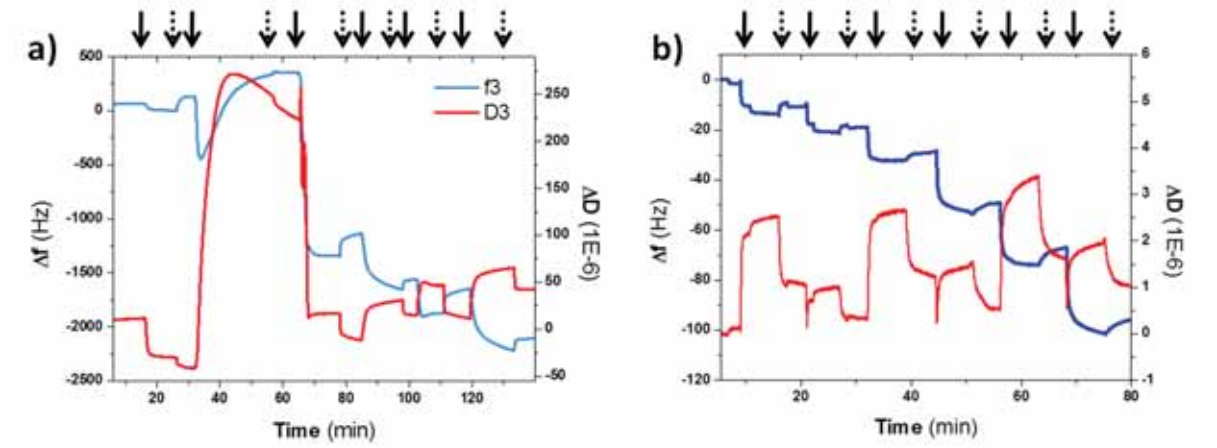

Figure 58 Assembly of 6 layers of PDADMAC/PSS in 0.5 M NaCl on top of a free-PSPM brush (a) and on top of a SiO_2 wafer (b), which is used as reference. The starting time of each deposition step and rinses are indicated by solid and dashed *arrows*, respectively.

Comparison between Figures 58(a) and 58(b) clearly shows how the presence of the PSPM brush underneath is affecting the assembly of PDADMAC/PSS polyelectrolyte pair. Among all the differences observed between both figures, the most striking feature would arise from the deposition of the two first layers of the PEM, which speaks about the complexity of the hybrid system formed. Assembly of the first PDADMAC layer on top of the brush made the frequency reaching positive values of almost +70 Hz, and of up to +290 Hz when polyanionic PSS was added while the same adsorption on bare SiO_2 showed to a continuous decrease of the frequency to -10 Hz and -17 Hz for the first two layers. Such a result could initially result very surprising, especially after defending the higher capacity of brushes to adsorb charged polyelectrolytes in comparison to bare charged surfaces. This phenomenon might be explained by the reorganization of negatively charged PSPM chains in order to form the electrostatically-driven complexation with the bulk positive chains of the incoming PDADMAC. As a consequence of the interaction between oppositely charged PDADMAC and PSPM the energy dissipation of the system

decreases (Fig. 58a) and a state of higher rigidity is reached. Since polyelectrolyte brushes are highly hydrated systems, the structural rearrangement of the system makes some of the water entrapped in the structure to be released. When negative PSS was added, the situation became even more extreme and the amount of water lost was bigger. Nevertheless, the main difference found in comparison to the first PDADMAC layer is that the adsorption of PSS raises ΔD values up to 250 x 10^{-6}, which is indicative of a softening of the film. To understand such behavior it must be taken into account how the adsorption of PSS chains is totally influenced by the layout of the PDADMAC chains already bound to the brush, which provide the binding sites for the electrostatically-driven interaction. Unbound chain regions of the first layer of PDADMAC may protrude into the bulk solution, and, therefore, a certain number of the incoming PSS chains can be anchored outside the PSPM brush. This causes the energy dissipation monitored upon shear stress to be much higher. However, such softening of the film disappeared as soon as the next PDADMAC layer was added and a high rigidity state was reached again. The incoming chains of PDADMAC bind to the negative PSS sites they find outside the brush and from this level onwards the assembly takes place on top of the brush rather than by diffusion in the structure of the PSPM. Assembly of this 3rd layer also had a dramatic effect in the frequency response and a shift from +290 to -1200 Hz was measured, which relates to a big mass being adsorbed. With successive layers deposited both frequency and dissipation followed a normal trend until final values of -2170 Hz and 50×10^{-6}, respectively, were observed for the last PSS layer adsorbed which are 20 and 50 times higher than those obtained for a same number of layers on top of a bare SiO_2 substrate, -96 Hz and 0.916×10^{-6} (Fig. 58b)

The same analysis was repeated for a PSPM brush grown in the presence of Cu (II) in order to control the polydispersity of the growing chain. Thus, QCM-D was employed to follow the alternate deposition of PDADMAC and PSS polyions, up to 6 layers in total, on top of a PSPM (4:1) brush. The recorded variation of the acoustic parameters f and D as the PEM was built can be seen in Figure 59.

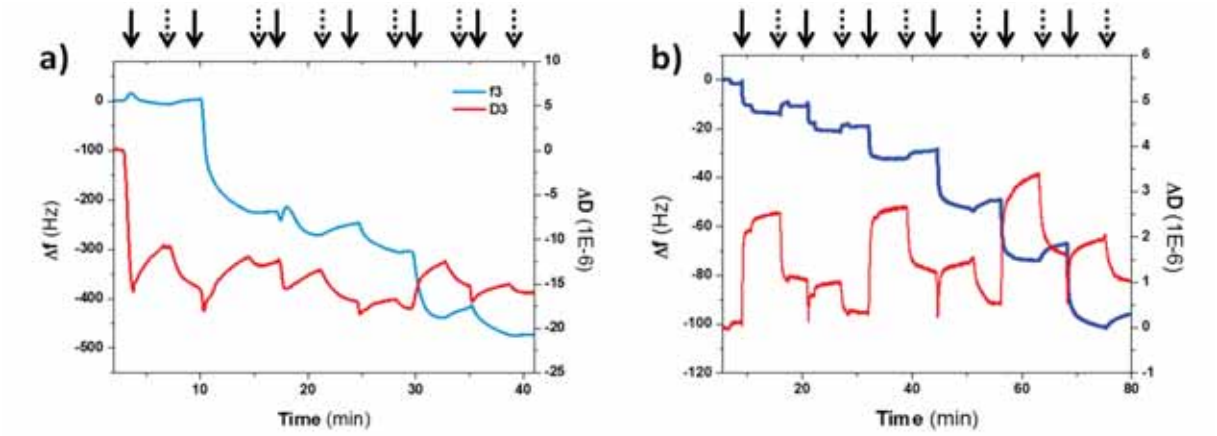

Figure 59 Assembly of 6 layers of PDADMAC/PSS in 0.5 M NaCl on top of a PSPM (4:1) brush (a) and on top of a SiO_2 wafer (b), which is used as reference. The starting time of each deposition step and rinses are indicated by solid and dashed *arrows*, respectively.

From Fig. 59a one can immediately notice that the tendency followed by the PEM in the assembly differs from that observed for the case of a free-PSPM brush. Though deposition of the first PDADMAC layer causes almost no variation in the frequency, from the 2nd layer on the frequency was measured to decrease rather progressively as more layers were added. Another important feature to highlight would be related to the almost constant energy dissipation measured all along the LbL assembly, which resembles the one observed for the

PDADMAC/PSS multilayer when adsorbed on bare silica (Fig. 59b). These results undoubtedly have direct connection with the higher compactness of PSPM (4:1) brushes in comparison to freely grown PSPM chains. Besides, the structural difference between both brushes is also reflected in the total amount of polyelectrolyte that can be assembled. Hence, the total frequency shift measured for deposition of 6 layers of PDADMAC/PSS on top of the PSPM (4:1) brush results of -470 Hz, while around -2200 Hz were observed for the same number of layers on top of a free-PSPM brush and thus the mass being assembled in the latter case is almost five times bigger.

6.2.1.2. PAH/PSS deposition on top of brushes

The LbL assembly of weak, positively charged PAH and negative PSS polyelectrolytes on top of PSPM brushes was also followed in situ by means of QCM-D (Fig. 60). In agreement to the protocol shown above for PDADMAC/PSS polyelectrolyte pair, the system was again built up to 6 total layers.

Fig. 60a displays the variations of acoustic parameters f and D as recorded from the in situ monitoring of the assembly. Comparison of Fig. 60a with Fig. 60b highlights how the presence of a preformed brush of PSPM underneath leads the system to move away from its characteristic linear growth trend.

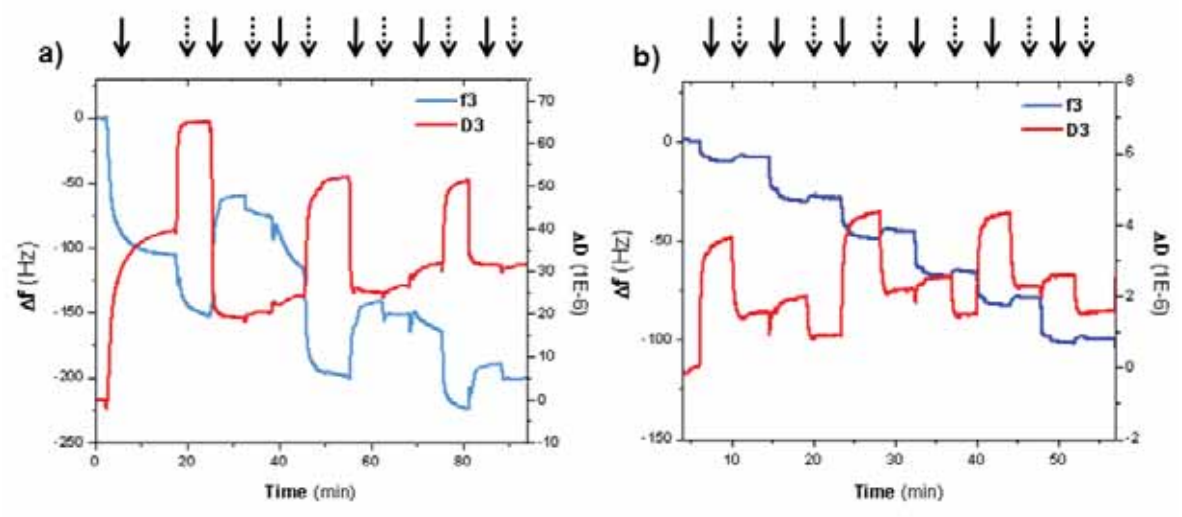

Figure 60 Assembly of 6 layers of PAH/PSS in 0.5 M NaCl on top of (a) a free-PSPM brush and (b) on top of a SiO_2 wafer, which is used as reference. The starting time of each deposition step and rinses are indicated by solid and dashed *arrows*, respectively.

For instance, deposition of the first PAH layer originated a decrease in frequency values down to almost -150 Hz, even lower than the total variation measured for the assembly of 6 layers of PAH/PSS on a bare SiO_2 surface. Such frequency decrease is accompanied by a great increase in the dissipation values to almost 70×10^{-6} which is related to a very soft coating. Then, subsequent adsorption of a PSS layer on top allowed for a partial recovery of both frequency and dissipation values in the system. This behavior could only be explained by the release of a certain amount of water as the negative chains of PSS interact with the positive sites of already bound PAH, and is reflected as the achievement of a more rigid structure. Assembly of the 3rd layer (PDADMAC) brought the situation back to higher dissipation values and lower frequencies, as observed for the 1st PDADMAC layer added. From this level onwards the system went under the same oscillatory performance described for the first two layers. However, the amplitude of the oscillations tends to decrease as the number of layers is increased. The final frequency measured for the assembly

of 6 total layers reached -200 Hz which doubles that of the multilayer directly attached to a SiO_2 surface and, at the same time, dissipation value is also almost 15 times higher. It can be undoubtedly concluded that the PSPM brush underlying promotes the adsorption of polyelectrolytes although overall values remain far away from those obtained for the assembly of PDADMAC and PSS. The significant mass difference between PDADMAC/PSS and PAH/PSS is probably due to a different behavior of the chains during deposition.

6.2.2. Block co-polymer brush-based systems

Assembly of complex systems could still be taken a step further by employing a multi-responsive copolymer brush, as the one described in section 4.2.3, as substrate for LbL deposition of polyelectrolytes on top. As the copolymer mentioned was formed by synthesis of a freely grown PSPM brush on top of a thermally-responsive PNIPAAM brush, in addition to the new responsiveness endowed, the outermost part of the hybrid film kept the negative charge needed for the subsequent electrostatic binding of polyelectrolyte chains.

The in situ QCM-D monitoring for the LbL assembly of 6 layers of PDADMAC and PSS on top of the PNIPAAm/PSPM copolymer brush is shown in Figure 61.

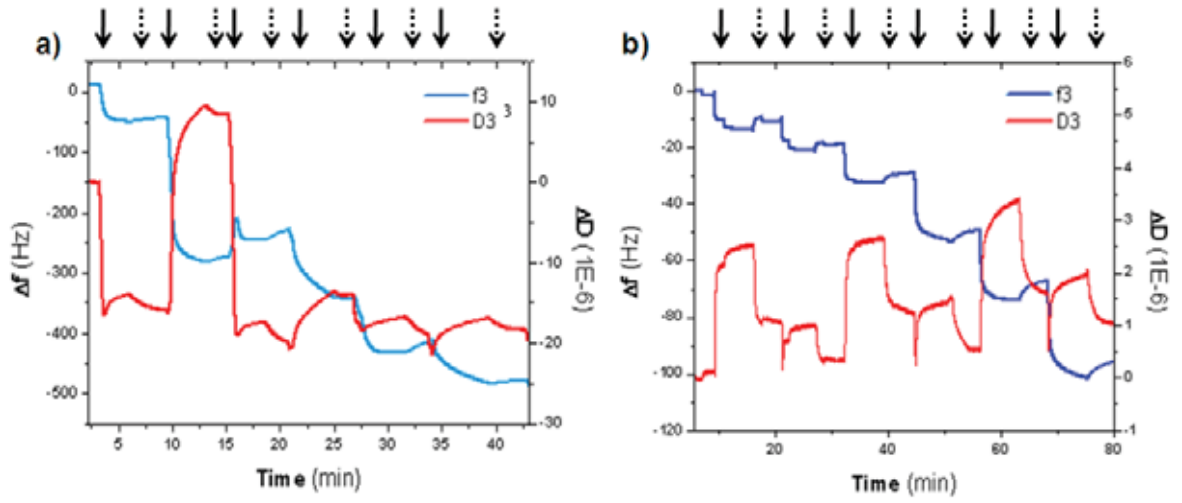

Figure 61 Assembly of 6 layers of PDADMAC/PSS in 0.5 M NaCl on top of (a) a PNIPAAm/PSPM copolymer brush and (b) on top of a SiO_2 wafer, which is used as reference. The starting time of each deposition step and rinses are indicated by solid and dashed *arrows*, respectively.

The difference between Figures 61a and 61b is again clearly noticeable as for previous LbL assemblies on PSPM brushes studied. By comparison of Fig. 61a with both Figs. 58a and 59a it can be checked out whether the presence of a PNIPAAm block underneath is affecting or not to the buildup of the multilayer. Such a comparison brings very interesting results since the trend in the frequency variations monitored for case of the assembly on top of the copolymer can be considered a combination of the other two. For instance, the type of assembly and the final frequency measured (-500 Hz) resemble, on one hand, what observed for a PSPM (4:1) brush. On the other hand, dissipation is closer to the behavior of freely grown PSPM, since it is also characterized by a significant increase after deposition of the second layer of the multilayer, corresponding to negatively charged PSS.

These results might be explained as follows: the non-tethered ends of the PSPM on top of the copolymer interact with the bulk solution as in a single block of free-PSPM since both brushes

were synthesized in the same conditions and in the absence of Cu (II) inhibitor and the first polyelectrolyte layers may lead to a similar state. Nevertheless, the presence of PNIPAAm beneath makes the PSPM block growing to a much lesser degree and, therefore, the amount of polyelectrolytes that can be deposited decreases as well. The smaller the size of the brush the lower the chain mobility and this will restrict the diffusion of the incoming polyelectrolytes through the preformed brush. To a certain extent this situation can originate a better packed brush which would be comparable to PSPM (4:1) brushes, or at least with similar restrictions.

6.2.3. Topological features of the complex system

The topology of PSPM brushes and its changes after consecutive adsorption of polyelectrolytes according to the LBL protocol were studied by AFM imaging. The micrograph in Figure 62a shows a free-PSPM brush before polyelectrolyte coating. The image in Figure 62b corresponds to the freely grown PSPM brush after five cycles of adsorption of PDADMAC and PSS have been conducted (5 PDADMAC/PSS bilayers). The image reveals sharply elevated closed, and a few open rings, which cover the entire surface. The original brush shown in Figure 62a, in contrast, can be best described as a rough surface lacking any noticeable regular structure. For the sake of comparison, PDADMAC was substituted by PAH in the assembly. Figure 62c shows that, when PAH was used instead of PDADMAC, the resulting brush/polyelectrolyte multilayer surface was homogeneous with a roughness of the order of 10 nm.

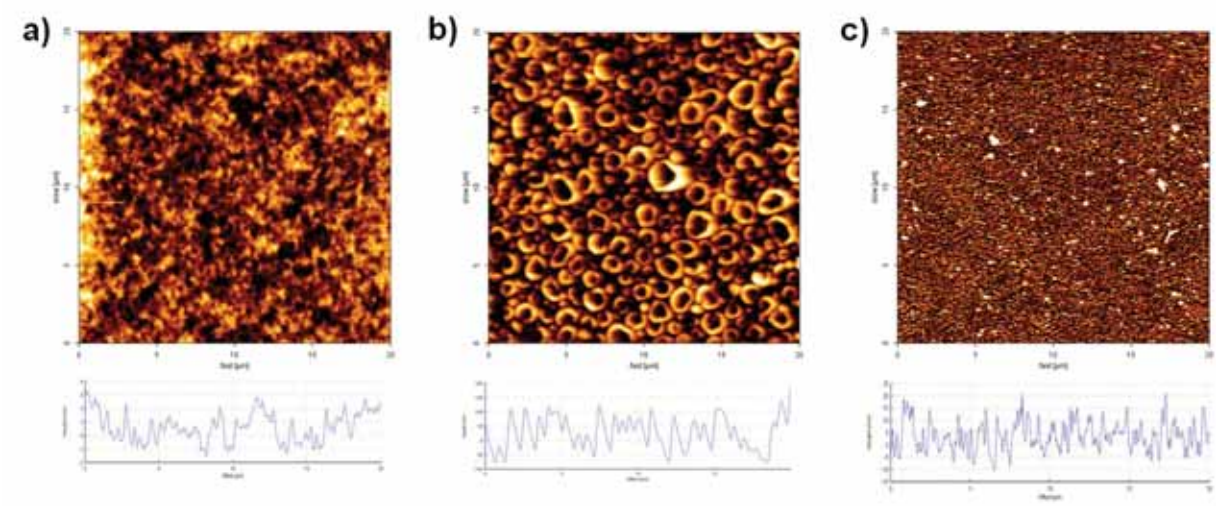

Figure 62 AFM height micrograph of a) a gold surface covered with a PSPM *free* brush; b) a gold surface covered with a free-PSPM brush coated with 10 layers of PDADMAC/PSS; c) a gold surface covered by a free-PSPM brush and 10 layers of PAH/PSS. A typical height profile is displayed below each micrograph.

Additionally to their growth from monolayers of polymerization initiator molecules, PSPM brushes were also grown from a patterned surface. Brushes grew from selected areas, which had been previously stamped with the initiator, according to the shape of the stamp employed: 5x5 μm squares carrying the initiator separated from each other by 3 μm wide initiator-free gaps.

When PDADMAC and PSS were adsorbed consecutively onto such a patterned brush, a quite unusual topology formed by polymer rings was observed as Figure 63 shows.

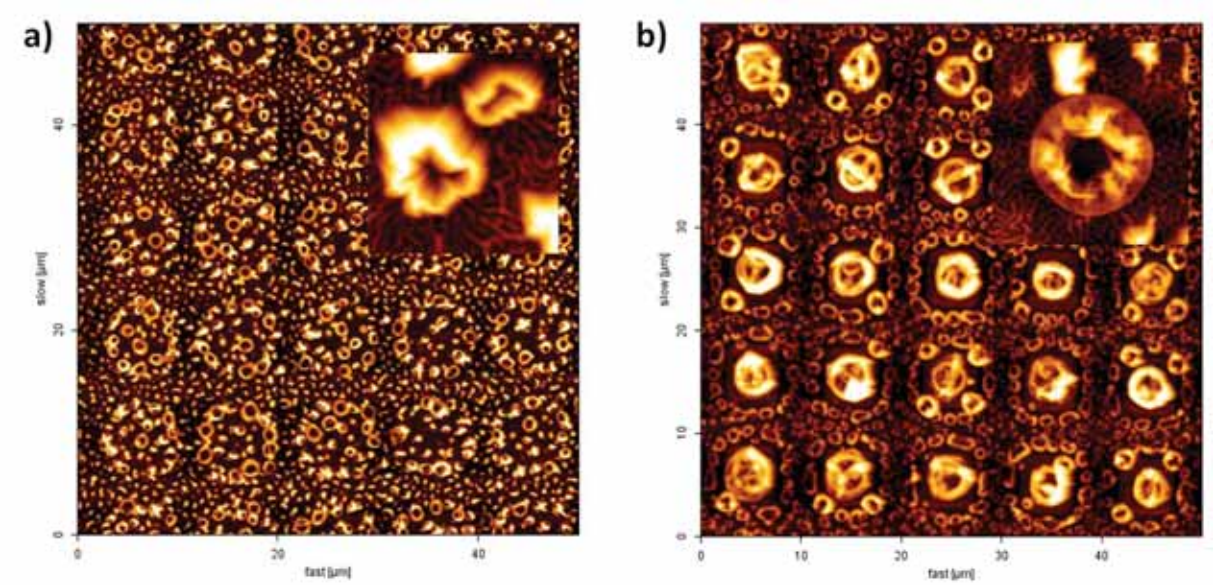

Figure 63 AFM micrograph of PDADMAC/PSS 10 LBL multilayer deposited on top of surfaces patterned with (a) PSPM (4:1) and (b) free-PSPM brushes.

The diameter of the rings being formed appears to depend on the original height of the brush placed beneath. For the thinner brush (Fig. 63a), the ring diameter varied between 0.8 and 2.2µ m with a distribution maximum at 1.6 µm while a larger and more complex ring extending over almost the entire square was observed for the multilayers built on freely grown brushes, as can be observed from Fig. 63b. These peculiar rings which have their centers in the middle of the stamped square show a height ranging from 200 to 400 nm a the diameter of the large central ring structure of 4.75 µm, which is very close to the edge length of the stamped area. At the same time the smaller rings formed at the edges of the patterned square ranged from 200 to 700 nm.

The presence of ring structures during LBL assembly of PEI/PSS had been observed previously.[8-9] Authors interpreted it as the result of the collapse of different polyelectrolyte complexes into an ordered structure which could minimize hydrophobic interactions.[10] But

attending to the results shown here, a different reasoning comes up: the toroid-like structure could be explained to take place as a consequence of the formation of a non-homogeneous layer when the first PDADMAC molecules are adsorbed. More likely, PDADMAC chains form complexes with the oppositely charged brush molecules, either scattered or more regularly distributed over the brush surface, depending on whether the original brush was a continuous monolayer or it was patterned. These complexes may then serve as the preferential attachment sites for the next incoming polyelectrolyte species. This explains the exponential growth regime. Besides, the first incoming PDADMAC molecules are thought to attract PSPM segments, quite likely belonging to different PSPM chains. This would create a locally higher charge density of the PSPM chains caused by the interaction with the PDADMAC chain. Such interaction with the positively charged PDADMAC would counterbalance the electrostatic repulsion of the PSPM segments. Therefore, there is an increased probability that the next adsorbing PDADMAC chains will attach to highly charged regions caused by the first adsorbed PDADMAC. In this way, growth may preferentially occur at the sites, where the first incoming PDADMAC molecules were initially adsorbed. A central element in this explanation is the spatial extension of the PSPM chains together with their flexibility. If these chains are drawn to the PDADMAC molecule forming a corona around it, the surface in between becomes depleted of PSPM, which in turn reduces the probability of sustained adsorption of PDADMAC in these regions. PSS as the following oppositely charged poly-ion may partially remove these less strongly bound PDADMAC polymers. This mechanism would support the strongly inhomogeneous growth of PDADMAC/PSS on PSPM brushes. With PAH the situation is different, since there is a large probability that PAH forms hydrogen bonds, in addition to the electrostatic interaction with

PSPM. Such a result would imply a stronger interaction with the sulfonate groups of PSPM, which would make desorption less likely. The high flexibility of PAH compared with PDADMAC would be a factor facilitating a more homogeneous mode of adsorption, since PAH could more easily adapt to the conformation of PSPM. Another question is the suspiciously geometric structure of the complexes. They occur as curved walls or in many instances even as closed rings. The circumference of these structures is larger or comparable with the contour length of a polymer chain. The width of the wall is much smaller than the contour length. Therefore these structures correspond to a stretched conformation of the adsorbed PDADMAC. Such a stretched conformation would maximize the electrostatic interaction with PSPM and minimize intra-molecular self-repulsion, respectively. Rings may form since, as discussed above, the next adsorbing PDADMAC molecule will try to align with the contour defined by the adsorption of previous PDADMAC molecules. This may close a previously open contour. The process will continue following the initial pattern of assembly. For a proper quantitative understanding of the assembly mode and the structure on laterally homogeneous and patterned brushes, further experiments and theoretical simulations would be required.

6.2.4. Response with the ionic strength

The high responsiveness shown by the individual components of PE brush-PEM complexes suggested that the way such a structure behaves in the presence of salts is worth an analysis. In case of PEMs composed of PDADMAC/PSS assembled on bare SiO_2 substrates, for instance it has been already demonstrated (section 2.2.1) that the structure undergoes a reversible collapse

upon exposure to high ionic strength when PDADMAC appeared as last layer, while for multilayers capped with PSS no apparent changes were observed. Likewise, analysis of individual PSPM-free and PSPM (4:1) brushes in situations of high ionic strength resulted in thickness decreases of about 20 nm and water releases of the 32 and the 16 %, respectively. The combination of both systems would be thus expected to have an outstanding ionic strength-responsive behavior.

But, surprisingly, exposure of the PEM-PE brush hybrid system to 1 M NaCl resulted in the stripping-off of the porous PDADMAC/PSS film instead of in a collapse of the structure. The image in Figure 64a shows the completely recovered patterned structure of the brush after removal of the adsorbed polyelectrolyte.

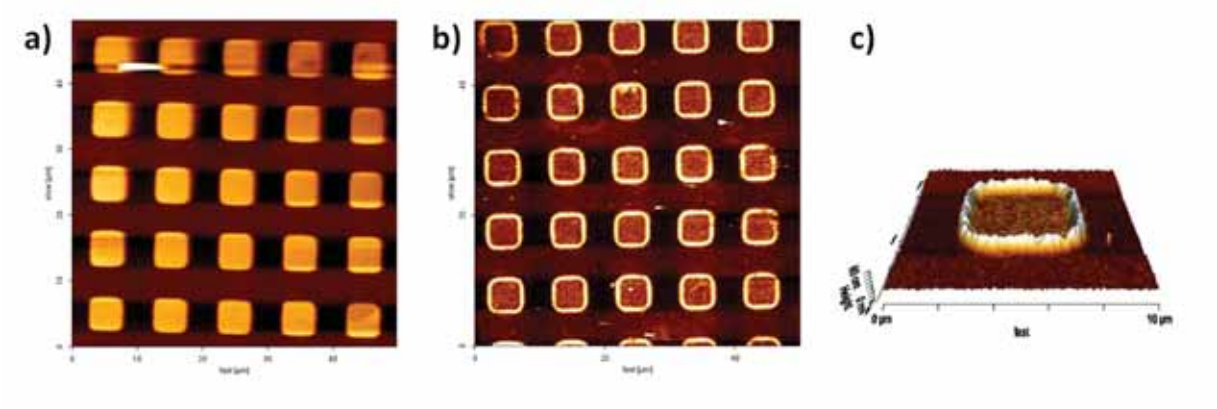

Figure 64 AFM height micrographs of PSPM patterned surfaces after removal of PDADMAC/PSS: a) complete removal of the multilayer; b) partial removal; c) detail of a square of patterned surface after the partial removal.

This process can be considered to be ‘reversible’, in the sense that the total recovery of the initial PSPM structure would permit to re-start the PDADMAC/PSS adsorption cycle again to re-establish the porous polyelectrolyte rings. From that point of view, the situation more or less resembles that explained for PDADMAC/PSS multilayers assembled on silica, when exposure to quaternary ammonium surfactant concentrations over the CMC led to a total removal when PDADMAC was the outermost layer.

But the removal process is also featured by proceeding progressively over a certain period of time after the surface becomes exposed to the NaCl solution, so the process can be interrupted at any time. In this case, a certain part of the original adsorbed polyelectrolytes remains on the brush surface. This situation is depicted in Figure 64. One can see in (b) and (c) that a proper treatment in NaCl has left the adsorbed polyelectrolyte preferentially at the edges of the squares forming a thin wall, bordering the brush on the stamped square. Figure 64c shows this border wall, which was measured to be around 60 nm thick, in greater resolution. Obviously, it can be deducted that the thicker the brush used, the thicker the walls that can be obtained. Then, by controlling the amount of $CuCl_2$ employed, through the Cu(I)/Cu(II) ratio, one would be able not only to tune the height of the brush assembled but the height of the walls resulting from the partial removal of the PDADMAC/PSS multilayer placed on top. This turns of main importance for the different applications these 3D structures may have.

6.3. Conclusions

In this 6th chapter the formation of complex systems formed by layer-by-layer assembly of PDADMAC/PSS on top of negatively charged PSPM brushes has been described.

First, the deposition of the PEMs on PSPM brushes, grown either in the presence or in the absence of Cu (II), was followed in situ by means of the QCM-D technique. Hence, depending on the protocol employed to synthesize the brush, the way the multilayer adsorbs is shown to be changed. Although a similar supra-linear growing tendency is observed for all the examples studied, in case of PEMs assembled on top of a freely grown PSPM brush both the mass being adsorbed and the viscoelastic properties of the film show higher values than those measured for multilayers built on top of PSPM (4:1) brushes for a same number of layers. While for PDADMAC/PSS on free-PSPM total shifts in the frequency and the dissipation of -2200 Hz and 50 x 10^{-6} are shown, the latter reaches around -500 Hz and shows a negligible variation in the dissipation which speaks about the rigidity of the film. These values differ rather remarkably from LbL adsorption on bare SiO_2 substrates as seen in Chapter 1.

When the polyelectrolyte pair being assembled on top of the PSPM brush is that formed by PAH and PSS, the growth has been shown to diverge quite considerably from the typical linear trend characterizing this system and, instead, tends to follow an oscillatory tendency. Thus, adsorption of PAH layers results in significant increases of both the mass adsorbed and the dissipation. On the contrary, assembly of each layer of PSS promotes some water to be released from the structure and dissipation drops.

PDADMAC and PSS were also employed to build a multilayer on top of a multi-responsive PNIPAAm/free-PSPM copolymer brush. In that case the presence of another system underneath limits partially the freedom of PSPM chains and the acoustic response is closer to that observed for single PSPM (4:1) brushes, although some viscoelastic features are shared with a freely grown PSPM brush.

In the second part of the chapter, topological studies done on the complex systems revealed the formation of well defined three-dimensional structures appearing as sharp curved walls or even closed rings with holes inside. The wall radius of curvature and the diameter of the rings range from below μm to several μms, depending on the height of PSPM brush. The walls may have a height of a few hundred nanometers. At patterned brushes, impressive symmetrical ring ornaments can be created. In addition, these structures can be completely or partially removed in mild conditions developing the original brush structure. This phenomenon gives an additional degree of freedom in the design of 3D structures on interfaces. Combination of soft polyelectrolyte brushes providing a flexible charge distribution with the self assembly provided by LBL adsorption may generate a general and simple way of obtaining interesting three-dimensional structures on the nanoscale in a controlled fashion, which may find interesting applications in a variety of fields.

6.3. References

(1) Dubas, S. T.; Schlenoff, J. B. *Macromolecules* 1999, 32, 8153-8160.

(2) Zhang, H.; Rühe, J. *Macromolecules* 2003, 36, 6593-6598.

(3) Farhan, T.; Huck, W. T. S. *Eur. Polym. J.* 2004, 40, 1599–1604.

(4) Kumar, A.; Biebuyck, H. A.; Whitesides, G. M. *Langmuir* 1994, 10, 1498-1511.

(5) Bruening, M. L.; Dotzauer, D. M.; Jain, P.; Ouyang, L.; Baker, G. L. *Langmuir* 2008, 24, 7663.

(6) Estrela-Lopis, I.; Leporatti, S.; Clemens, D.; Donath, E. *Soft Matter* 2009, 5, 214-219.

(7) Yang, S. Y.; Kim, D. L.; Jeong, S. M.; Park, J. W. *Macromol. Rapid Commun.* 2008, 29, 729-736.

(8) Picart, C.; Mutterer, J.; Ritchert, L.; Luo, Y.; Prestwich, G. D.; Schaff, P.; Voegel,J. C.; Lavalle, P. *PNAS* 2002, 99, 12531-12535.

(9) Jaber, J. A.; Schlenoff, J. B. *Langmuir* 2007, 23, 896-901.

(10) Menchaca, J. L.; Flores, H.; Cuisinier, F. J. G.; Pérez, E. A. *J. Phys.: Condens. Matter* 2004, 16, S2109-S2117.

Summary

The work developed in this thesis has described the assembly and the responsiveness of supramolecular structures based on stimuli-responsive polyelectrolyte chains. Two different types of assemblies have been built according to the protocol followed for the anchoring of polyelectrolyte chains to the surface coated: electrostatic adsorption of oppositely charged polyelectrolytes has been used for the formation of multilayered systems, while the growth of the chains from chemically modified surfaces has resulted in brush-like structures. The analysis done for both multilayers and brushes has revealed very interesting properties and, in some of the cases, a remarkable potentiality for their use in different applications.

In the first section, a general approach to polyelectrolyte multilayers composed of standard polyelectrolyte pairs PDADMAC/PSS and PAH/PSS has been done. The main information extracted from the analysis could be summarized as follows:

- Layer-by-layer assembly of PAH/PSS has been shown to produce a linearly growing film that contains almost no water in its interior when assembled with rinses in salt solution, while the assembly with rinses in pure water produced a film that contained more than 40% water. On the contrary, supralinear growth of PDADMAC/PSS PEMs, exhibits a strong dependence on both the ionic strength employed and the last layer deposited. While for multilayers built with NaCl rinses the hydration values oscillate around the 40% in water content, in conditions of low ionic strength the film is capable to soak water up to 70% of the total multilayer mass when the last incubation step is with PDADMAC. Adsorption of a new PSS layer on top of such system lead the multilayer to a more

compact and rigid state, which makes the water content in the film to decrease down to the 30%.

- Exposure of PDADMAC/PSS multilayers with PDADMAC as top layer to high ionic strengths cause reversible decreases in the film thickness of >100 nm (~58%) and in the water content of about the 50% that can be recovered by exchanging NaCl for water. Nevertheless, when PSS is the top layer such variations do not take place.

- A specific interaction between ClO_4^- and PDADMAC and $H_2PO_4^-$ and PAH in LbL multilayer systems has been demonstrated to take place. While in case of perchlorate/PDADMAC a partial removal of polyelectrolytes from the top layer is shown, the Phosphate/PAH union is explained to take place through hydrogen bonding between the primary amines and the anions.

- The specific nature of the interaction of the quaternary ionic surfactant TTAB with polyelectrolyte multilayers results in the strip off the multilayer depending of the polyelectrolyte pair chosen. PAH/PSS multilayers, for instance, remain stable while PDADMAC/PSS multilayers can be removed in a controlled manner.

- Exposure of hybrid systems, composed of sequentially assembled PAH/PSS and PDADMAC/PSS PEMs, to TTAB reduces the removal of the PDADMAC/PSS layers. Furthermore, the extent of the stabilization increases with the number of layers of PAH/PSS placed underneath.

- Spectroscopic studies of polyelectrolyte complexes have provided new insights in the interaction between PAH and PSS. For instance, dry PSS/PAH complexes display the $\nu(SO_2)$ and $\nu s(SO_3^-)$ bands at positions that are indicative of the presence of hydrogen bonds between PSS and PAH that may account for the exceptional stability of multilayers of PAH/PSS.

In the second section, both the growth (via ATRP from chemically activated gold surfaces) and the responsiveness of brushes composed of ionic strength-responsive PMETAC and PSPM polyelectrolytes and of thermo-sensitive PNIPAAm have been studied. Main results deriving from such analysis are described in the following list:

- For brushes grown from a monolayer of initiator thiol, PMETAC brushes show the highest hydration, of approximately the 65 %, while the lowest water content, of the 40%, is observed for PNIPAAm brushes. In case of PSPM brushes the content of water varies with the growing conditions: for PSPM assembled in the presence of Cu (II) inhibitor the water content stays close to the 45%. On the contrary, Cu (II)-free PSPM brushes, which show a significantly higher film thickness, allow reaching a 49% of entrapped water in the structure. Knowing these initial water content/hydration values, calculation of the percentage of water lost during collapse of the brushes has been shown to be possible. On one hand, PMETAC and PSPM (4:1) polyelectrolyte brushes lost a maximum of around a 30 % of their water content at 1 M NaCl, and freely grown PSPM only released a 16% of

its aqueous content upon treatment with the same ionic strength. The thermally-responsive PNIPAAm, on the other hand, showed a water release of the 80% of its water content at a temperature of 40º C.

- PMETAC brushes grown from a wide range of initiator percentages (between 1% and 100%) show an almost constant content of water. This observation implies that the water associated to the monomers represents most of the water in the brush independently of the packing of the brush chains in the brush and the small differences in water content between the different brushes must be, thus, due to water entrapped in the structure of the brush. In case of PSPM brushes the study basically has shown the effect of whether incorporating Cu (II) or not in the polymerization reaction at the same time that the grafting density was also varied. Surprisingly, same water content values have been calculated for both PSPM (4:1) and free-PSPM brushes at the different initiator densities employed. Exposure of PMETAC brushes, grown from different initiator densities, to increasing ionic strengths of NaCl permits calculating a removal of around the 30-40% of the water in the brush is observed for 0.5 and 1 M NaCl solutions while only a 10% is eliminated at ionic strengths below 0.1 M NaCl. The amount of water released would mostly come from entrapped water but changes in the hydration of the monomers can take place as well in response to high ionic strengths. However, the total dehydration of the brush could not be reached in any case.

- The assembly of a multi-responsive copolymer brush composed of a first brush of PNIPAAM and a second block of PSPM on top has been achieved by reactivation of the ATRP process to originate a highly hydrated structure where a 65 % of the mass corresponds to water. The alternate exposure of such multi-responsive brush to either an increase in the temperature over the LCST or high ionic strength solutions showed the selective response of the structure built.

- The formation of a hybrid system formed by layer-by-layer assembly of PDADMAC/PSS on top of negatively charged PSPM brushes has been also characterized. For multilayers built on top of a freely growing PSPM brush it has been shown that thicker films of higher viscoelastic properties can be generated in comparison to those measured for multilayers built on top of PSPM (4:1) brushes for a same number of layers. Topological studies done reveal that such systems promote the formation of well defined three-dimensional structures appearing as rings with holes inside, where the radius of curvature and the diameter of the rings range from below μm to several μms, depending on the height of PSPM brush. In addition, these hybrid structures can be completely or partially removed in mild conditions developing the original brush structure.